

Appendix

DEVELOPMENT OF SCENARIO EARTHQUAKE STRONG GROUND MOTIONS AND LIQUEFACTION POTENTIAL

Appendix

Ground motion and liquefaction assessment

To properly couple earthquake source variability (nucleation point and asperity distribution) into variability in nonlinear site response as well as liquefaction demands and capacities, equivalent linear site response has been combined into a finite fault simulation code (Silva et al., 1999). Source and site parameters (shear-wave velocity, layer thicknesses, depth to bedrock, and G/G_{max} and hysteretic damping curves) are varied randomly (following empirical distributions) and resulting motions (time histories and response spectra) as well as at-depth cyclic shear stress, strain energy density (Dobry et al., 1981), and Arias intensity (Kayen and Mitchell, 1997) are evaluated for each realization. Selective variation of parameters permits impact assessments on both motions and parameters which affect liquefaction triggering.

Ground motion model. The effects of a large finite source including rupture propagation, directivity, and source-receiver geometry can profoundly influence strong ground motions in terms of frequency content and duration. To accommodate these effects, a methodology that combines the aspects of finite-earthquake-source modeling techniques (Hartzell, 1978) with the stochastic point-source ground motion model has been developed to produce response spectra and time histories appropriate for engineering design (Silva et al., 1990; Silva and Stark, 1992; Schneider et al., 1993; Beresnev and Atkinson, 1997). The approach is very similar to the empirical Green function methodology introduced by Hartzell (1978) and Irikura (1983). In this case however, the stochastic point source is substituted for the empirical Green function and peak amplitudes; PGA, PGV, and response spectra (when time histories are not produced) are estimated using random vibration theory (RVT). Use of the stochastic point source as a Green function is motivated by its demonstrated success in modeling ground motions in general and particularly strong ground motions (Boore, 1983, 1986; Silva and Stark, 1992) and the desire to have a model that is truly site and region specific. The model can accommodate a region specific crustal $Q(f)$, Green function sources are arbitrary moment or stress drop, and site specific kappa values (Anderson and Hough, 1984). The necessity of regional and site specific recordings or the modification of empirical Green functions is eliminated.

Crustal response effects are accommodated by using vertically propagating shear waves through a vertically heterogeneous crustal structure. Propagation path damping, through a $Q(f)$ model, is incorporated from each fault element to the site. Near-surface crustal damping is incorporated through the kappa operator. To model crustal propagation path effects, the method of Ou and Herrmann (1990), is used for each subfault.

Site effects on ground-motion amplitude. The conventional computational approach in modeling site response involves a selection of suitable time histories to serve as control (rock) motions and a suitable computational formulation to transmit the motion through the soil profile. The computational scheme which has been most widely employed to evaluate one-dimensional site response assumes vertically propagating shear waves. Departures of

Appendix

soil response from a linear constitutive relation are treated in an approximate manner through the use of the equivalent-linear approach (Schnabel et al., 1972).

The computational scheme used in this study is the equivalent-linear analyses described in Schneider et al. (1993; EPRI, 1993). In this method, the site response is computed using the finite-fault model to generate the power spectral density and spectral acceleration of the control motion. This power spectrum is then propagated through the one-dimensional soil profile using plane-wave propagators for SH waves. Possible non-linear behavior of the soils is treated through the equivalent-linear formulation. Random vibration theory (RVT) is used to predict the peak time domain values of shear strain based upon the shear-strain power spectrum. In this sense, the procedure is analogous to the program SHAKE except that peak shear strains in SHAKE are measured in the time domain. The frequency domain approach does not require a time domain control motion, and this eliminates the need for multiple analyses based on a suite of input time histories. This occurs because each time domain analysis may be viewed as a single realization of a random process. Several realizations of the random process must be sampled to yield statistically stable estimates of the site response. In the frequency domain approach, the estimates of peak strain as well as response spectral values are, as a result of RVT, fundamentally probabilistic in nature. Stable estimates of site response with respect to a suite of input time histories representing varying distributions of energy with time can be obtained with just one run.

This RVT based equivalent-linear approach has been validated against several nonlinear codes (DESR-2C, TESS, and SUMDES) at high strain levels with recorded motions at the deep soil sites Treasure Island, Gilroy #2, California, Lotung, Taiwan, and Port Island, Japan. All four- simulation procedures were found to provide comparably good fits to the recorded motions (EPRI, 1993, BSC, 2004).

Approach in Computing Probabilities of Liquefaction. The occurrence of liquefaction is dependent upon the susceptibility of the soil, the amplitude and duration of the ground shaking, and the depth of the water table. The evaluation of a soil's resistance to liquefaction involves the estimation of both the capacity to resist liquefaction as well as the demand placed on the soil by ground shaking.

To assess liquefaction potential, three approaches have been incorporated into the RVT equivalent-linear portion of the finite-fault simulation code: cyclic stress ratio (CSR; Seed and Idriss, 1971), strain energy density (Dobry et al., 1981, 1982; Ostadan et al., 1996), and Arias intensity at-depth (Kayen and Mitchell, 1997). Because the finite-fault simulations represent the control motions for the stresses, and strains, entire profile, the effects of rupture directivity on spectral content, as well as duration are captured in a natural manner. Additionally, to provide estimates of the soil capacity, the number of cycles is estimated using random process theory. For close-in sites, the number of cycles increases or decreases for rupture away or toward the site. This allows appropriate and self consistent adjustments to the CSR capacity estimates.

Liquefaction Resistance. Site-specific evaluation of liquefaction resistance involves use of empirical correlations between the observed occurrence of liquefaction and the results of field measurements. Accepted field measurements include the Standard Penetration Test (SPT), the Cone Penetration Test (CPT), and V_s measurements (Youd et al., 2001). All of

Appendix

these field measurements are proportional to density, effective stress, and grain characteristics, which along with saturation conditions determine the soil's resistance to liquefaction, in terms of a cyclic resistance ratio (CRR).

Considering the available data and the adaptability of the various procedures, it was decided to estimate the CRR for the soils in the Mississippi embayment using V_S data. Use of the more established approaches in estimating dynamic strength such as SPT and CPT would have involved developing median values of blow count and tip resistance as well as statistical models for their uncertainties across the study region. The availability and maturity of statistical models for the variability of V_S , layer thickness, and nonlinear dynamic material properties were compelling arguments for implementing a V_S approach to estimate cyclic capacities.

A particularly attractive advantage in using the V_S approach in liquefaction assessment is that it is straightforward and it directly accommodates profile parametric uncertainty in a statistically rigorous manner. Profile variability (spatial variation within the study area), V_S , as well as nonlinear dynamic material properties, can be incorporated in a manner consistent with developing ground motions, arriving at median and fractile estimates of liquefaction potential that are consistent with median and fractile estimates of ground motions.

The equation for determining the CRR from V_S is empirical, and based on case history studies at sites that did and did not liquefy during earthquakes (Andrus and Stokoe, 2000). The equation is:

$$\text{CRR} = 0.022 (K_C V_{S1}/100)^2 + 2.8 [1/V_{S1C} - K_C V_{S1}] - 1/V_{S1C} \cdot \text{MSF} \quad (1)$$

$$\text{where MSF} = (M/7.5)^{-2.56} \text{ (a magnitude scaling factor)} \quad (2)$$

and V_{S1} is the stress-corrected V_S , V_{S1C} is a correction factor that depends on fines content, and K_C is a correction factor for cementation and aging. Because there is currently no widely accepted method for estimating K_C (Andrus and Stokoe, 2000), it was taken as 1 for this study. A fines content of 24% was assumed appropriate for the site. The actual fines content is expected to vary with depth. However, in the analysis by Andrus and Stokoe (2000), equation (1) was derived from sands and gravels that were classified into three broad categories with regards to fines content: $\leq 5\%$, 6 to 34%, and $> 35\%$. Based on this classification, variabilities in fines content is expected to have a minimal effect on the median probability of liquefaction.

Liquefaction Demand. Cyclic demands are expressed as the ratio of the average seismically induced shear stress to the vertical effective overburden stress within a liquefiable zone, generally within about 15m (50 ft) of the ground surface. This ratio, known as the cyclic stress ratio (CSR), is defined as:

$$\text{CSR} = \tau_{\text{cyc}} / \sigma_v' \quad (3)$$

where τ_{cyc} is the cyclic shear stress in the soil and σ_v' is the effective vertical stress (Seed and Idriss, 1971). In practice, demands are usually computed using approximate and generic

Appendix

relations between surface peak acceleration and at-depth cyclic shear stress (Youd et al., 2001),

For this study, the average CSR for the soil susceptible to liquefaction is determined during the finite rupture simulation. Conditions which determine the CSR are: (1) PGA at the ground surface, (2) σ_v , the total vertical stress, and (3) σ'_v . Calculation of the total and effective stress condition requires estimation of the density of the overlying material. A constant wet density of 2.20g/cm^3 along with a dry density of 1.80g/cm^3 and a water table depth of 10 ft (3m) was used.

Model of liquefaction probability. Liao et al. (1988) developed a parametric model to predict the probability of liquefaction as a function of magnitude-normalized CSR and Standard Penetration Test (SPT) blow count in the liquefiable stratum. Youd and Noble (1997) and Noble (1998) extended the analyses of Liao et al., (1988) using new case histories and adding magnitude and fines content explicitly into the equations for the liquefaction probability. Approaches that calculate results in terms of a probability of liquefaction, rather than a yes/no value, acknowledge that the onset of liquefaction cannot be predicted exactly, given a few scalar parameters. These methods capture the scatter in liquefaction case history data, rather than define a conservative estimate for use in design. This is consistent with the practice in ground-motion equations where model results are given as the probability distribution of ground-motion amplitude (in the form of a median and a standard deviation) given magnitude and distance. Probabilistic models of liquefaction have been used in dam studies (Vick, 1994), regional liquefaction hazard studies (Budhu et al., 1987; Hashash, 1987), risk analyses for nuclear material storage facilities (Arango et al., 1996), and loss-estimation studies (RMS, 1997).

Factor of Safety. The ratio of capacity (CRR) to demand (CSR) is termed the factor of safety (FS) against liquefaction. Liquefaction is predicted to occur when FS is at or below 1, and not to occur when it exceeds 1. To provide a more rational basis for assessing risk levels, Juang et al. (2002) cast the deterministic factor of safety into an expression for the probability of liquefaction (P_L). This mapping function is given by:

$$P_L = 1/(1 + \text{FS}/0.8)^{3.5} \quad (4)$$

It is based on SPT field performance data and accommodates the occurrence of sites that should have liquefied but did not, as well as those that did and provides the mechanism for translating liquefaction hazard into liquefaction risk. Subsequent work by Juang et al. (2002) has shown that the V_s field performance data compiled by Andrus and Stokoe (2000) provides a probability mapping function close to Equation 4.

Computation of Liquefaction Susceptibility. To incorporate uncertainty in dynamic material properties, the shear-wave velocities, G/G_{max} , and hysteretic damping curves are randomized using probabilistic models. These models are based on probabilistic analyses of about 500 measured shear-wave velocity profiles (Silva et al., 1997) and results of multiple laboratory dynamic tests (EPRI, 1993). To accommodate uncertainty in source and path parameters, slip model and nucleation points are randomized along with $Q(f)$ and κ values (Table A1). The model for the slip distribution preserves the statistical properties of slip models derived from well recorded earthquakes. Nucleation points are also randomized

Appendix

within a rectangular nucleation zone (Silva, 1992). Probabilistic models have been developed for $Q(f)$ and kappa variability (Silva, 1992; EPRI, 1993). At the site, one obtains a value of CSR and CRR along with the FS, P_L , and N (number of cycles) at each depth in 10 ft increments down to 80 ft for each realization of source, path, and site properties. Randomness in liquefaction is introduced by computing the liquefaction probability, using the geotechnical characteristics of the site, for all realizations. One could also introduce uncertainty in surficial geotechnical characteristics (e.g., variations in blow counts within each liquefaction zone) at this stage. The resulting value of liquefaction probability embodies the natural scatter in ground motions, liquefaction susceptibility, as well as site dynamic material properties.

An important aspect of any numerical modeling approach is a validation of the model against data and a proper statistical estimate of uncertainty. The appropriate validation of the model is in the estimation of ground motions and liquefaction prediction. The liquefaction parameters, although incorporated into the model, have all been validated or calibrated with appropriate case histories (Andrus and Stokoe, 2000; Juang et al., 2001). The model validation for motions consists of estimating the model bias (e.g. systematic under-prediction or over-prediction of the data) and the modeling uncertainty of the prediction due to complexities in the source and path effects that are not included in the model.

A quantitative assessment of the model bias and modeling uncertainty (Abrahamson et al., 1990) associated with the finite-fault and equivalent-linear RVT numerical predictions has been computed for 16 earthquakes at over 150 sites within a 20 km rupture distance (Silva et al., 1997). For rock and soil-sites which did not have available shear-wave velocity profiles, generic profiles were used appropriate for soft rock and deep soil. Generic depth dependent modulus reduction and damping curves appropriate for rock and both cohesive and cohesionless soils (as appropriate) were used to model nonlinear soil effects (EPRI, 1993; Silva et al., 1997). In this validation, magnitudes ranged from 5.8 to 7.4 with rupture distances ranging from 1 to about 20 km. CEUS type earthquakes included the M 6.8 Nahanni, Canada.

The modeling uncertainty and bias estimates are shown in Figure A1. The model bias is not significantly different from zero over the frequency band of 0.2 to 100 Hz. Over this frequency range, the simple model using a Brune omega-square point-source as a source function coupled with simple Ou and Herrmann (1990) geometrical attenuation and RVT equivalent-linear site response provides accurate and unbiased predictions of strong ground motions at both rock and soil sites. Using a similar stochastic finite fault model and linear crustal response for rock site conditions, Beresnev and Atkinson (2002) found similar results for both WNA and CEUS earthquakes. Interestingly Hartzell et al., (1999) for the Northridge earthquake, found comparable accuracy using much more seismologically rigorous source and wave propagation models, including a three dimensional crustal and basin model.

To provide validation for the liquefaction estimation using the combined model of ground motion, site response, and liquefaction, Silva et al. (1999) obtained results for the demand side calculations of CSR and strain energy during the Kobe earthquake. In this DOE-sponsored project, 580 sites were modeled to assess liquefaction prediction. The results show high CSR's and energies in areas with mapped ground failure or liquefaction. The

Appendix

rapid falloff of CSR's and energies toward Osaka, where liquefaction was sparse, means that the procedure does not predict liquefaction where none had occurred. This validation reflects near-source, (within 20 km) conditions. To provide validation at larger distances, soils at Treasure Island, the Bay Bridge approach, and the Marina District (all at about 70 km distance were modeled), all of which had extensive liquefaction. These sites have been studied in detail so site properties are readily available. The procedure showed high CSR's when the input motion characteristics were those of recorded rock motion at Treasure Island, further validating the method.

SOURCE, PATH, AND SITE PARAMETERS

Source Parameters. The Hayward scenario earthquake assumes a two segment (north and south) rupture with a length of 75 km. Assuming a rupture width of 15 km, the resulting area (1125 km²) corresponds to a **M** 7.1, based on Wells and Coppersmith (1996). The rupture distance was taken as 5 km and the rupture mechanism was vertical strike slip. The remaining finite rupture parameters are rupture velocity, taken at 2.88 km/sec or 0.8 times the crustal shear-wave velocity of 3.6 km/sec, slip velocity, and subevent stress drop (stress parameter; Boore, 1983). The slip velocity is held constant over the rupture surface, resulting in spatially varying rise times for spatially varying slip amplitudes (or location of asperities). Based on the validations, slip velocity was taken as 100 cm/sec and the subevent stress drop was set to 60 bars. This stress drop value is appropriate for WUS conditions and oblique slip sources, based on inversions of the Abrahamson and Silva (1997) attenuation relation (Silva et al., 1997).

Path parameters. The $Q(f)$ model used was $176 f^{0.6}$ with a kappa value of 0.04 sec. Both parameter values are appropriate for the Bay area, based on inversions of strong motions from the Loma Prieta, Coyote Lake, and Morgan Hill earthquakes. The crustal model, Figure A2, is taken from the Wald et al. (1991) Loma Prieta crustal model with the shallow site profile (Figure A3) merged at the appropriate shear-wave velocity (Silva et al., 1997).

Site Parameters. The shear-wave velocity profile is based on available measurements (except for the shallow rock-fill section) at the Port of Oakland and is shown in Figure A3 to a depth of 500 ft. G/G_{max} and hysteretic damping curves assumed for the site are shown in Figure A4.

STRONG GROUND MOTION AND LIQUEFACTION TRIGGERING

Response spectra (5% damped), median and $\pm 1 \sigma$, for a variation of all (source, path, and site) parameters are shown in Figure A5. The median peak acceleration is 0.34g, seemingly low for such proximity to a **M** 7.1 earthquake, but compares reasonably well with those at the comparably soft Port Island site (about 2-3 km rupture distance) from the **M** 6.9 Kobe earthquake. The range in motions (median to plus 1σ) is about 1.3 and is reasonably uniform with frequency from 0.1 to 100.0 Hz. Varying only site parameters (Figure A6), the variability dramatically decreases for frequencies below about 0.5 Hz, suggesting the soft profile (top 350 ft, Figure A3) controls this frequency range. Conversely, varying only source parameters, Figure A7 shows a decrease in variability at high (≥ 2 Hz) frequency,

Appendix

suggesting the influence of nucleation point (rupture directivity) and asperity distribution at low frequency. To easily see these largely distinct influences, Figure A8 shows the variabilities (σ_{in}) in response spectral estimates for the three cases (all, site, and source variation). The variability due to source variation decreases rapidly for frequencies above about 1 Hz, where the site variability increases. Variabilities for both source and site exceed the variability for both sets of parameters varied simultaneously, suggesting some expected and unmodeled coupling between the effects of source and path parameters, perhaps due to the nonlinearity in site response.

To examine how this selective variation in parameters affects liquefaction triggering, Figure A9 shows median estimates of liquefaction probabilities for the three cases versus depth. The median probabilities range from about 5% near the surface to about 10% at depth, with the site variability (site as well as source and site) showing a much steeper increase with depth from about 5 ft to about 30 ft. The corresponding variabilities (σ_{in}) are shown in Figure A10 and quantify the extremely large impacts of site variability on liquefaction triggering. At a depth of about 15 ft, the variability in median estimates of liquefaction probability is about 1.25, a factor of 3.5 about the median, whereas the variability in peak acceleration is about 0.25 (a factor of about 1.30, Figure A8). For berth facilities susceptible to liquefaction induced displacements, these results suggest that variabilities in liquefaction triggering and downstream consequences (pile loading due to soil deformation) will likely dominate variabilities in loss estimation (repair cost and down time). Source variabilities (conditional on magnitude and distance) will dominate loss estimation for structures, systems, and components with high fragility to shaking at low frequency (≤ 0.5 Hz). These results are, of course, source, path, and site dependent but the methodology presented illustrates an approach to assess and quantify the impacts of uncertainties (variabilities) in earthquake source and path as well as site parameters on cyclic loads, including both ground shaking and liquefaction triggering. Figure Sets A11, A12, and A13 summarize all at-depth liquefaction triggering parameters; liquefaction probability, factor-of-safety, cyclic stress ratio, number of cycles, strain energy density, and Arias intensity for all, site, and source parameters respectively. Figure Sets A14, A15, and A16 show corresponding surface acceleration, velocity, and displacement time histories for each realization.

Appendix

REFERENCES

- Abrahamson, N.A., Somerville, P.G., Cornell, C.A. (1990). "Uncertainty in numerical strong motion predictions," *Proc. Fourth U.S. Nat. Conf. Earth. Engin.*, Palm Springs, CA., 1, 407-416.
- Andrus, R.D., and Stokoe, K.H., II. (2000) Liquefaction resistance of soils from shear-wave velocity, *Journal of Geotechnical and Geoenvironmental Engineering*, 126(11), 1015-1025.
- Arango, I., F. Ostadan, M.R. Lewis, and Gutierrez (1996). "Quantification of Seismic Liquefaction Risk," *Proc. ASME Pressure Vessel and Piping Conf.*, Montreal.
- Bechtel SAIC Company, LLC (2004) "*Development of earthquake ground motion input for preclosure seismic design and postclosure performance assessment of a geologic repository at Yucca Mountain, NV*" Final Report to U.S. Department of Energy, Contract Number DE-AC28-01RW12101.
- Beresnev, I.A. and G. M. Atkinson (2002). "Source parameters of earthquakes in Eastern and Western North America." *Bull. Seism. Soc. Am.*, 92(2), 695-710.
- Beresnev, I.A. and G. M. Atkinson (1997). "Modeling finite-fault radiation from the ω " spectrum." *Bull. Seism. Soc. Am.*, 87(1), 67-84.
- Boore, D.M. (1986). "Short-period P- and S-wave radiation from large earthquakes: implications for spectral scaling relations." *Bull. Seism. Soc. Am.*, 76(1) 43-64.
- Boore, D.M. (1983). "Stochastic simulation of high-frequency ground motions based on seismological models of the radiated spectra." *Bull. Seism. Soc. Am.*, 73(6), 1865-1894.
- Brune, J.N. (1971). "Correction." *J. Geophys. Res.* 76, 5002.
- Brune, J.N. (1970). "Tectonic stress and the spectra of seismic shear waves from earthquakes." *J. Geophys. Res.* 75, 4997-5009.
- Dobry, R., R. S. Ladd, F. Y. Yokel, R. M. Chung and D. Powell (1982). "Prediction of pore water pressure buildup and liquefaction of sands during earthquakes by the cyclic strain method." *NBS Building Science Series 138*, National Bureau of Standards.
- Dobry, R., K.H. Stokoe II, R.S. Ladd, and T. L. Youd (1981). "Liquefaction susceptibility from S-wave velocity." In situ testing to evaluate liquefaction susceptibility. New York: ASCE, Geotechnical Engineering Division, St. Louis, MO (pre-print 81-544), 1-15.

Appendix

- Electric Power Research Institute (1993). "Guidelines for determining design basis ground motions," Palo Alto, Calif: Electric Power Research Institute, vol. 1-5, EPRI TR-102293.
- Hartzell, S., S. Harmsen, A. Frankel, and S. Larsen (1999). "Calculation of broadband time histories of ground motion: Comparison of methods and validation using strong-ground motion." *Bull. Seism. Soc. Am.*, 89(6), 1484-1504.
- Hartzell, S. H. (1992). "Site response estimation from earthquake data," *Bull. Seism. Soc. Am.*, 82(6), 2308-2327.
- Hartzell, S.H. (1978). "Earthquake aftershocks as Green's functions." *Geophys. Res. Letters*, 5, 1-4.
- Hough, S.E., J.G. Armbruster, L. Seeber, and J.F. Hough (2000). "On the Modified Mercalli intensities and magnitudes of the 1811-12 New Madrid earthquakes." *J. Geophys. Res.*, 105(B10), 23,839-23,864.
- Irikura, K. (1983). "Semi-empirical estimation of strong ground motions during large earthquakes." *Bull. Disaster Prevention Res. Inst.*, Kyoto Univ., 33, 63-104.
- Johnston, A.C., 1996. Seismic moment assessment of earthquakes in stable continental regions -III. New Madrid 1811-1812, Charleston 1886 and Lisbon 1755. *Geophys. J. International*, 126: 314-344.
- Johnston, A.C., and Schweig, E.S., 1996. The enigma of the New Madrid earthquakes of 1811-1812. *An. Rev. Earth Planet. Sci.*, 24: 339-384.
- Juang, C.H., Andrus, R.D., Jiang, T., and Chen, C.J., 2001, Probability-based liquefaction evaluation using shear wave velocity measurements, Proceedings, 4th International Conference on Recent Advances in Geotechnical Earthquake Engineering and Soil Dynamics, S. Prakash, (ed.), held 26-31 March 2001, San Diego, Calif. University of Missouri at Rolla, Paper 4.25.
- Kayen, R.E. and J.K. Mitchell (1997). "Assessment of liquefaction potential during earthquakes by Arias intensity," *J. Geot. And Geoenvironmental Engineering*.
- Liao, S.S.C., D. Veneziano, and R.V. Whitman (1988). "Regression Models for Evaluating Liquefaction Probability," *Journal of Geotechnical Engineering*, v. 114, no. 4, p.389-411.
- Noble, S. K. (1998). Probabilistic Evaluation of Soil Liquefaction Resistance, Technical Report CEG-98-02, Brigham Young University, Department of Civil and Environmental Engineering, Thesis Advisor: T.L. Youd.
- Ostadan, F., N. Deng and I. Arango (1996). "Energy Based Method for Liquefaction Potential Evaluation, Phase I- Feasibility Study." *NIST Report No. GCR 96-701*, Bechtel Corporation for NIST.

Appendix

- Ou, G.B., and Herrmann, R.B. (1990). "A statistical model for ground motion produced by earthquakes at local and regional distances." *Bull. Seism. Soc. Am.*, 80, 1397-1417.
- Schneider, J.F., W.J. Silva, and C.L. Stark (1993). Ground motion model for the 1989 M 6.9 Loma Prieta earthquake including effects of source, path and site. *Earthquake Spectra*, 9(2), 251-287.
- Seed, H. B. and I. M. Idriss (1971). "Simplified Procedure for Evaluating Soil Liquefaction Potential," *J. Soil Mechanics and Foundation Division, ASCE*, 97(9).
- Silva, W.J. and Costantino, C. (1999). "Assessment of liquefaction potential for the 1995 Kobe, Japan earthquake including finite-source effects." Prepared for U.S Army Engineer Waterways Experiment Station, Corps of Engineers Contract #DACW39-97-K-0015.
- Silva, W.J., N. Abrahamson, G. Toro, C. Costantino (1997). "Description and validation of the stochastic ground motion model." Submitted to Brookhaven National Laboratory, Associated Universities, Inc. Upton, New York.
- Silva, W.J. and C.L. Stark (1992). Near-field and in-structure monitorings of the aftershocks for the Loma Prieta. Palo Alto, Calif.: Electric Power Research Institute, Draft Final Report No. RP 3181-03.
- Silva, W.J., and Darragh, R.B., Stark, C., Wong, I., Stepp, J.C., Schneider, J., and Chiou, S.J. (1990). "A methodology to estimate design response spectra in the near-source region of large earthquakes using the Band-Limited-White-Noise Ground Motion Model". Fourth U.S. Nat'l Confer. Earthq. Engin., Palm Springs, California. EERI: 1:487-494.
- Vick, S.G. (1993). "*Design and Evaluation of Tailings Dams*". John Wiley & Sons, New York, 369p, ISBN 0-471-89829-5.
- Wells, D.L., Coppersmith, K.J. (1994). "New empirical relationships among magnitude, rupture length, rupture width, rupture area, and surface displacement." *Bull. Seism. Soc. Am.* 84(4), 974-1002.
- Youd, T.L., and S.K. Noble (1997). "Liquefaction Criteria Based on Statistical and Probabilistic Analyses," in Youd and Idriss, editors, *Proc. NCEER Workshop on Evaluation of Liquefaction Resistance of Soils*, National Center for Earthquake Engineering Research.
- Youd, T.L., Idriss, I.M., Andrus, R.D., Arango, I., Castro, G., Christian, J.T., Dobry, R., Finn, W.D.L., Harder, L.F., Jr., Hynes, M.E., Ishihara, K., Koester, J.P., Liao, S.S.C., Marcuson, W.F., III, Martin, G.R., Mitchell, J.K., Moriwaki, Y., Power, M.S., Robertson, P.K., Seed, R.B., Stokoe, K.H., II. (2001) Liquefaction resistance of soils: Summary report from the 1996 NCEER and 1998 NCEER/NSF workshop on evaluation of liquefaction resistance of soils, *Journal of Geotechnical and Geoenvironmental Engineering*, 127(10), 817-833.

Appendix

| Table A1 | | | |
|--|---------------------------|---|--------------|
| Parameters Varied | | | |
| Parameter | Median Value | Sigma | Distribution |
| 1. Kappa | 0.04 sec | 0.4 ¹ | Lognormal |
| 2. Q ₀ | 176 | 0.6 ¹ | Normal |
| 3. Profile | Base Case Profile | 0.3 | Lognormal |
| 4. Profile Depth | 350 ft | + 50 ft | Uniform |
| 5. G/G _{max} and hysteretic Damping | Depth Dependent | 0.3 ¹ at strain 3 x 10 ⁻² % | Lognormal |
| 6. Nucleation Point | Center of Nucleation Zone | Nucleation Zone ² | Uniform |
| 7. Slip Model | Wavenumber Spectrum | Random Phase | Normal |

¹ EPRI, 1997

² Nucleation Zone: Bottom half of rupture width and along strike to within 10% of rupture length of rupture ends.

Appendix

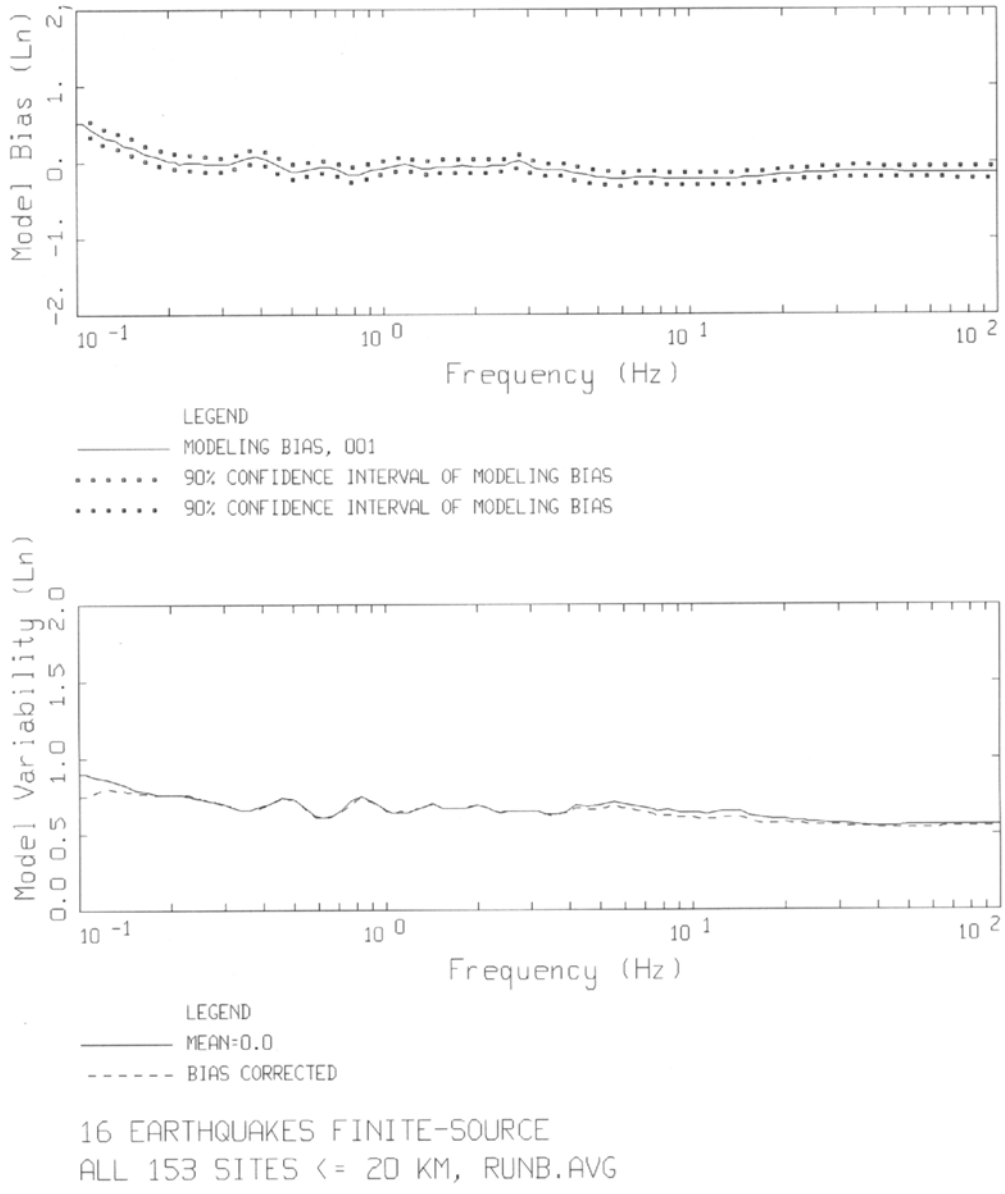


Figure A1. Validation of the stochastic finite source model for 5% damped response spectra for sites located within 20 km rupture distance.

Appendix

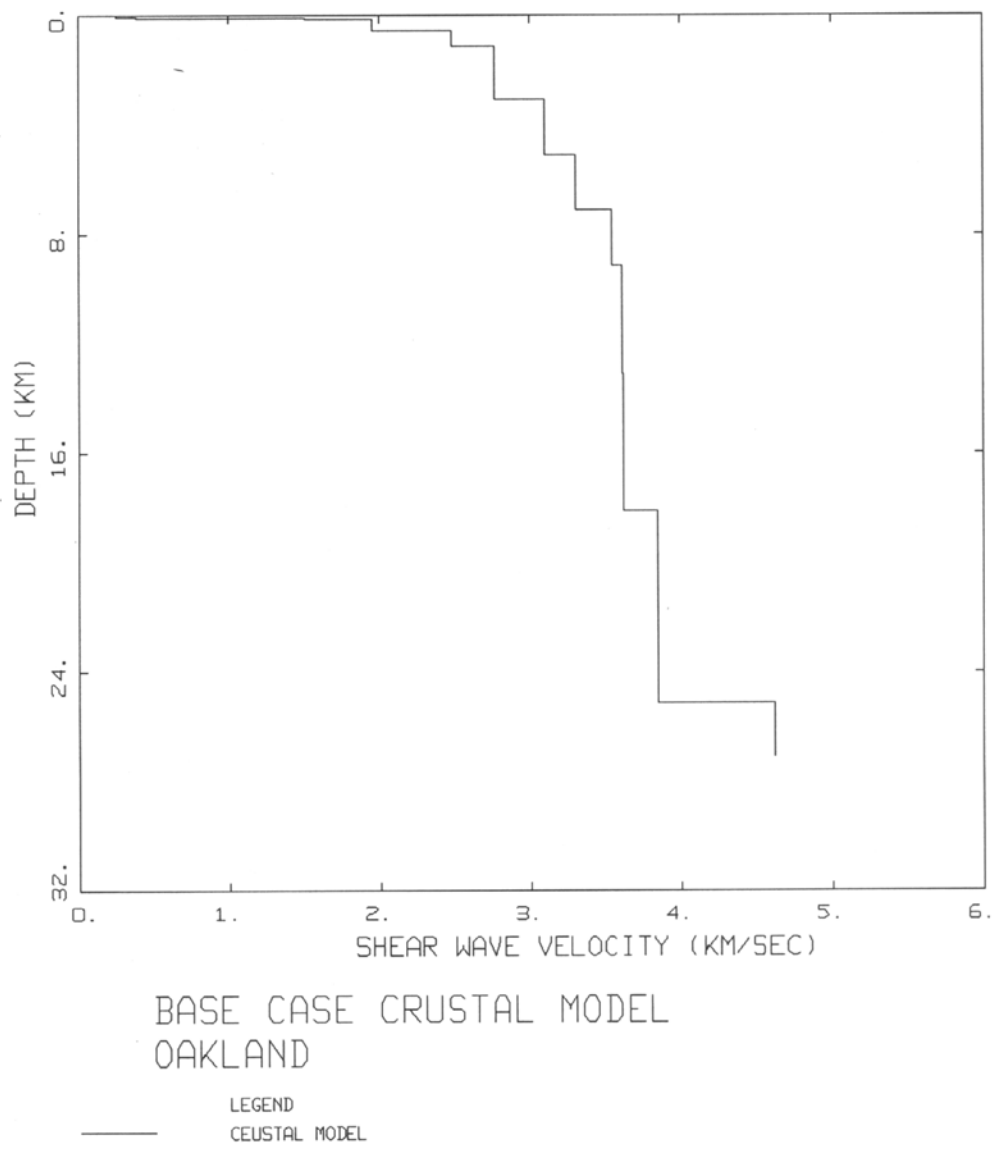


Figure A2. Deep crustal model used in simulations. Shallow site profile (Figure A2) was simply merged into Wald et al. (1991) Loma Prieta crustal model.

Appendix

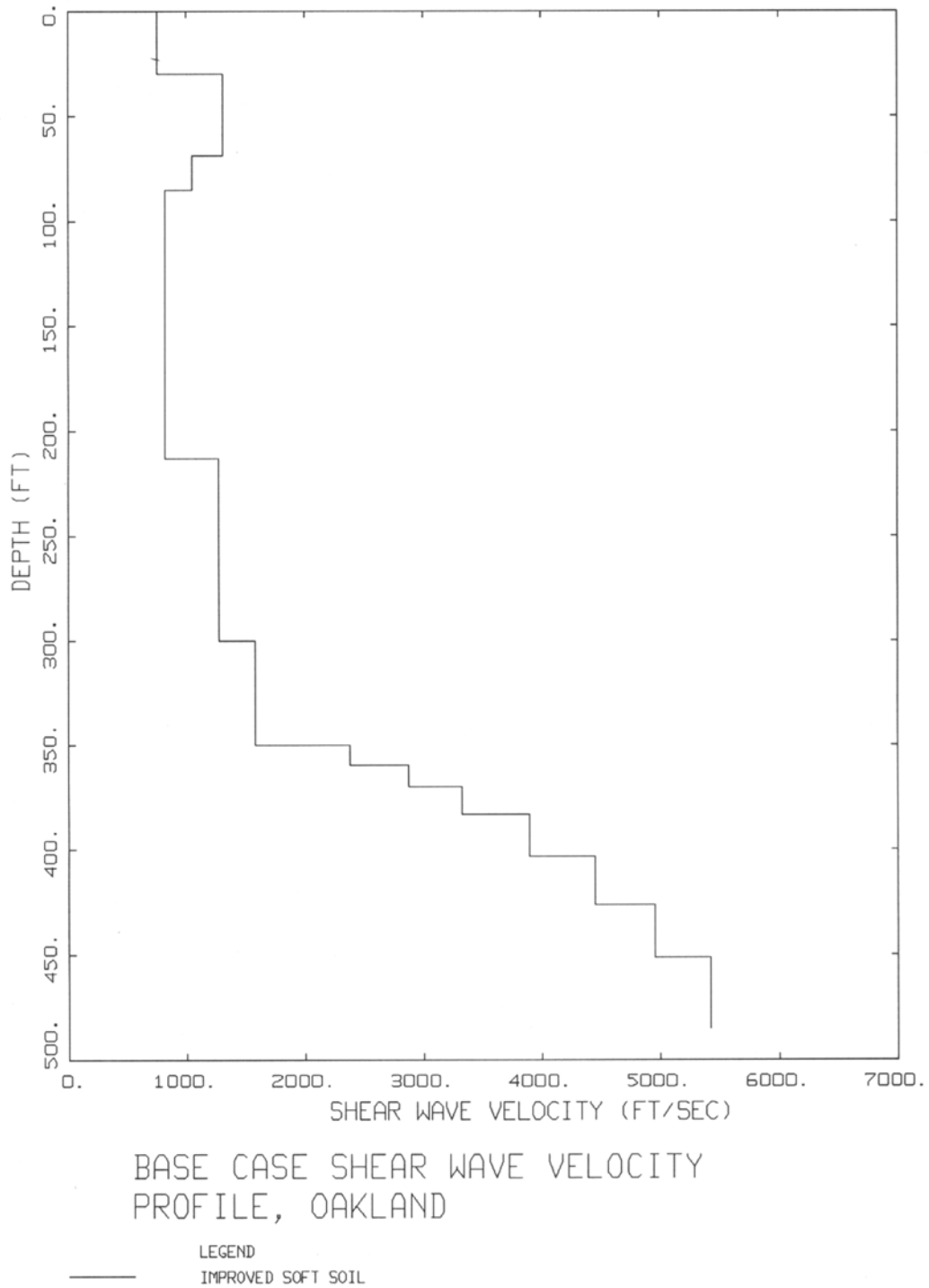
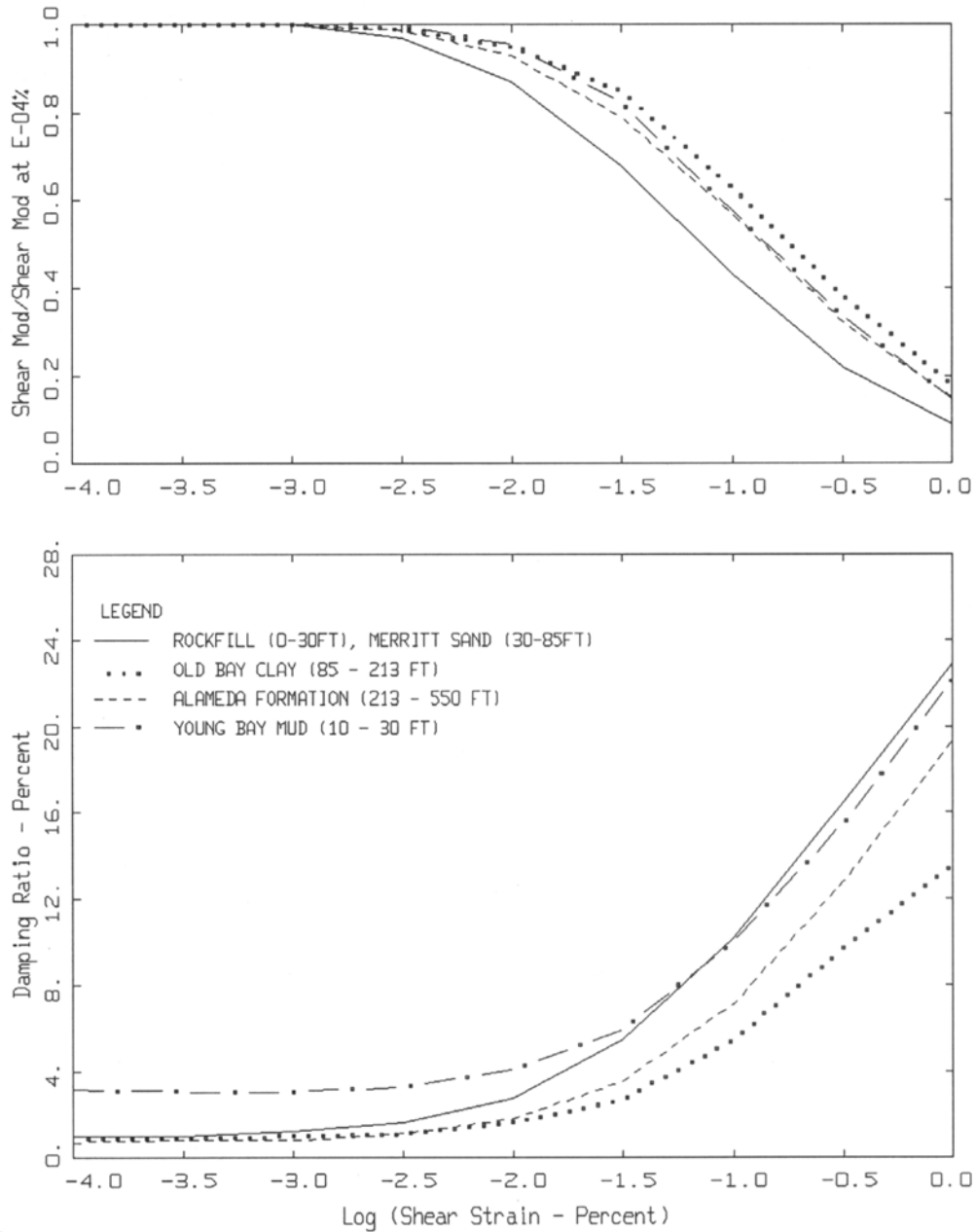


Figure A3. Base case shear-wave velocity profile based on a soft Bay mud (Port of Oakland) profile, improved in the top 30 ft by rock fill.

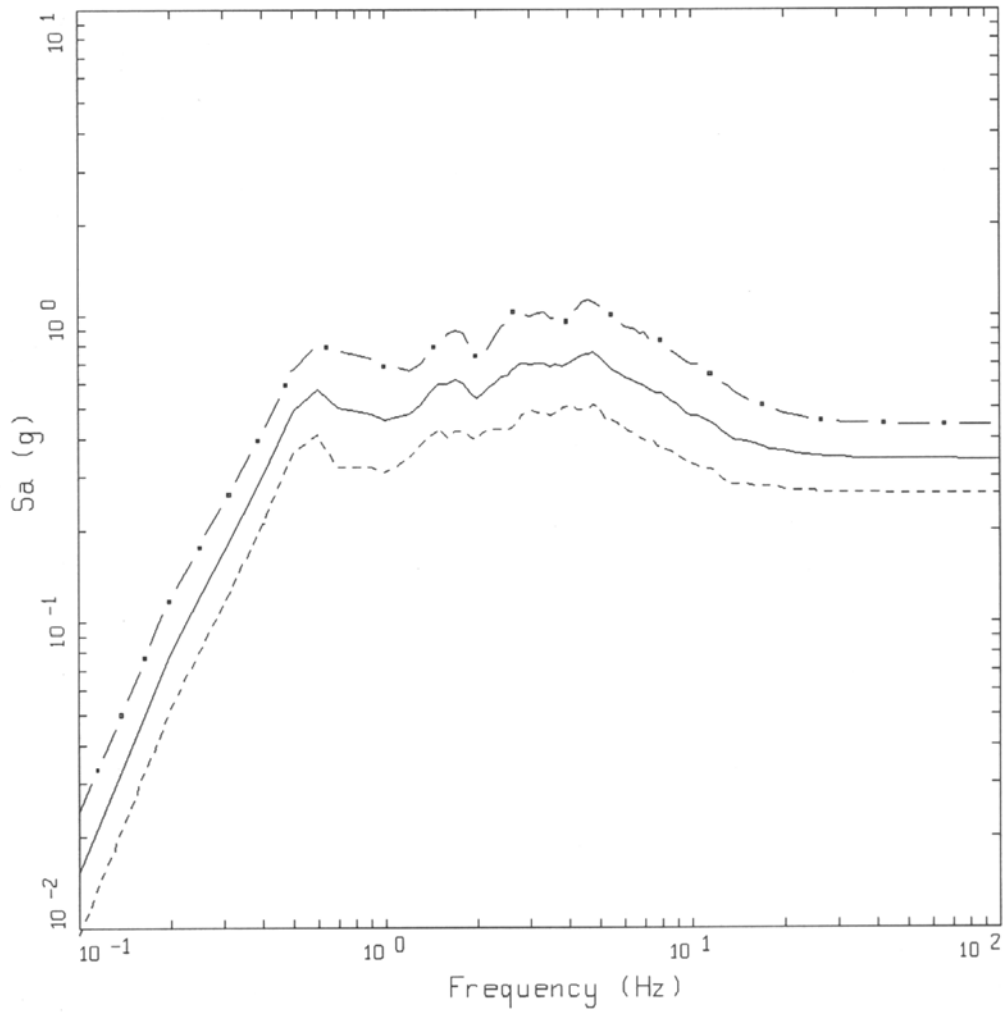
Appendix



MODULUS REDUCTION AND DAMPING CURVES FOR IMPROVED SOFT SOIL

Figure A4. G/G_{max} and hysteretic damping curves for the improved Bay mud profile. Young Bay mud curves were replaced with the rock fill curves and are shown for reference only.

Appendix



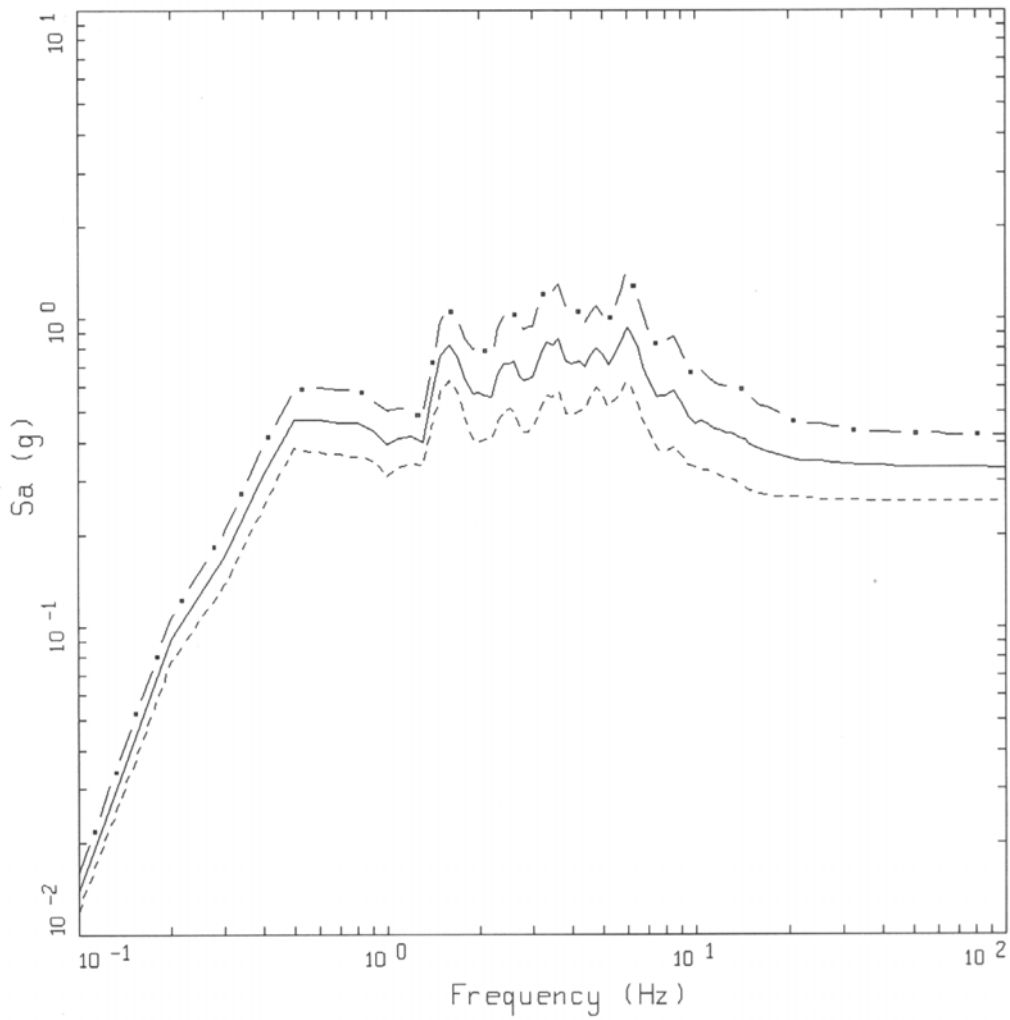
HAYWARD, M = 7.1, D = 5 KM
SOFT SOIL, VARIATION OF ALL PARAMETERS

LEGEND

- . - 84TH PERCENTILE, PGA = 0.440 G
- 50TH PERCENTILE, PGA = 0.340 G
- - - 16TH PERCENTILE, PGA = 0.263 G

Figure A5. Median and $\pm 1\sigma$ response spectra (5% damped) for variation of source, path, and site parameters.

Appendix



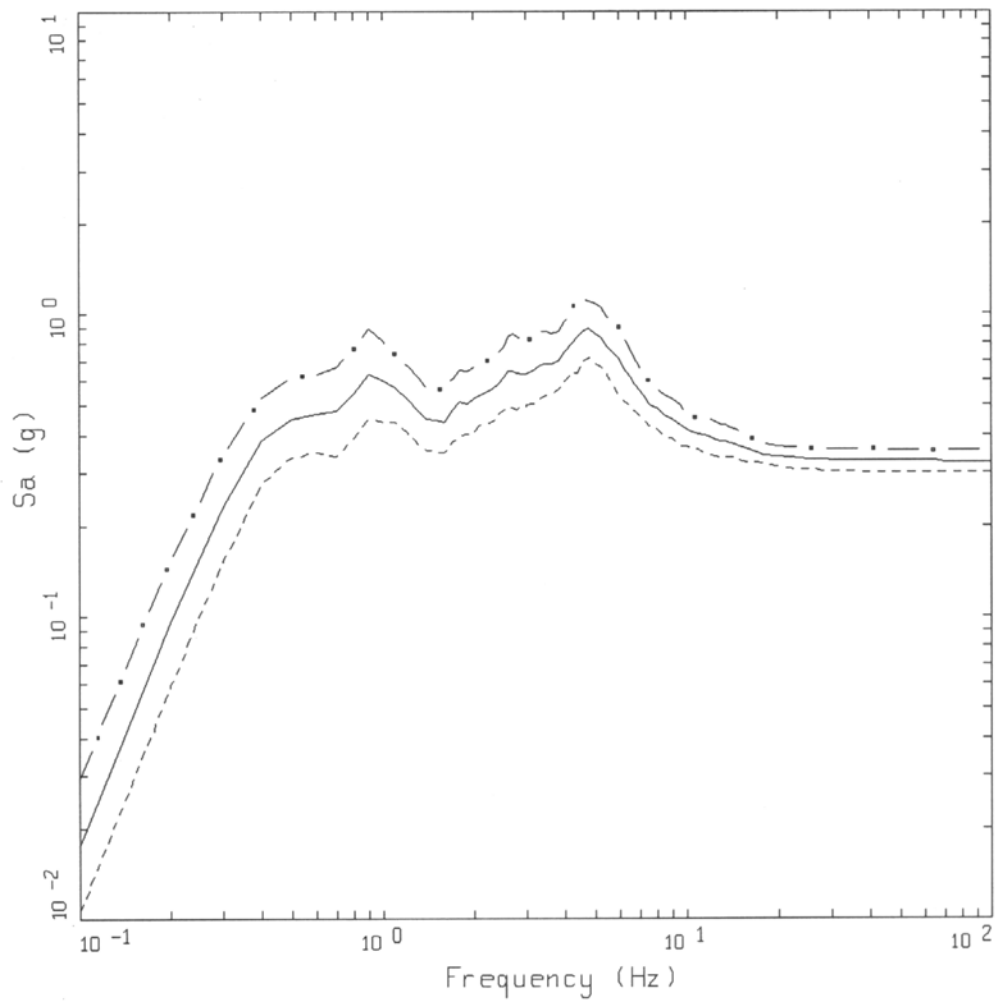
HAYWARD, M = 7.1, D = 5 KM
SOFT SOIL, VARIATION OF SITE PARAMETERS

LEGEND

- • — 84TH PERCENTILE, PGA = 0.422 G
- — — 50TH PERCENTILE, PGA = 0.329 G
- - - - 16TH PERCENTILE, PGA = 0.256 G

Figure A6. Median and $\pm 1\sigma$ response spectra (5% damped) for variation of site parameters.

Appendix

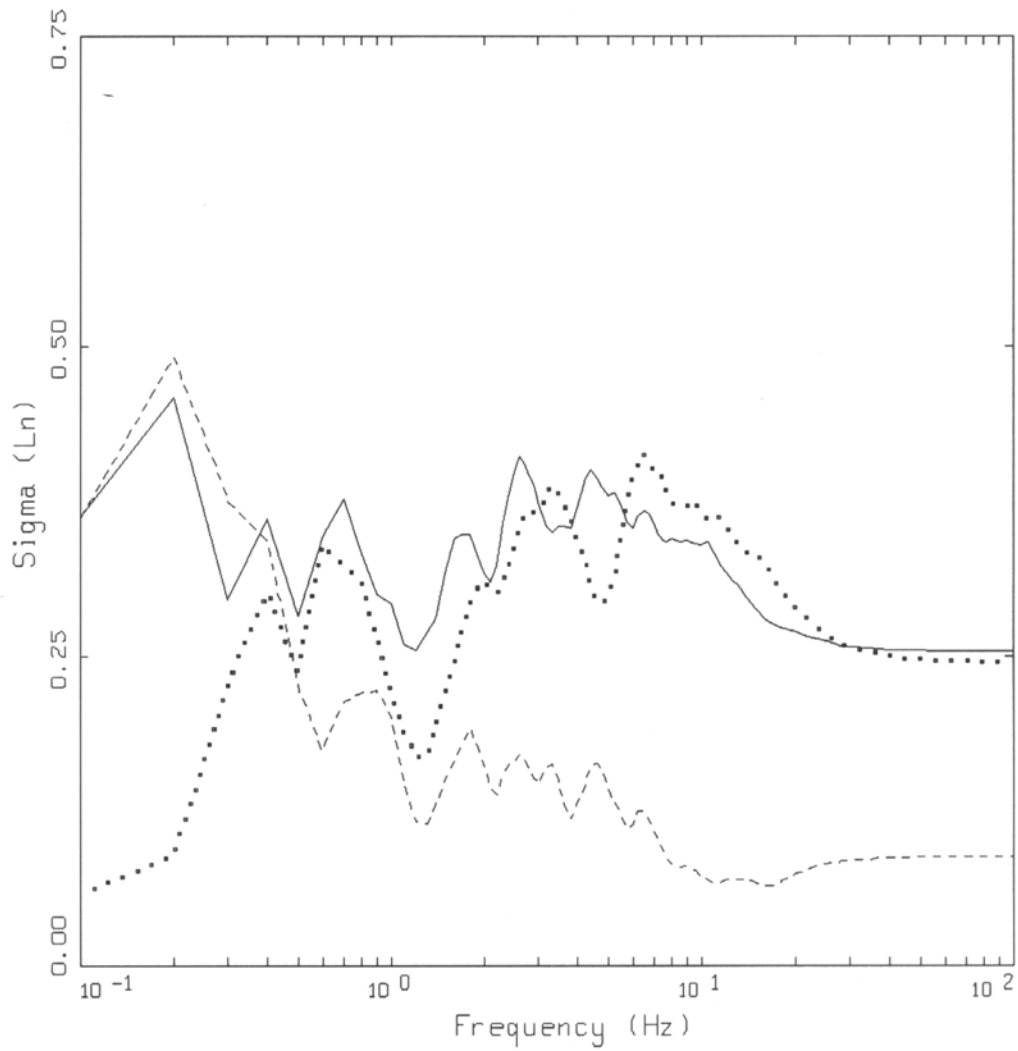


HAYWARD, $M = 7.1$, $D = 5$ KM
SOFT SOIL, VARIATION OF SOURCE PARAMETERS

LEGEND
- · - 84TH PERCENTILE, PGA = 0.355 G
— 50TH PERCENTILE, PGA = 0.325 G
- - - 16TH PERCENTILE, PGA = 0.298 G

Figure A7. Median and $\pm 1\sigma$ response spectra (5% damped) for variation of source parameters.

Appendix



HAYWARD, M 7.1, R = 5 KM
SIGMA(S_a) FROM VARIATION OF PARAMETERS

LEGEND
—— VARIATION OF ALL PARAMETERS
..... VARIATION OF SITE
- - - - VARIATION OF SOURCE

Figure A8. Variability (σ_{ln}) of response spectral estimates for variation of all, site, and path parameters.

Appendix

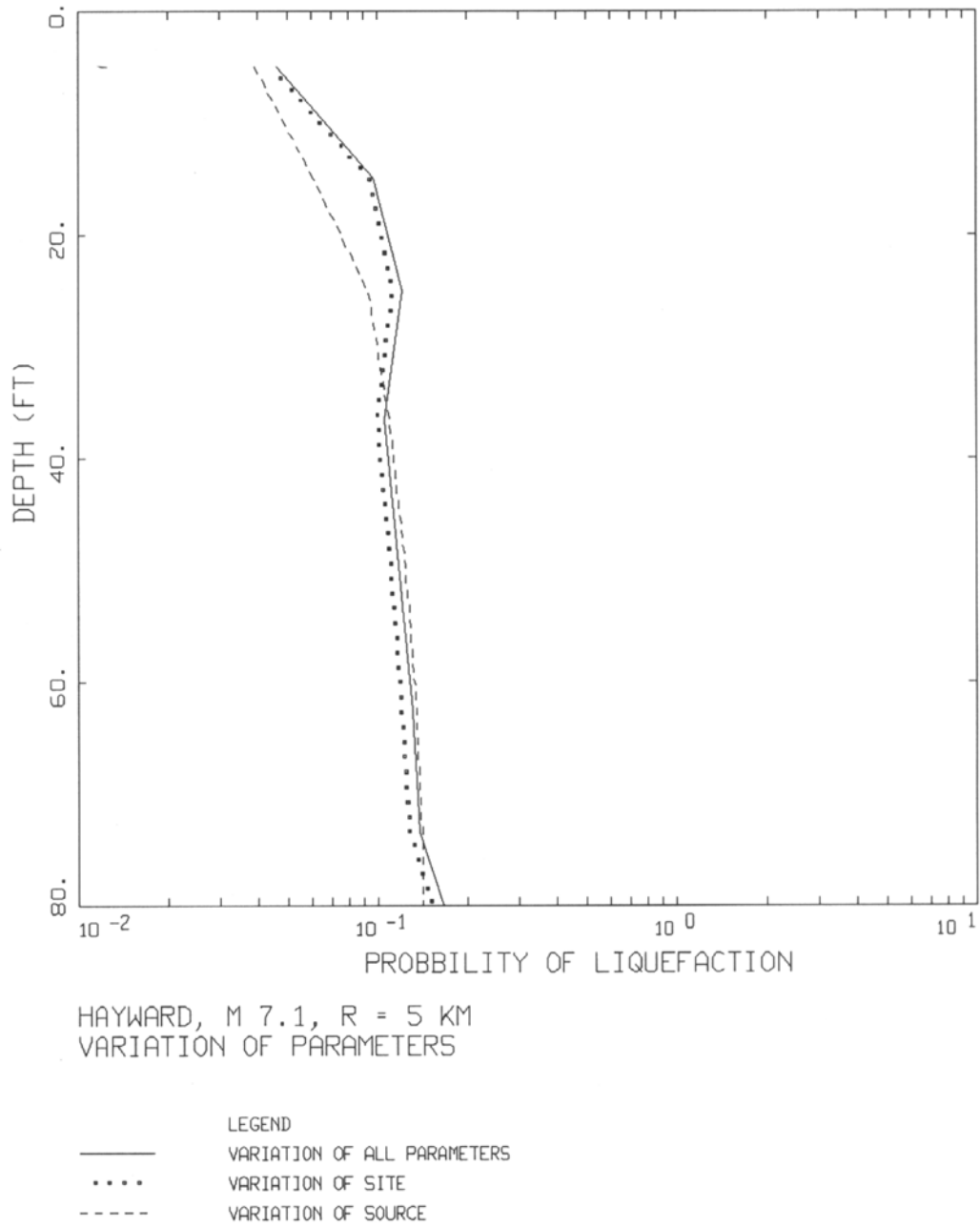
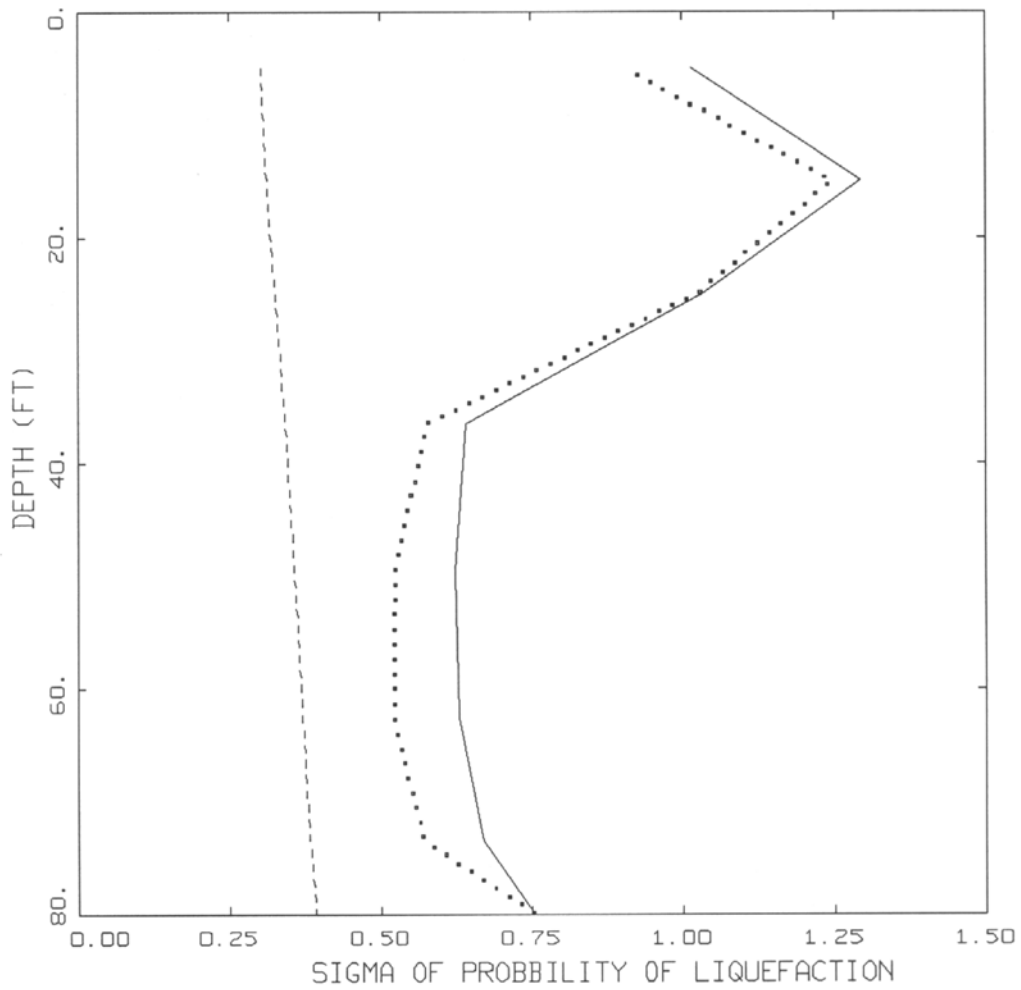


Figure A9. Median estimates of the probability of liquefaction verses depth for variation in all, site, and source parameters.

Appendix



HAYWARD, M 7.1, R = 5 KM
SIGMA(PL) FROM VARIATION OF PARAMETERS

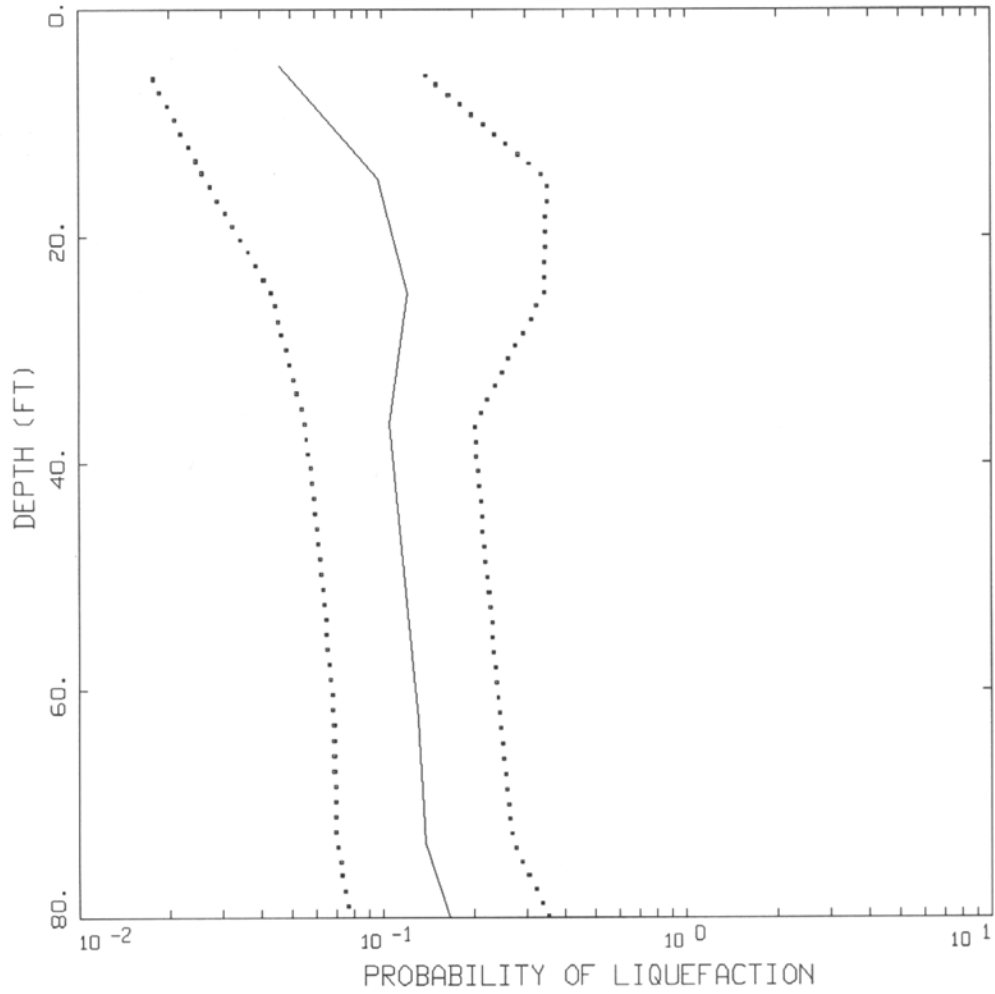
- LEGEND
- VARIATION OF ALL PARAMETERS
 - VARIATION OF SITE
 - VARIATION OF SOURCE

Figure A10. Variability (σ_{ln}) of liquefaction probability verses depth for variation in all, site, and source parameters.

Appendix

Figure Set A11. At-depth estimates of liquefaction probability, factor of safety, cyclic stress ratio, number of cycles, strain energy density, and Arias intensity for a variation of all parameters.

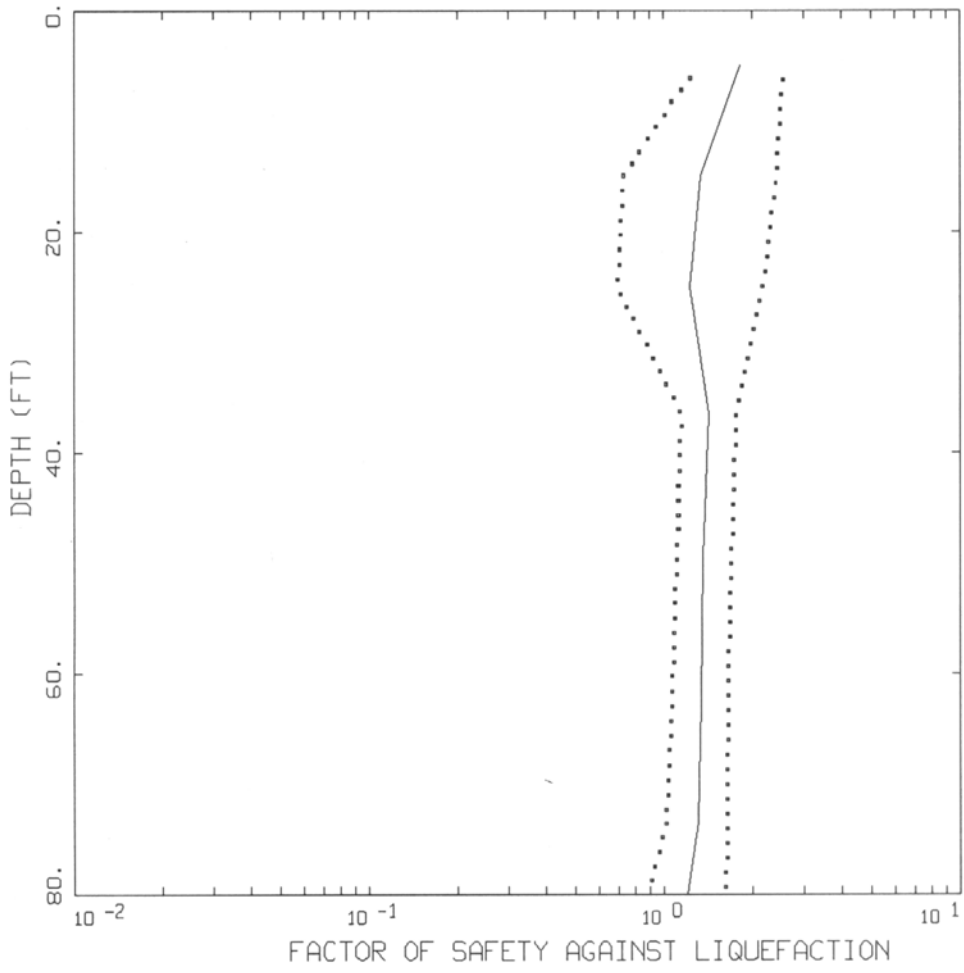
Appendix



HAYWARD, M 7.1, R = 5 KM
VARIATION OF ALL PARAMETERS

- LEGEND
- 84TH PERCENTILE
 - MEDIAN
 - 16TH PERCENTILE

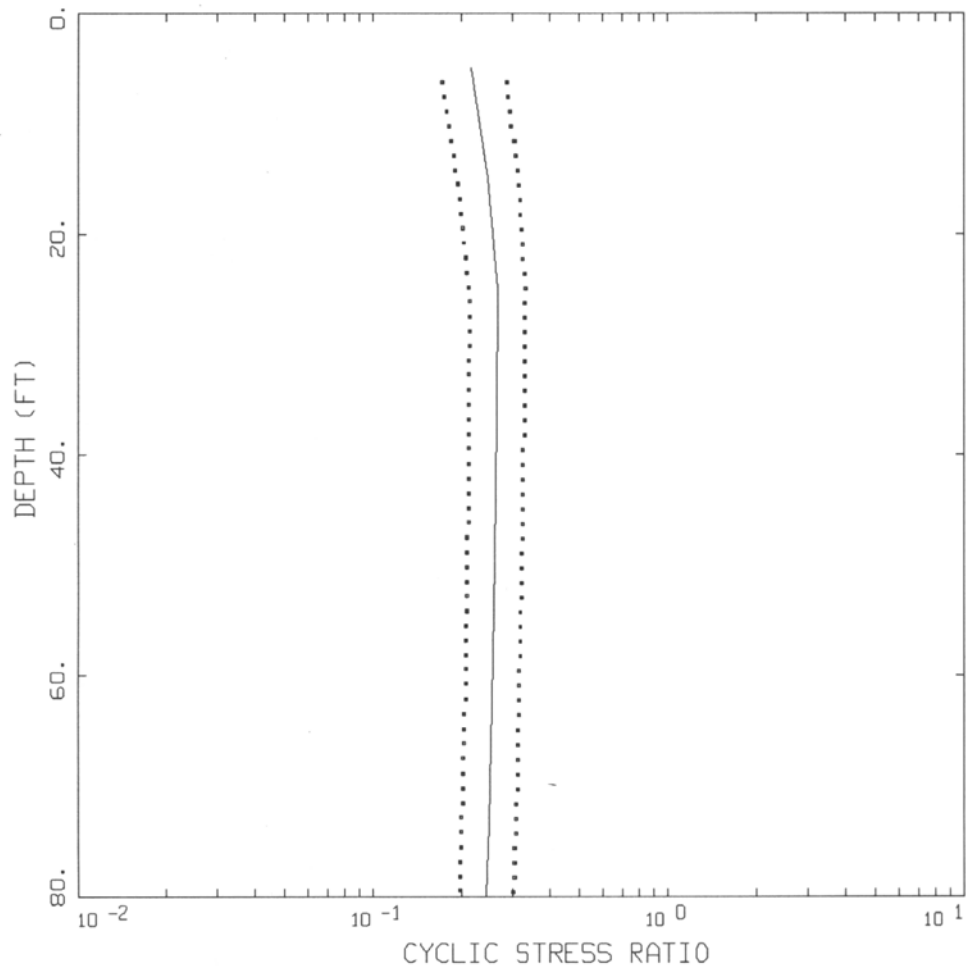
Appendix



HAYWARD, M 7.1, R = 5 KM
VARIATION OF ALL PARAMETERS

- LEGEND
- 84TH PERCENTILE
 - MEDIAN
 - 16TH PERCENTILE

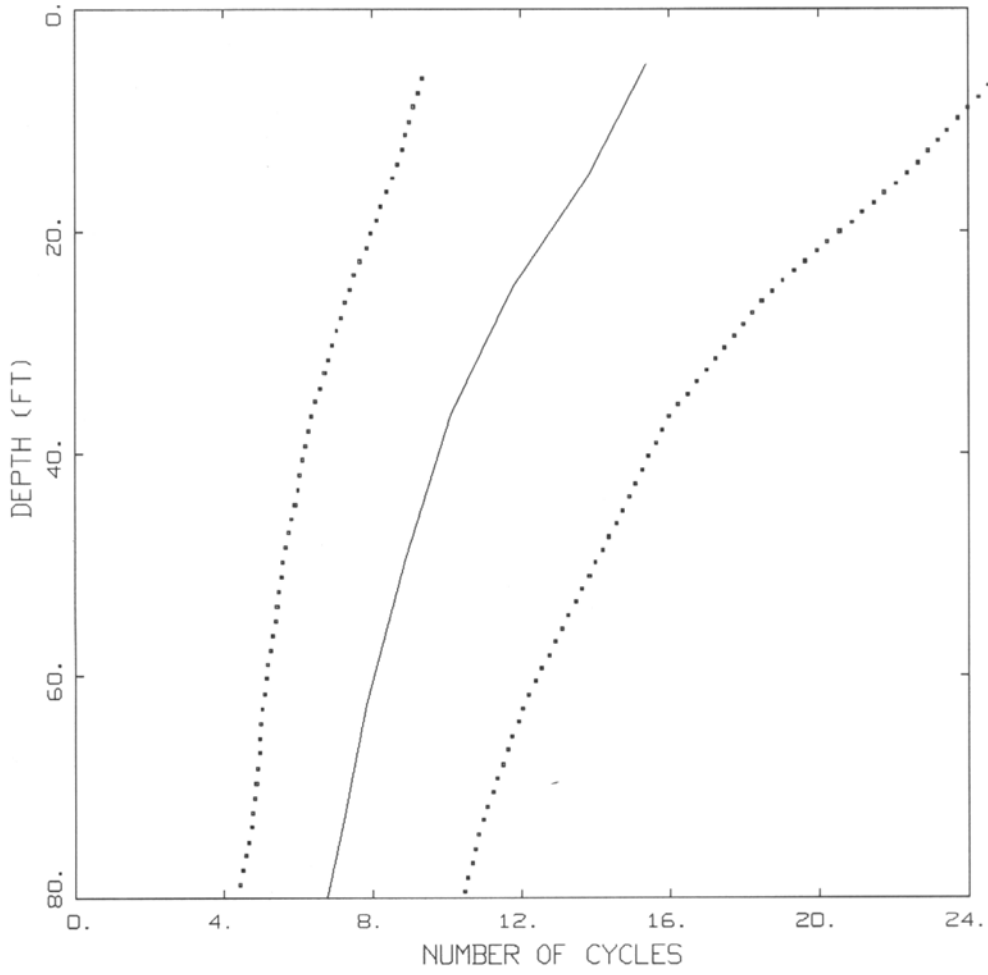
Appendix



HAYWARD, M 7.1, R = 5 KM
VARIATION OF ALL PARAMETERS

- LEGEND
- 84TH PERCENTILE
 - MEDIAN
 - 16TH PERCENTILE

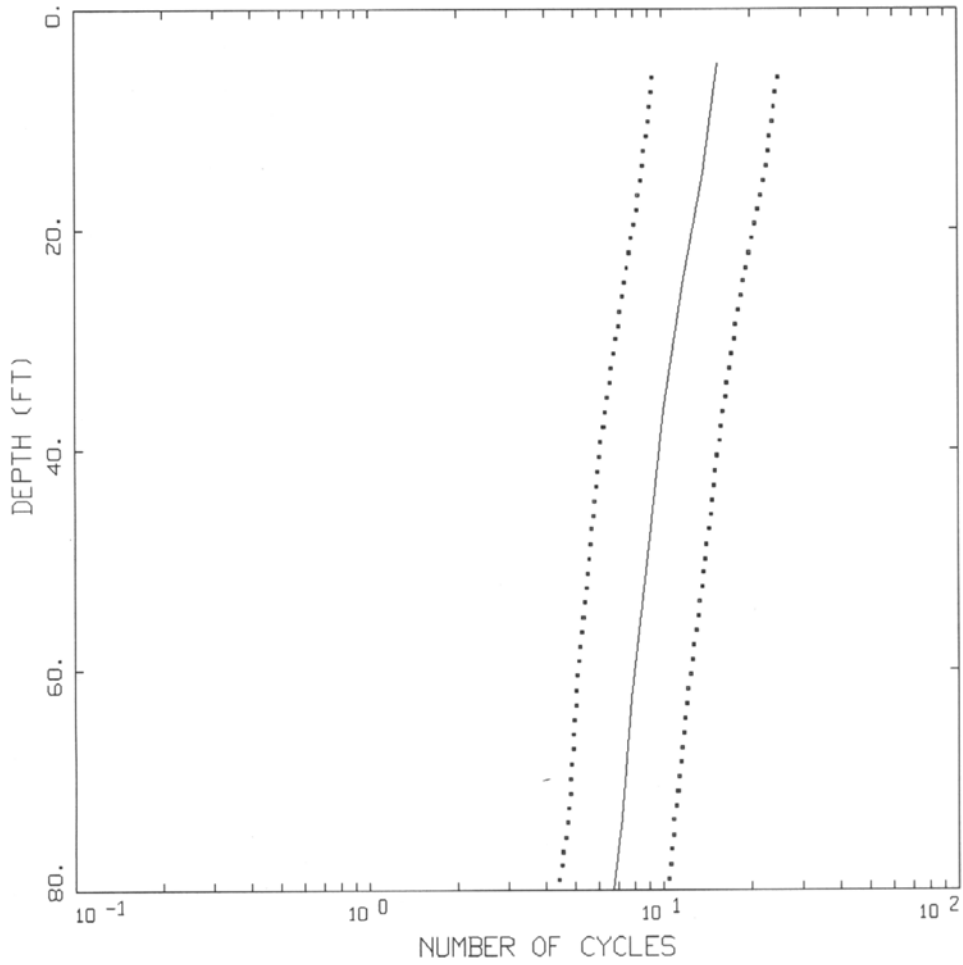
Appendix



HAYWARD, M 7.1, R = 5 KM
VARIATION OF ALL PARAMETERS

LEGEND
..... 84TH PERCENTILE
————— MEDIAN
..... 16TH PERCENTILE

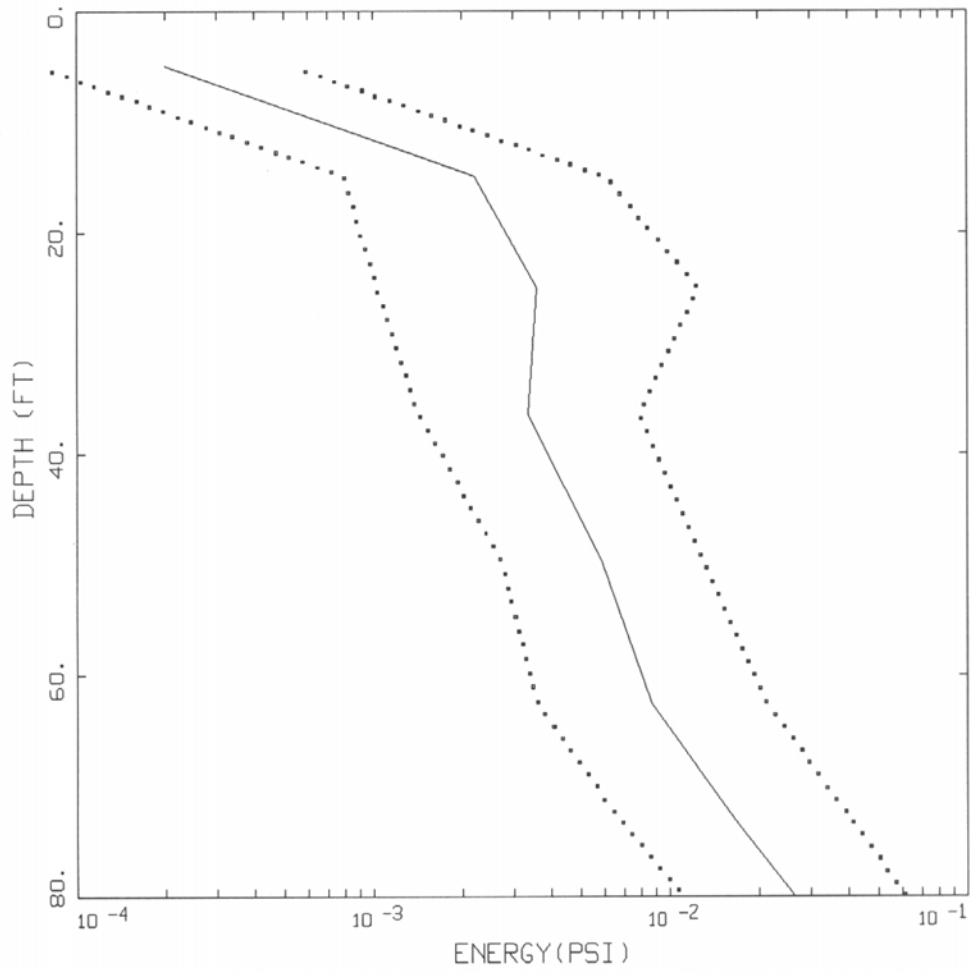
Appendix



HAYWARD, M 7.1, R = 5 KM
VARIATION OF ALL PARAMETERS

..... LEGEND
..... 84TH PERCENTILE
——— MEDIAN
..... 16TH PERCENTILE

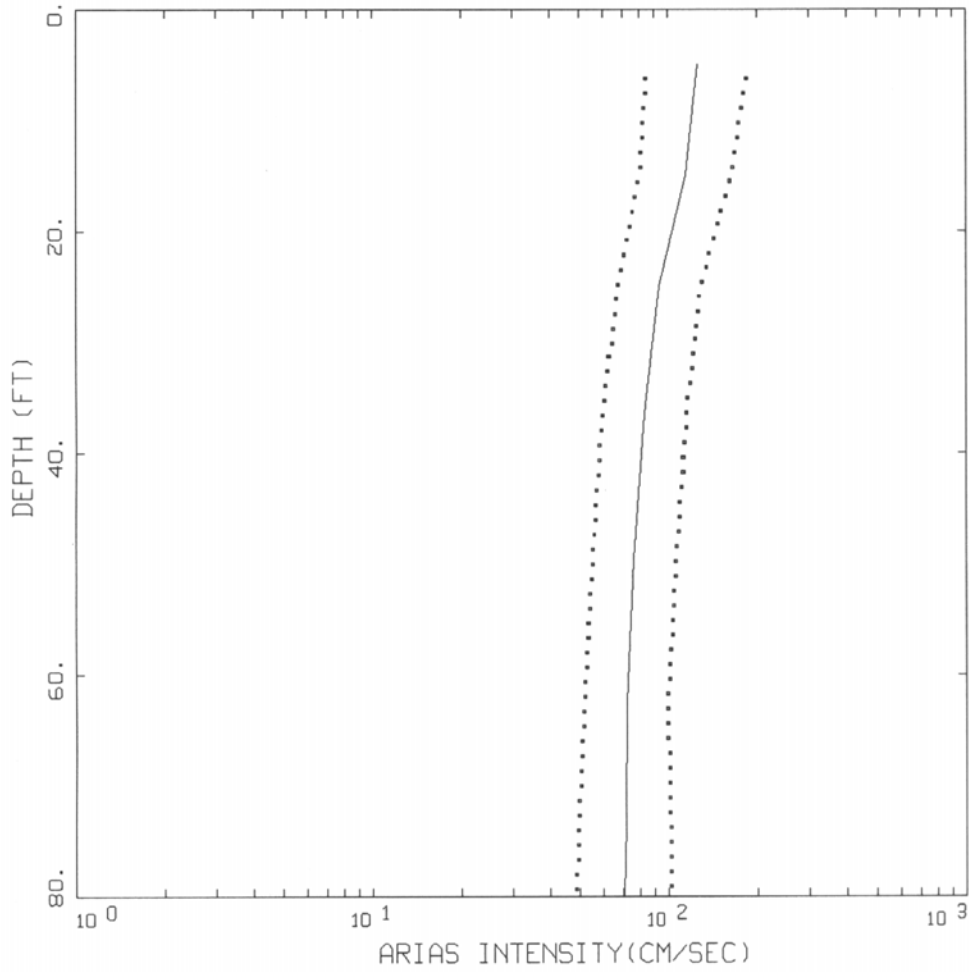
Appendix



- HAYWARD, M 7.1, R = 5 KM
VARIATION OF ALL PARAMETERS

LEGEND
..... 84TH PERCENTILE
———— MEDIAN
..... 16TH PERCENTILE

Appendix



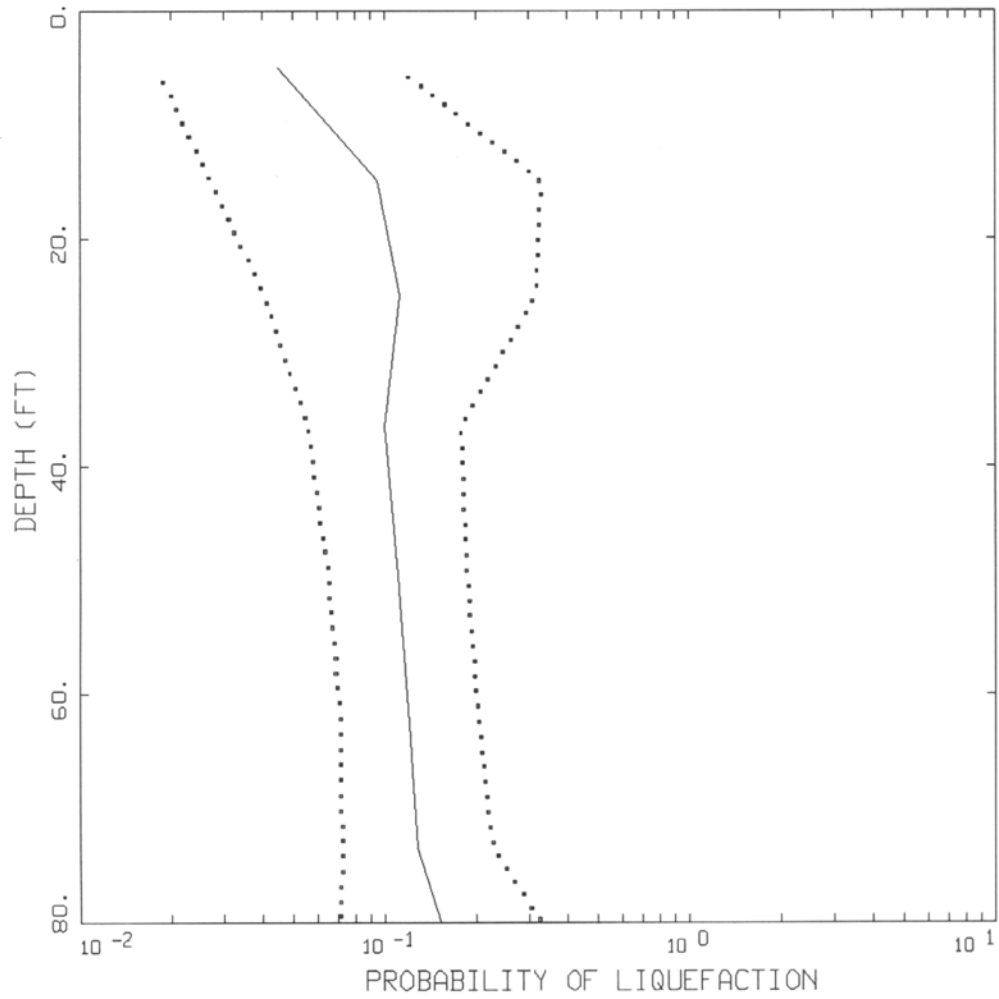
HAYWARD, M 7.1, R = 5 KM
VARIATION OF ALL PARAMETERS

- LEGEND
- 84TH PERCENTILE
 - MEDIAN
 - 16TH PERCENTILE

Appendix

Figure Set A12. At-depth estimates of liquefaction probability, factor of safety, cyclic stress ratio, number of cycles, strain energy density, and Arias intensity for a variation of site parameters.

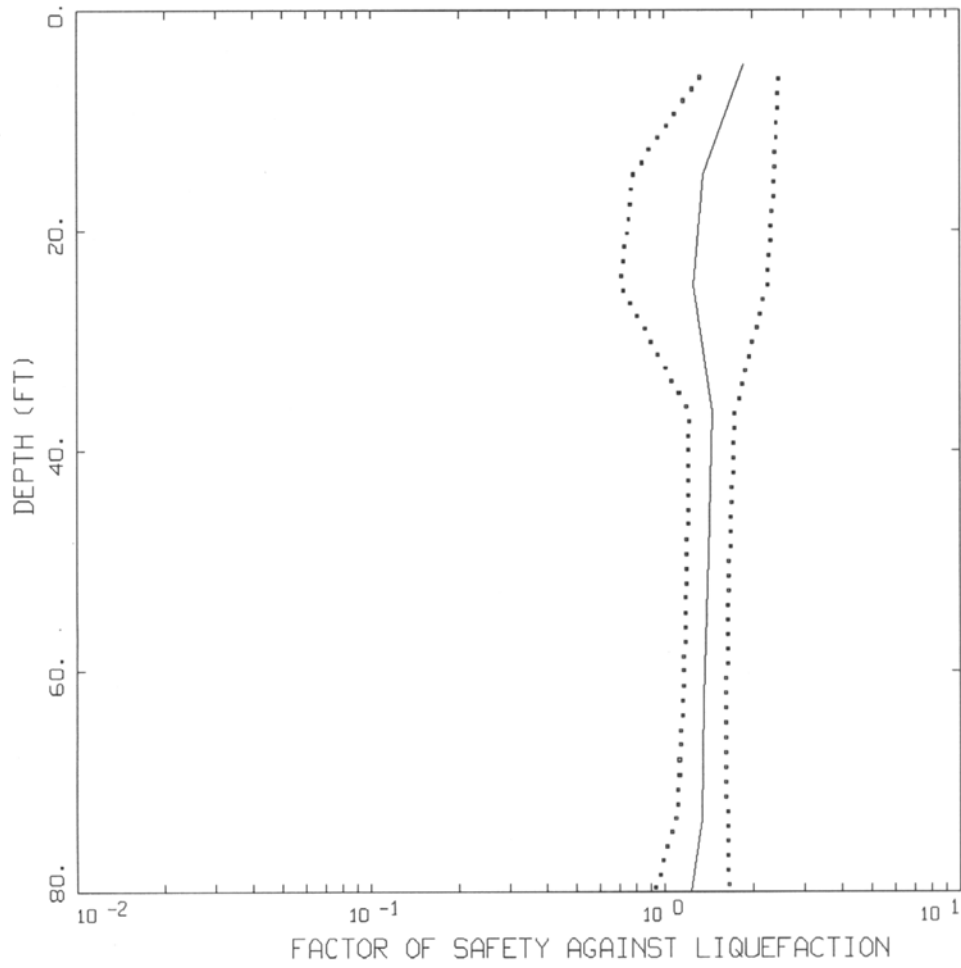
Appendix



HAYWARD, M 7.1, R = 5 KM
VARIATION OF SITE PARAMETERS

- LEGEND
- 84TH PERCENTILE
 - MEDIAN
 - 16TH PERCENTILE

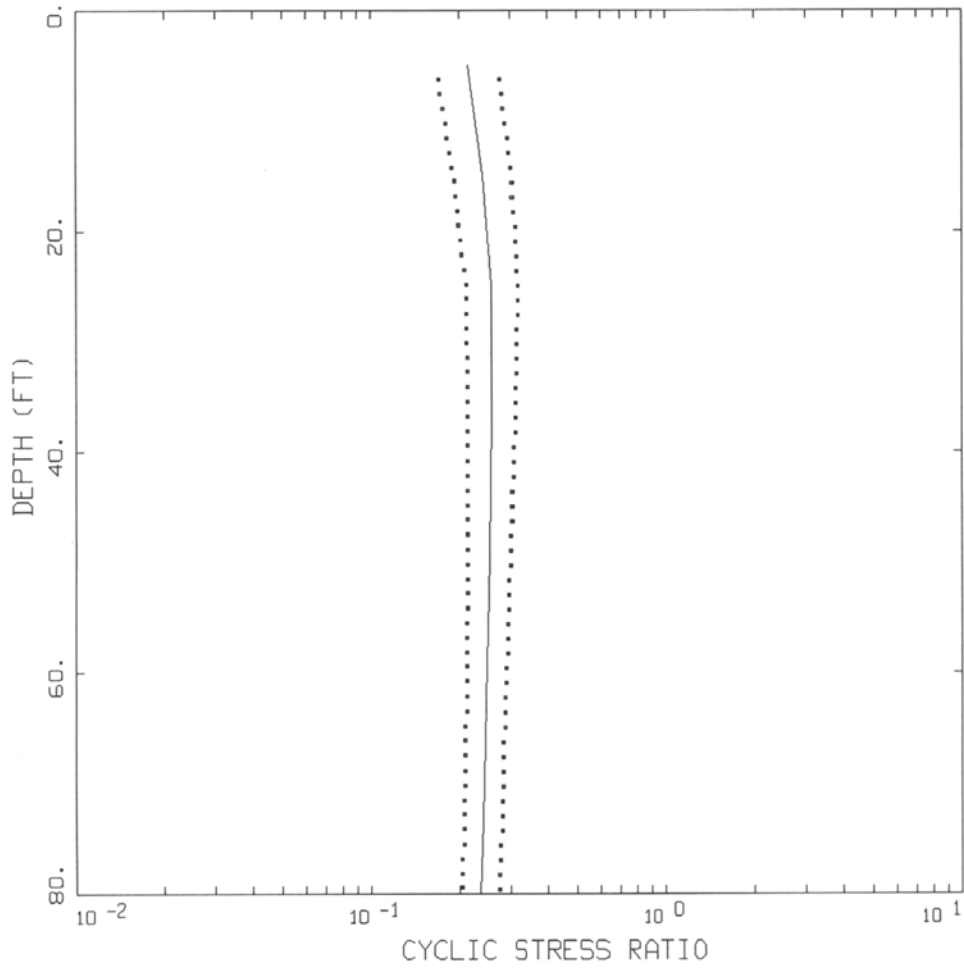
Appendix



HAYWARD, M 7.1, R = 5 KM
VARIATION OF SITE PARAMETERS

- LEGEND
- 84TH PERCENTILE
 - MEDIAN
 - 16TH PERCENTILE

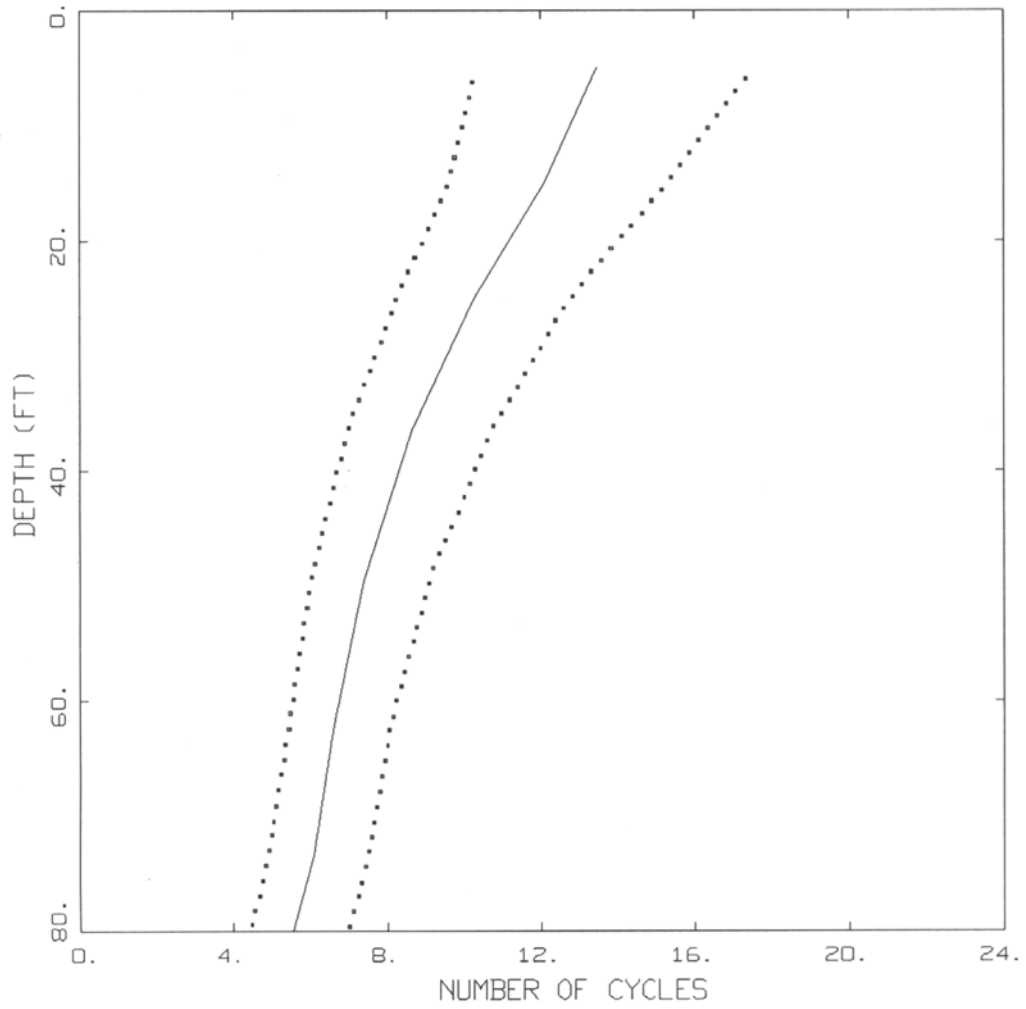
Appendix



HAYWARD, M 7.1, R = 5 KM
VARIATION OF SITE PARAMETERS

LEGEND
..... 84TH PERCENTILE
———— MEDIAN
..... 16TH PERCENTILE

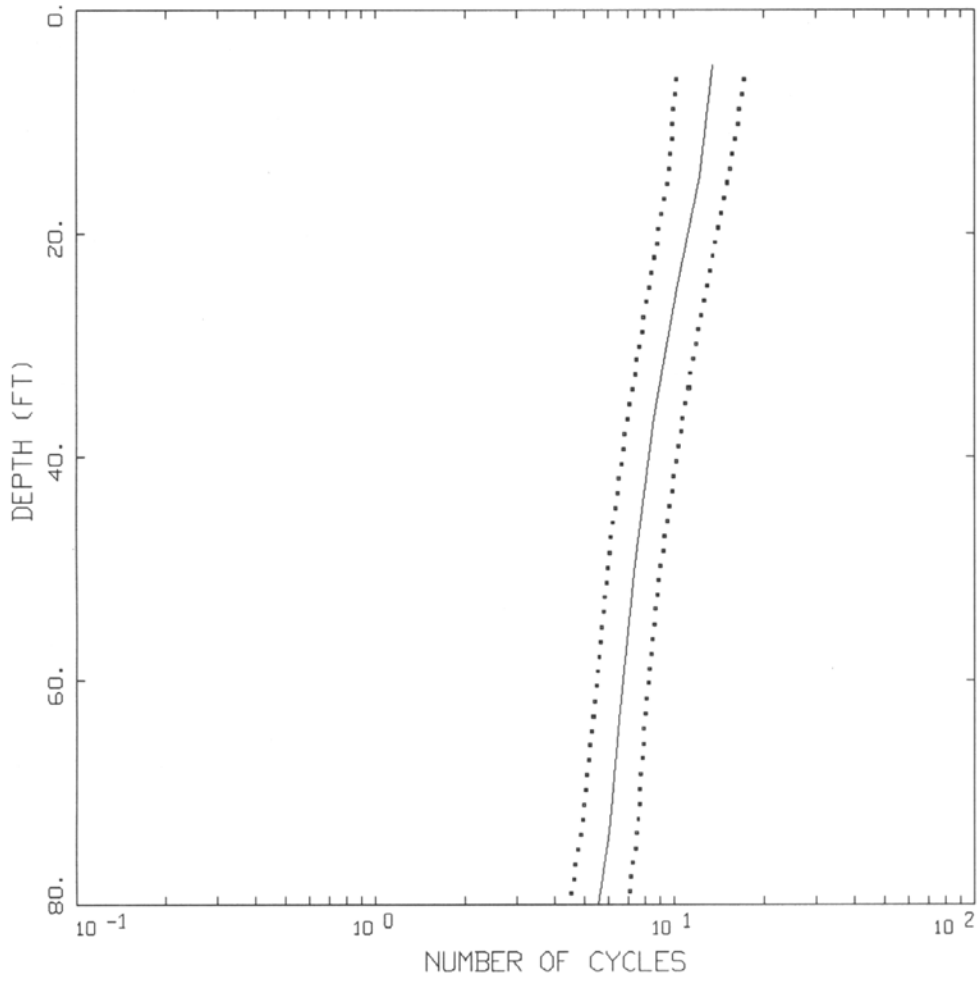
Appendix



HAYWARD, M 7.1, R = 5 KM
VARIATION OF SITE

- LEGEND
- 84TH PERCENTILE
 - MEDIAN
 - 16TH PERCENTILE

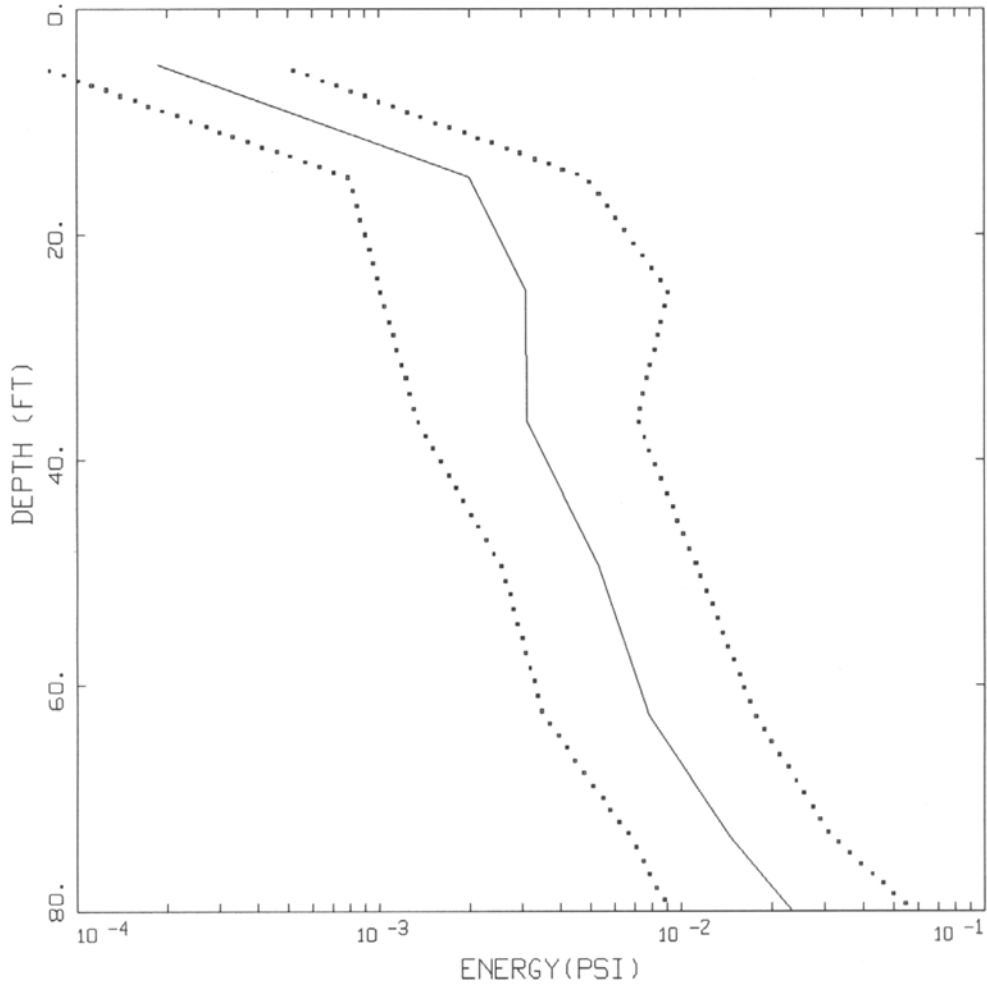
Appendix



HAYWARD, M 7.1, R = 5 KM
VARIATION OF SITE

LEGEND
..... 84TH PERCENTILE
———— MEDIAN
..... 16TH PERCENTILE

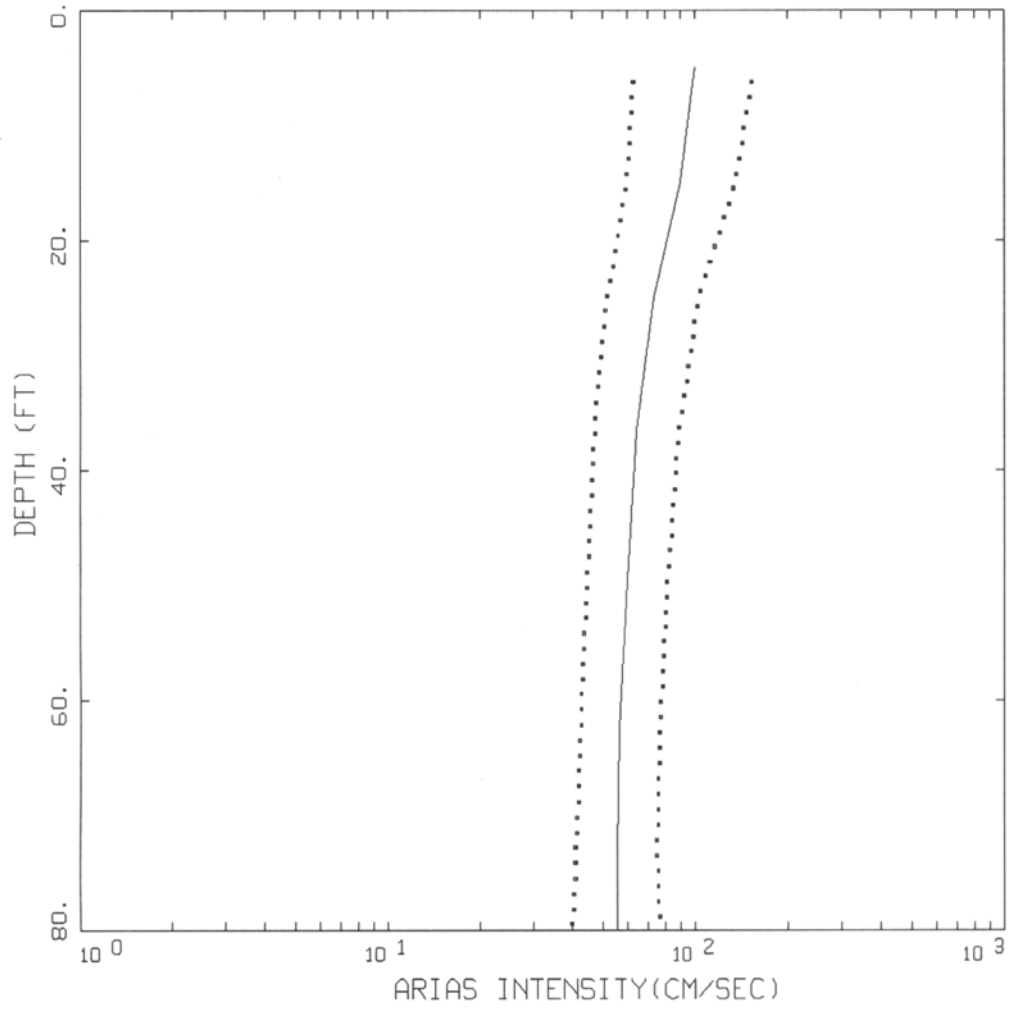
Appendix



HAYWARD, M 7.1, R = 5 KM
VARIATION OF SITE PARAMETERS

- LEGEND
- 84TH PERCENTILE
 - MEDIAN
 - 16TH PERCENTILE

Appendix



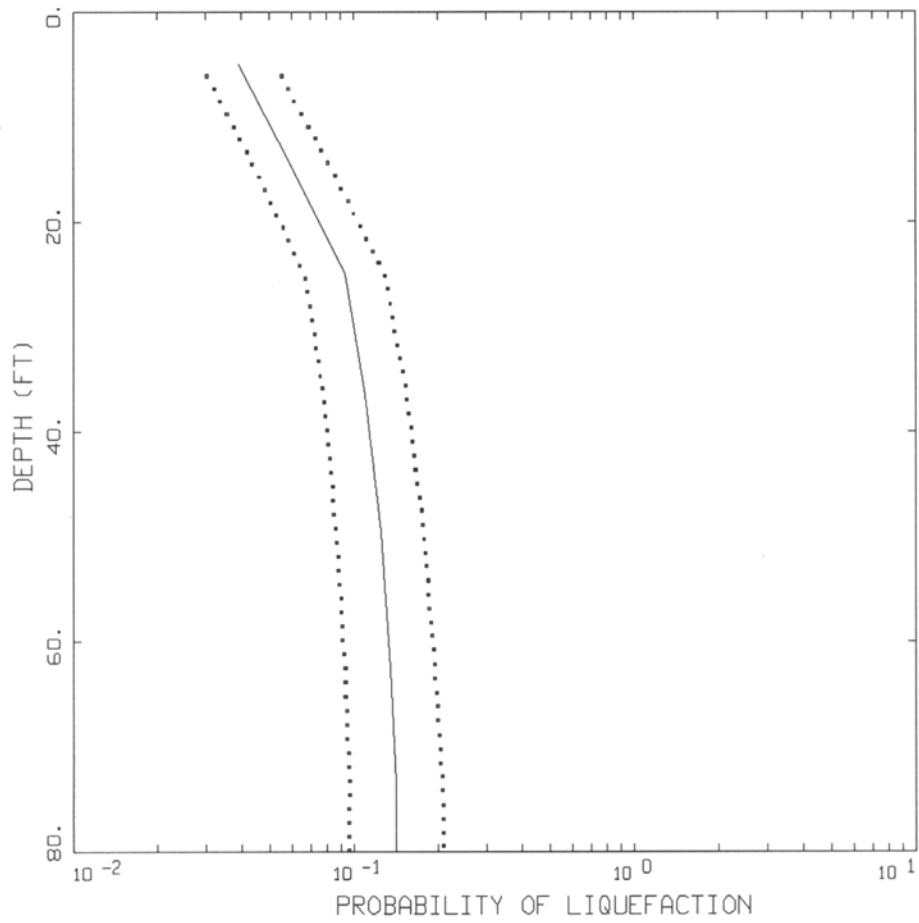
HAYWARD, M 7.1, R = 5 KM
VARIATION OF SITE PARAMETERS

LEGEND
..... 84TH PERCENTILE
———— MEDIAN
..... 16TH PERCENTILE

Appendix

Figure Set A13. At-depth estimates of liquefaction probability, factor of safety, cyclic stress ratio, number of cycles, strain energy density, and Arias intensity for a variation of all source parameters.

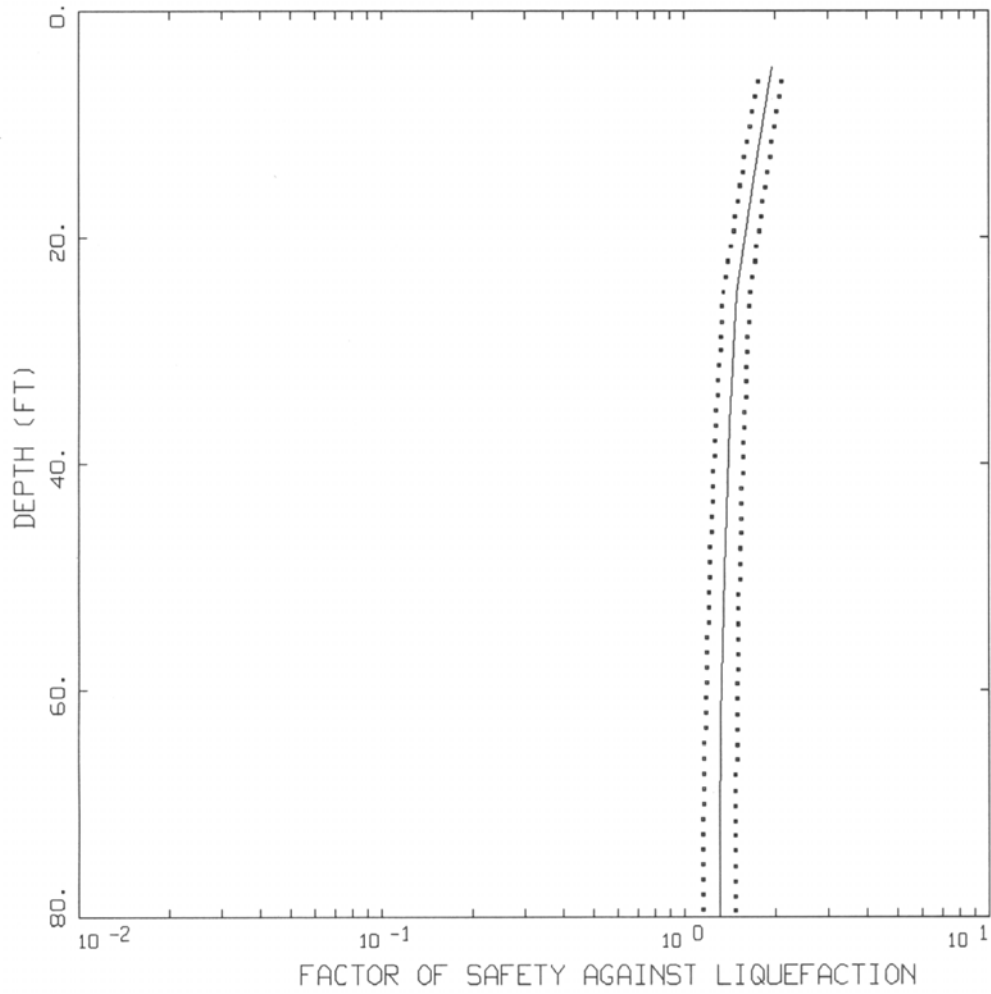
Appendix



HAYWARD, M 7.1, R = 5 KM
VARIATION OF SOURCE PARAMETERS

- LEGEND
- 84TH PERCENTILE
 - MEDIAN
 - 16TH PERCENTILE

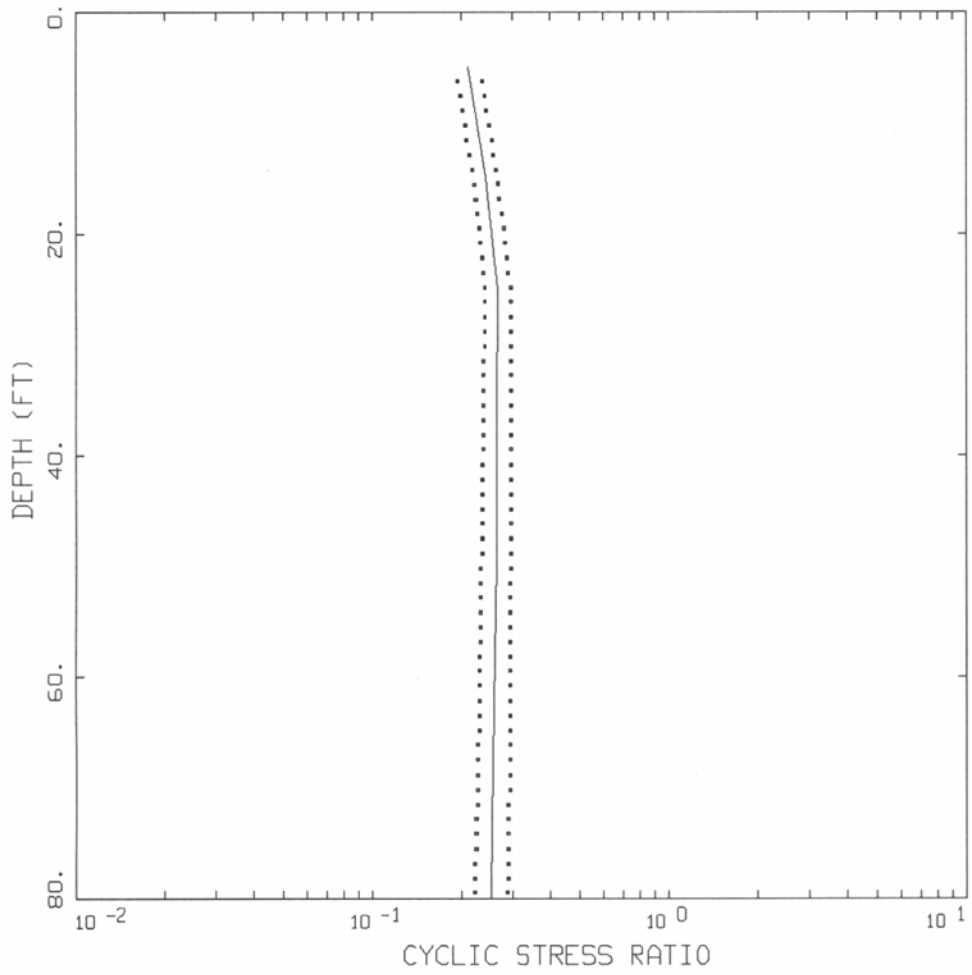
Appendix



HAYWARD, M 7.1, R = 5 KM
VARIATION OF SOURCE PARAMETERS

- LEGEND
- 84TH PERCENTILE
 - MEDIAN
 - 16TH PERCENTILE

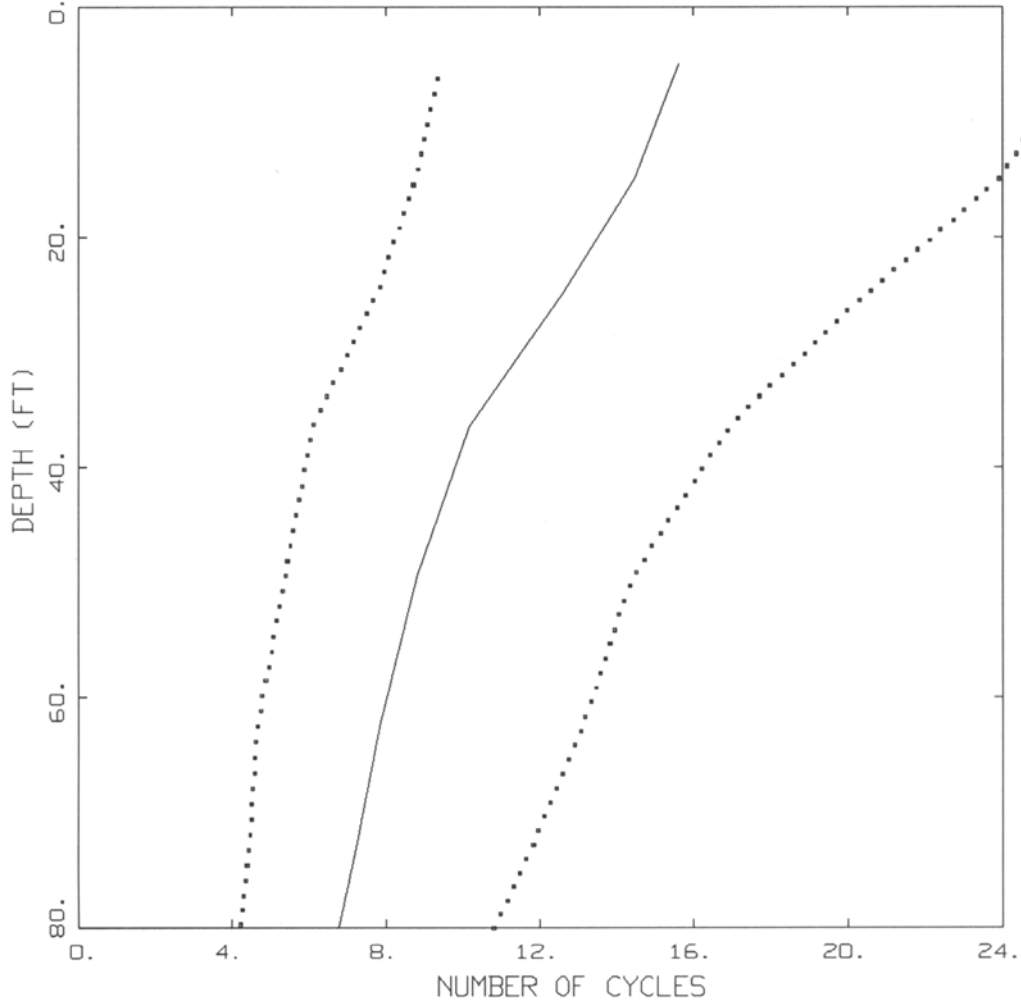
Appendix



HAYWARD, M 7.1, R = 5 KM
VARIATION OF SOURCE PARAMETERS

LEGEND
..... 84TH PERCENTILE
———— MEDIAN
..... 16TH PERCENTILE

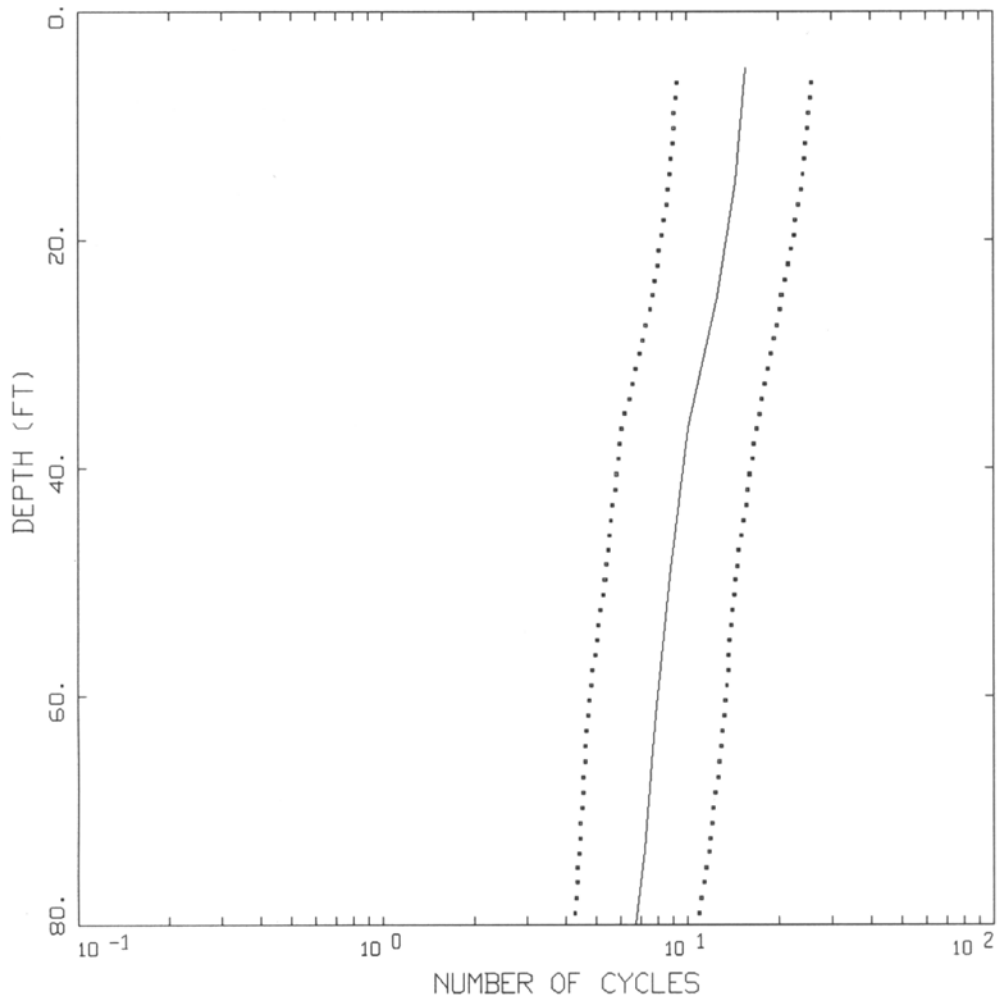
Appendix



HAYWARD, M 7.1, R = 5 KM
VARIATION OF SOURCE

- LEGEND
- 84TH PERCENTILE
 - MEDIAN
 - 16TH PERCENTILE

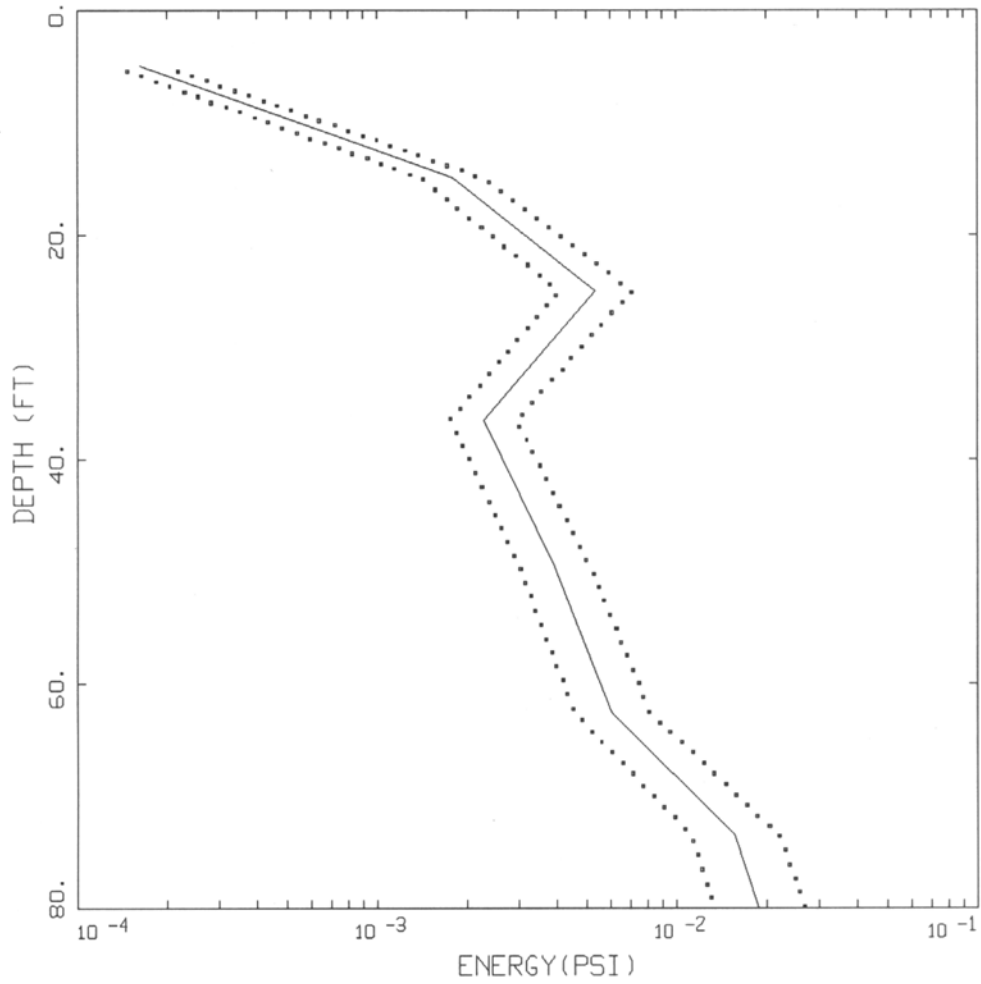
Appendix



HAYWARD, M 7.1, R = 5 KM
VARIATION OF SOURCE

- LEGEND
- 84TH PERCENTILE
 - MEDIAN
 - 16TH PERCENTILE

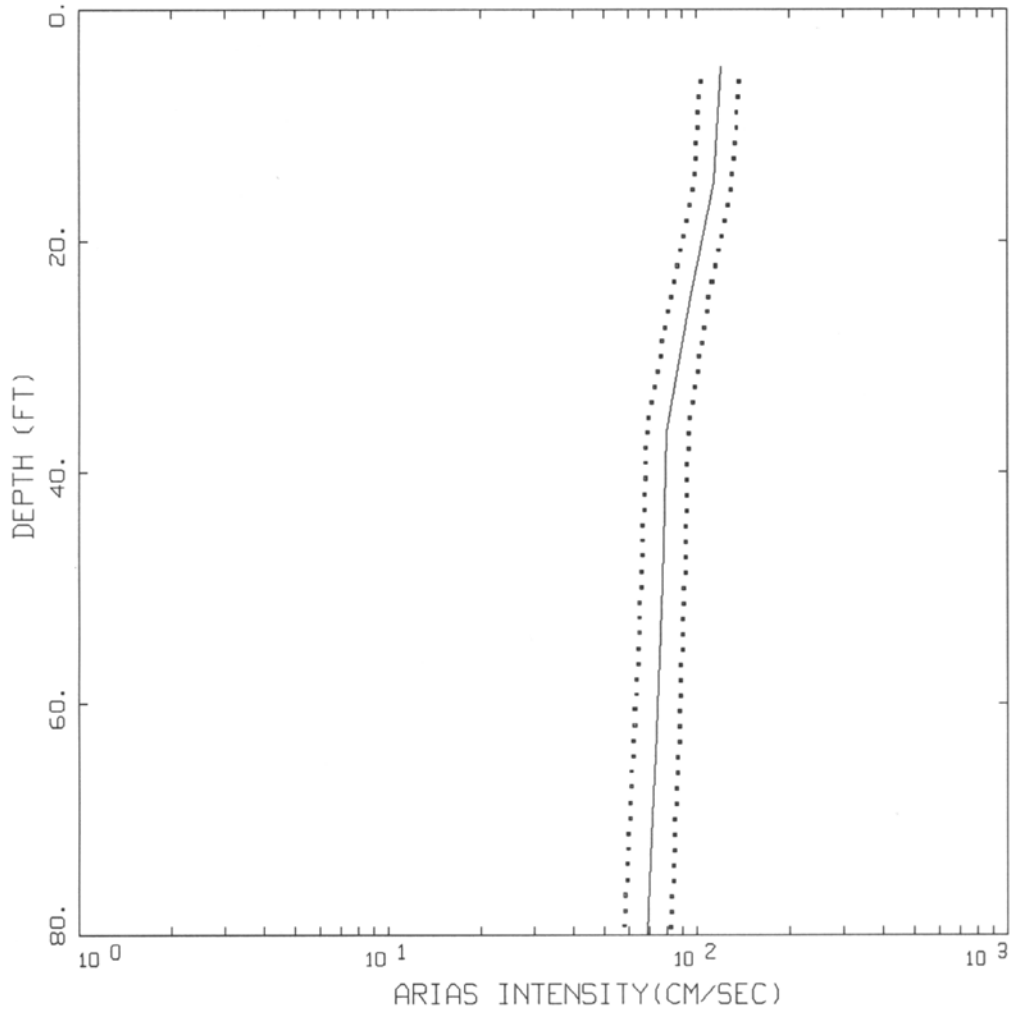
Appendix



HAYWARD, M 7.1, R = 5 KM
VARIATION OF SOURCE PARAMETERS

LEGEND
..... 84TH PERCENTILE
———— MEDIAN
..... 16TH PERCENTILE

Appendix



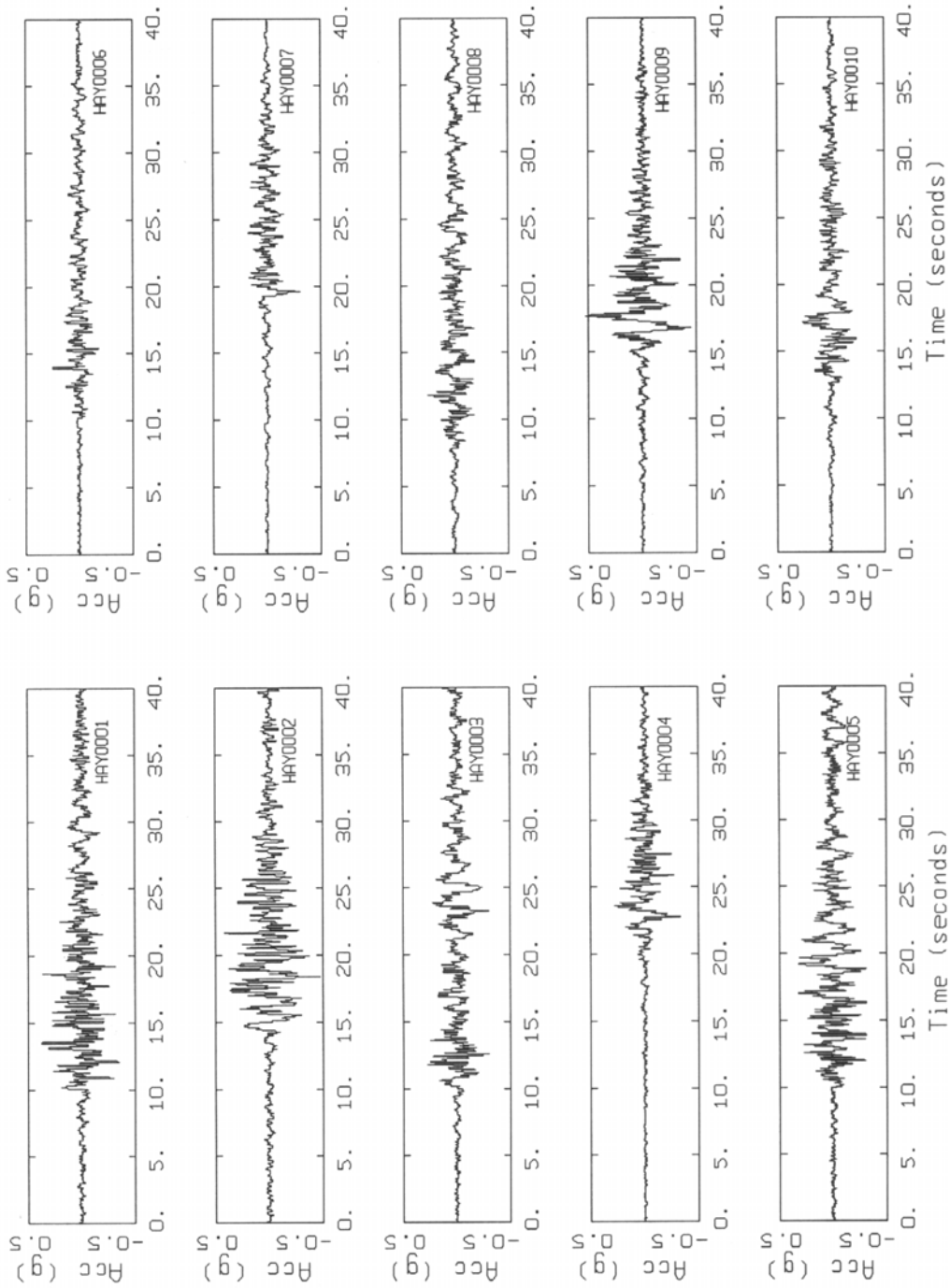
HAYWARD, M 7.1, R = 5 KM
VARIATION OF SOURCE PARAMETERS

LEGEND
..... 84TH PERCENTILE
———— MEDIAN
..... 16TH PERCENTILE

Appendix

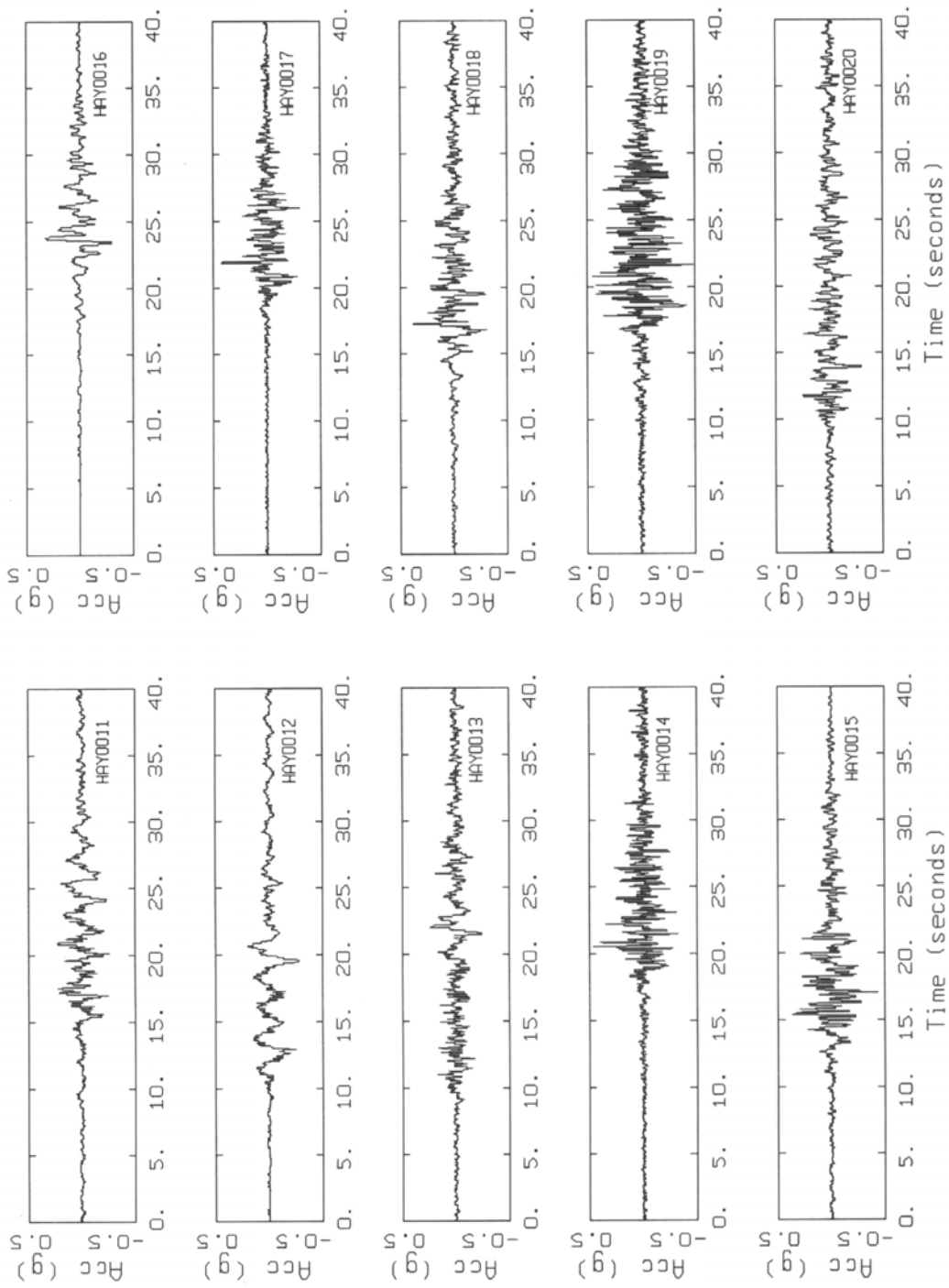
Figure Set A14. Plots of acceleration, velocity, and displacement time histories for an average horizontal component. Variation of source and site parameters.

Appendix



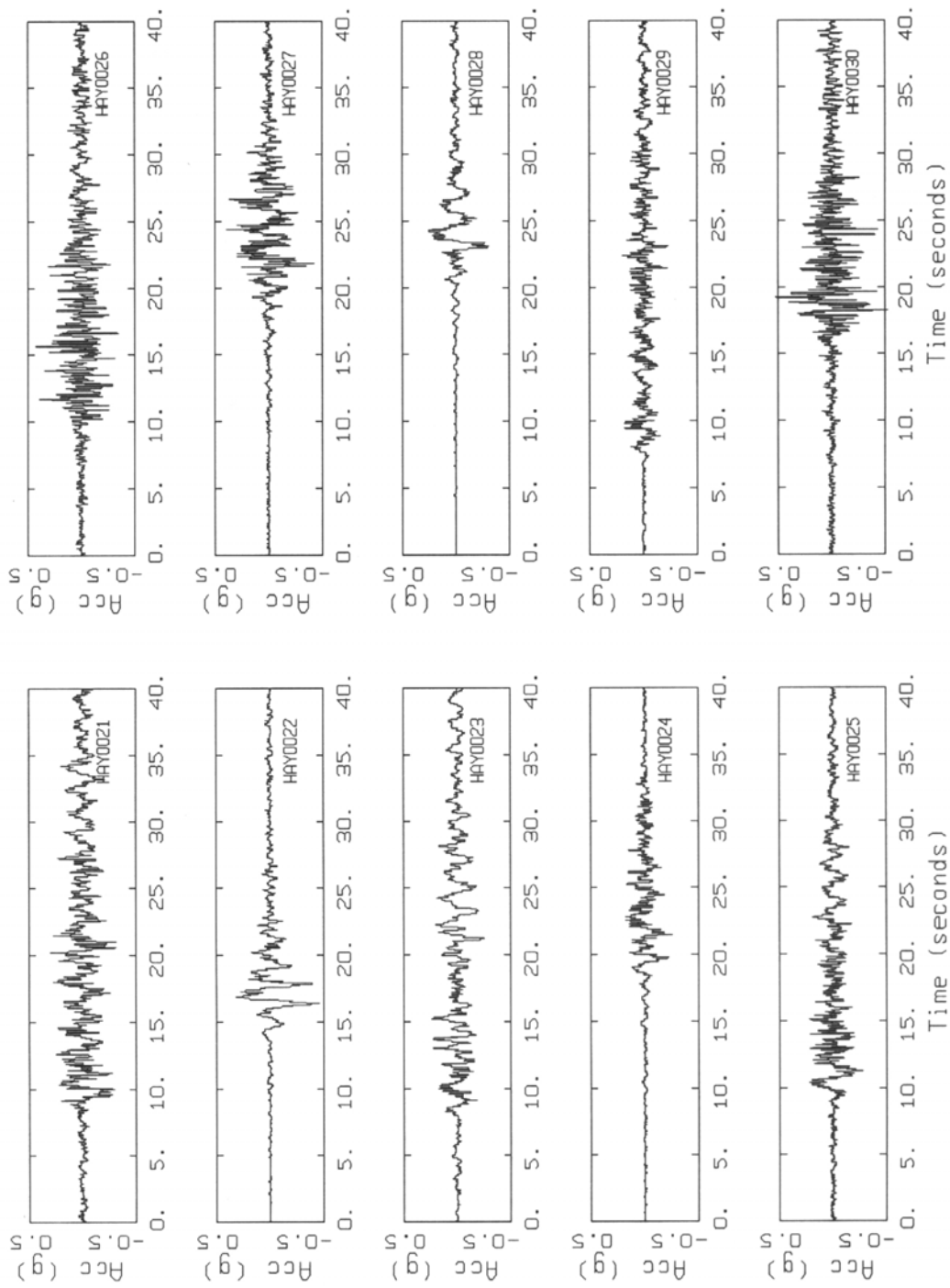
HAYWARD, M 7.1, SOFT SOIL, D = 5.0 KM, ALL

Appendix



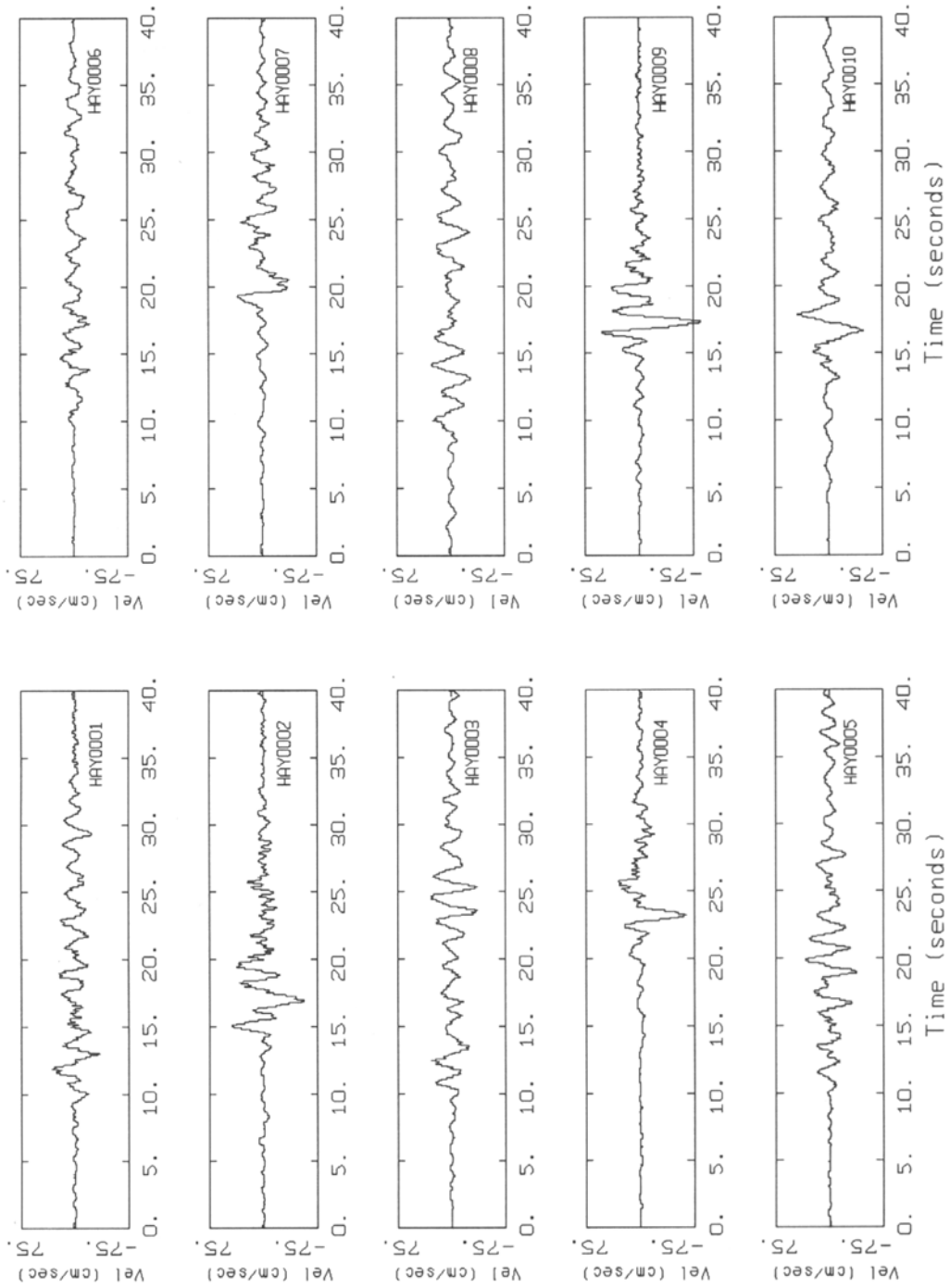
HAYWARD, M 7.1, SOFT SOIL, D = 7.5 KM, ALL

Appendix



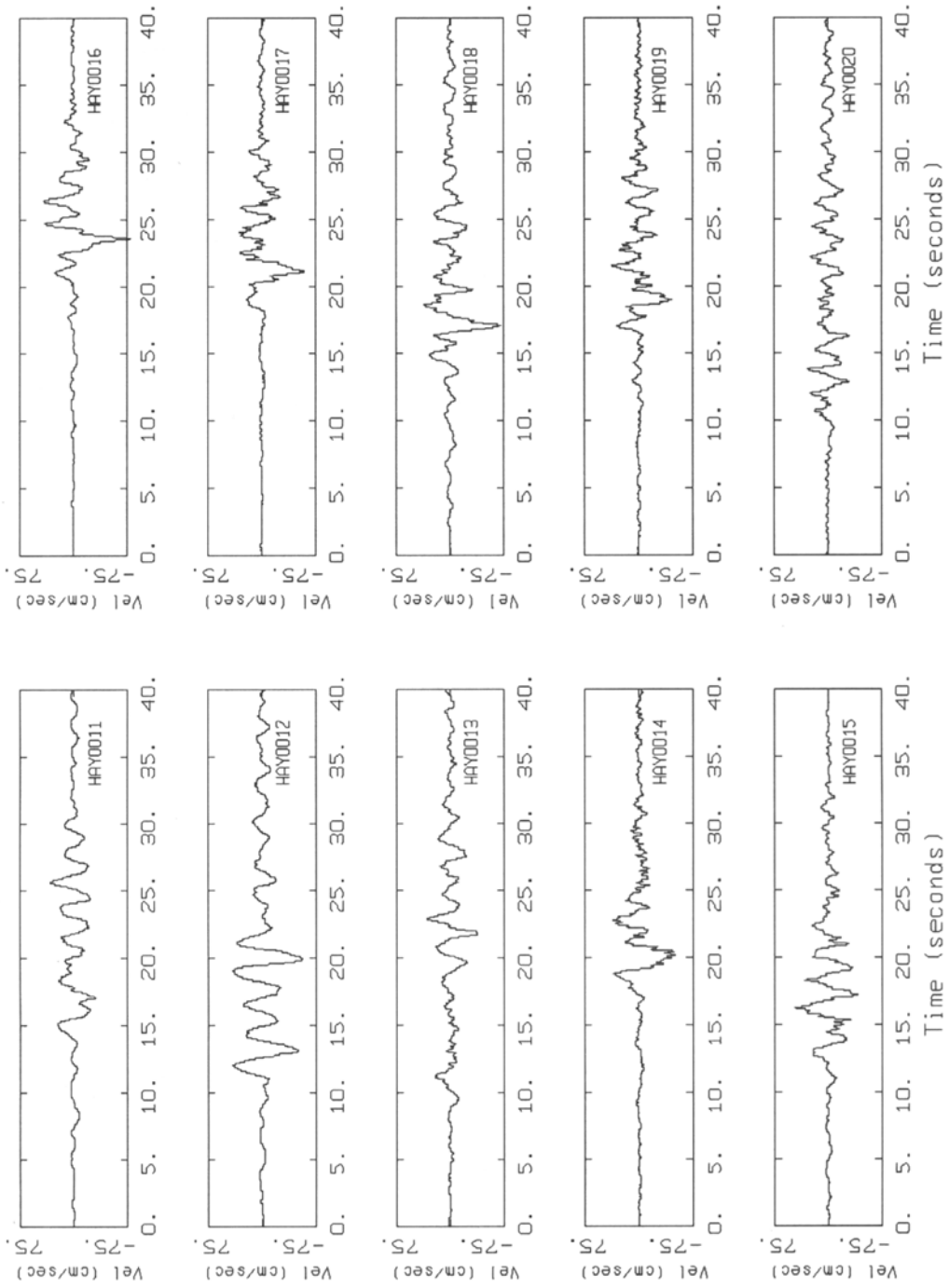
HAYWARD, M 7.1, SOFT SOIL, D = 7.5 KM, ALL

Appendix



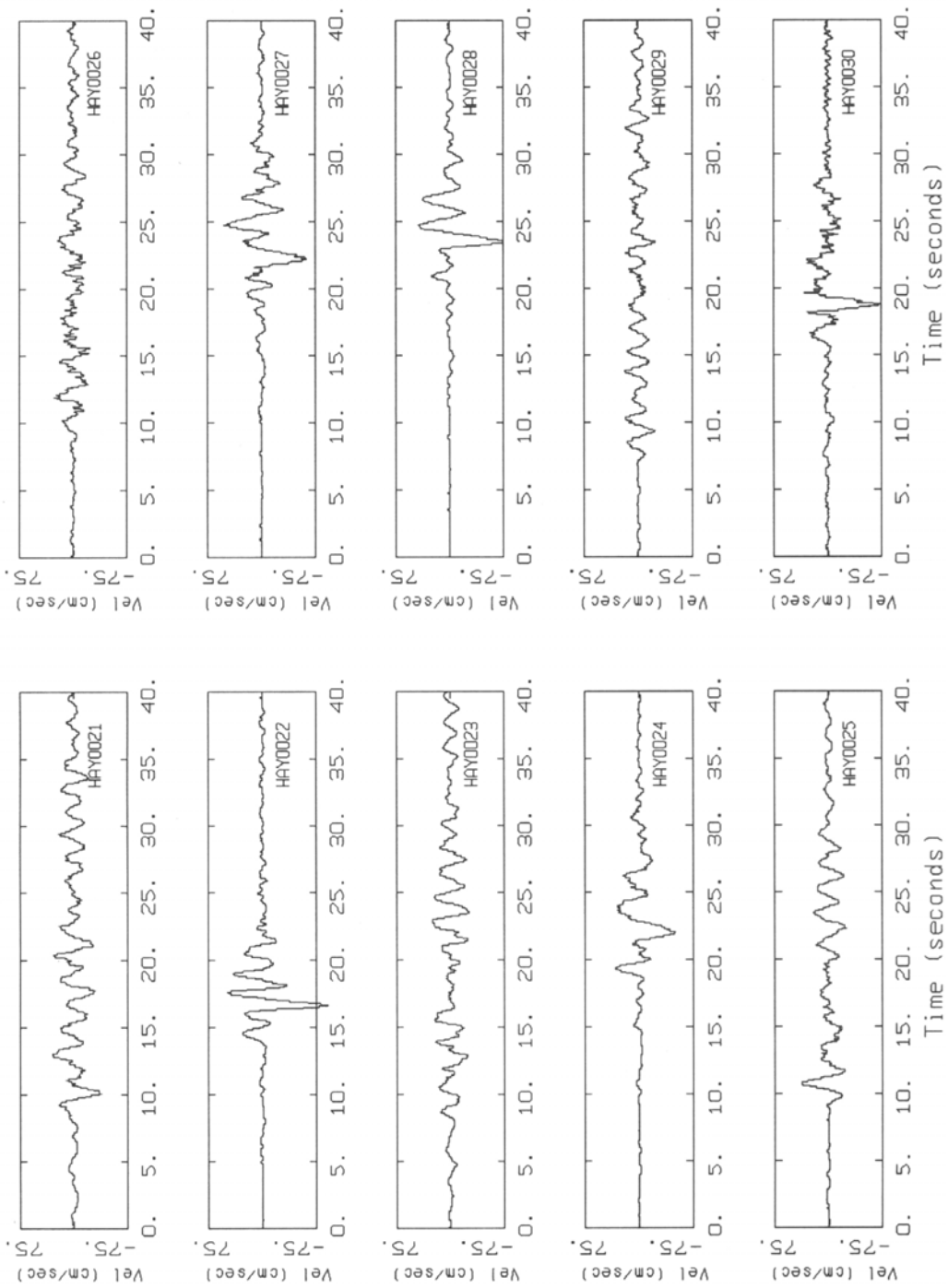
HAYWARD, M 7.1, SOFT SOIL, D = 5.0 KM, ALL

Appendix



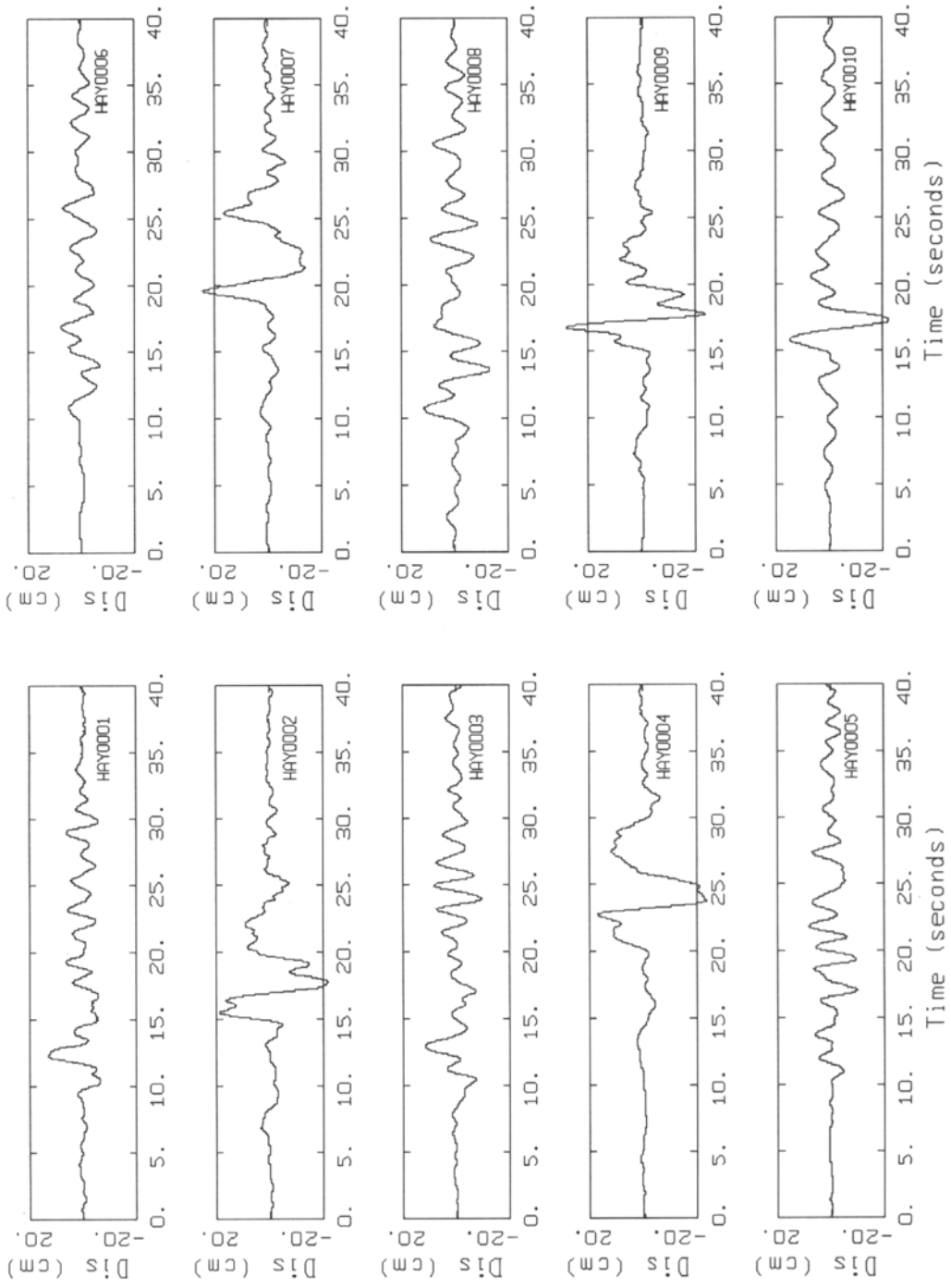
HAYWARD, M 7.1, SOFT SOIL, D = 5.0 KM, SOURCE

Appendix



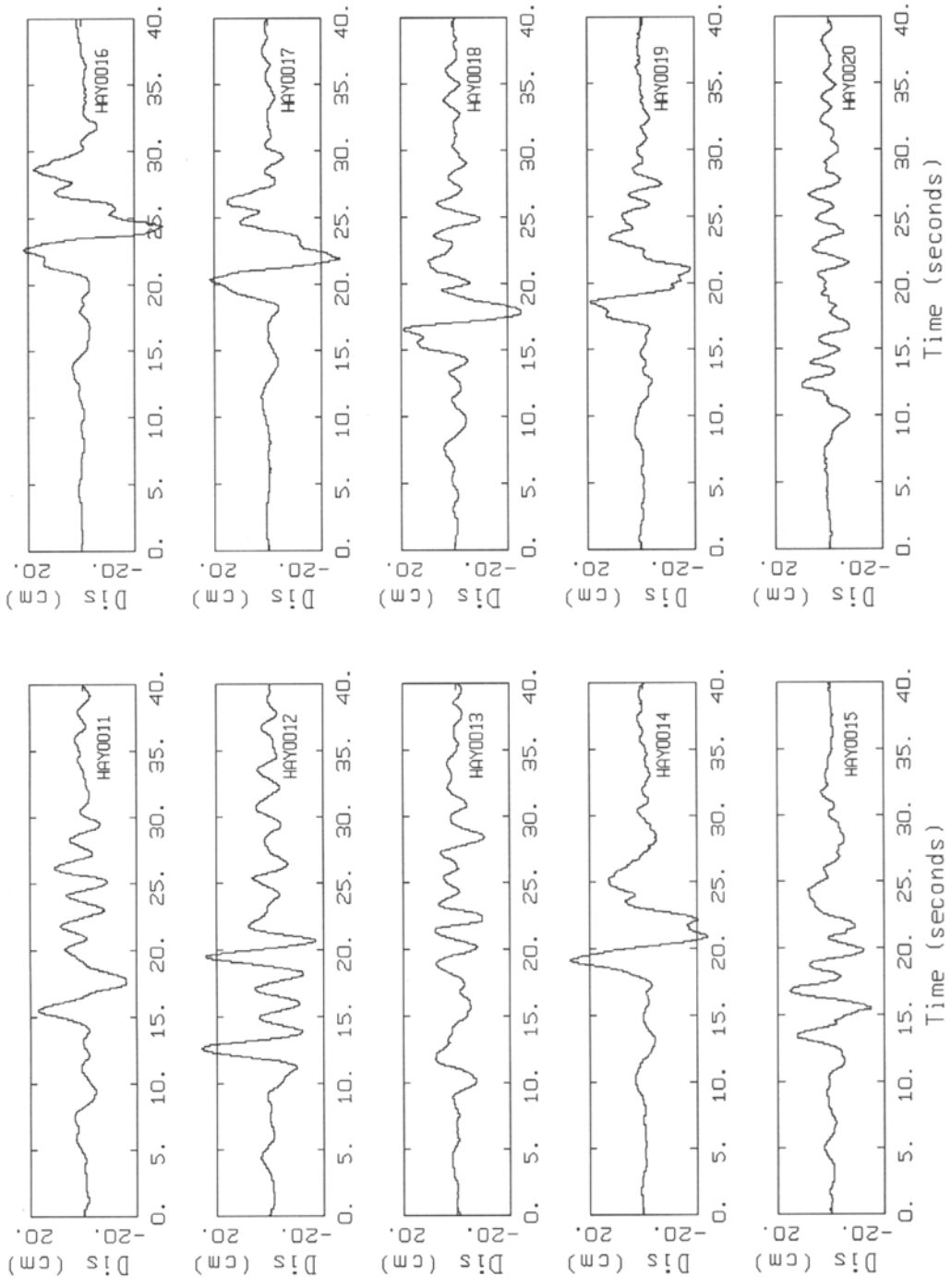
HAYWARD, M 7.1, SOFT SOIL, D = 5.0 KM, SOURCE

Appendix



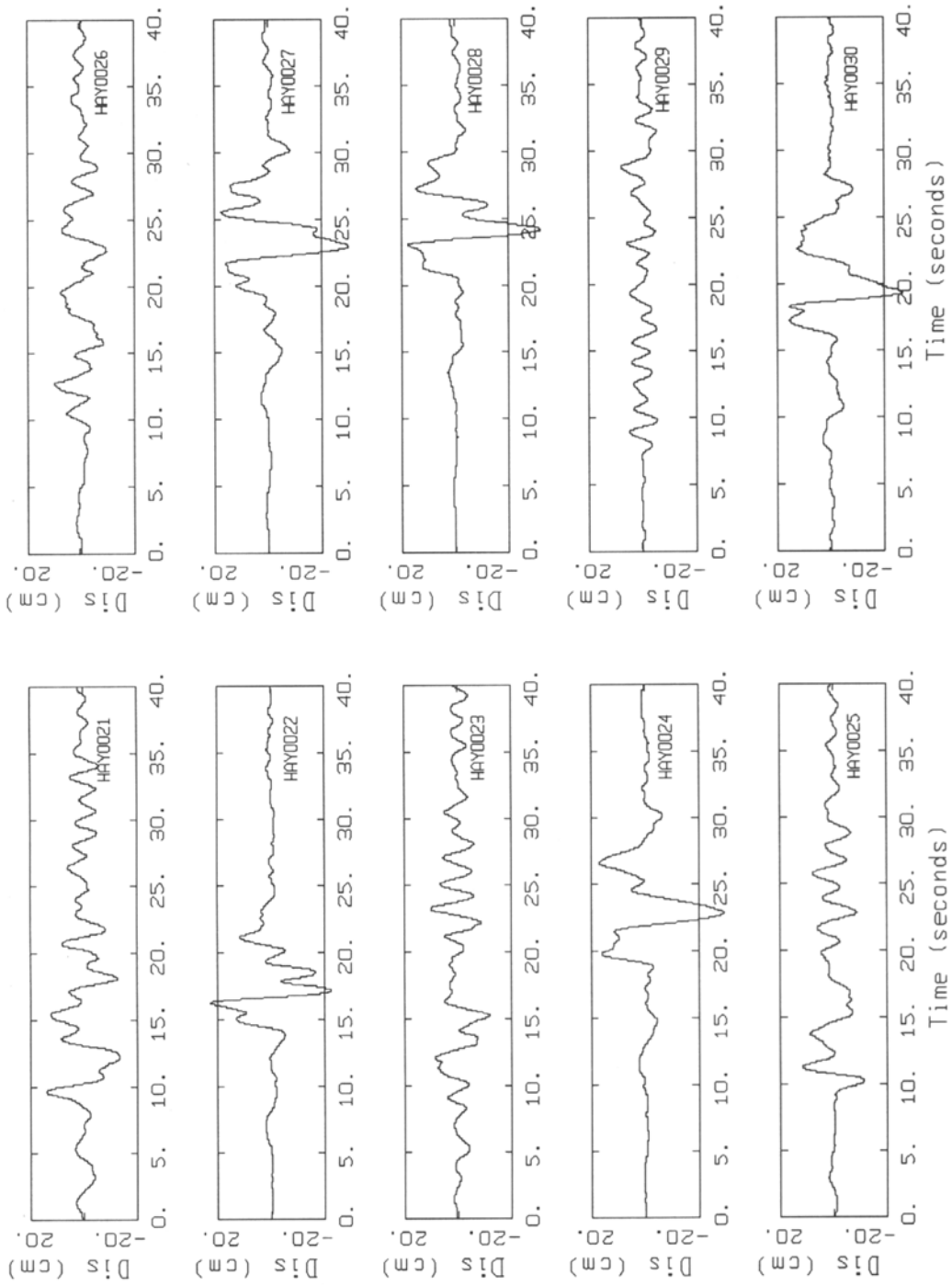
HAYWARD, M 7.1, SOFT SOIL, D = 5.0 KM, ALL

Appendix



HAYWARD, M 7.1, SOFT SOIL, D = 5.0 KM, SOURCE

Appendix

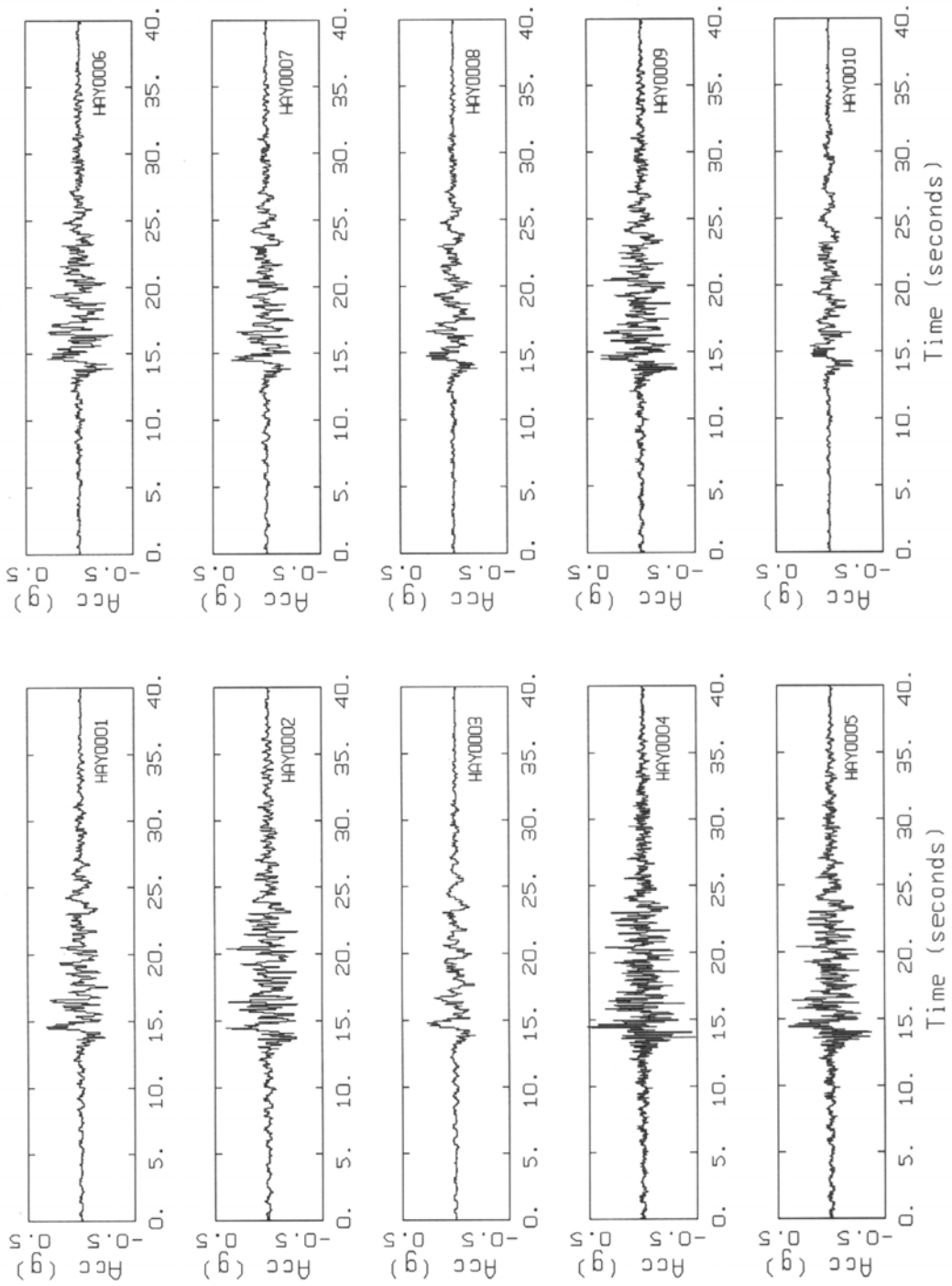


HAYWARD, M 7.1, SOFT SOIL, D = 5.0 KM, SOURCE

Appendix

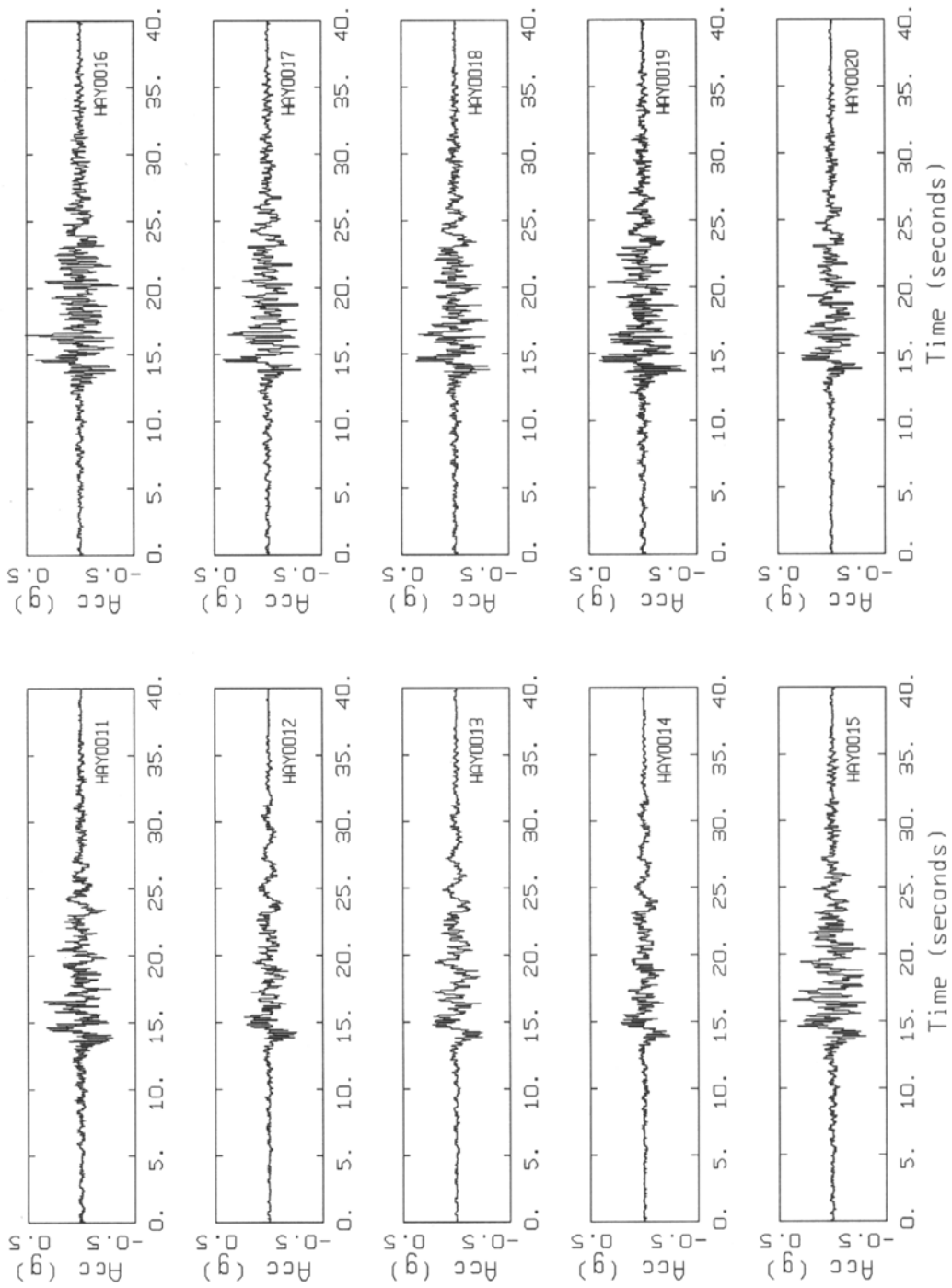
Figure Set A15. Plots of acceleration, velocity, and displacement time histories for an average horizontal component. Variation of site parameters.

Appendix



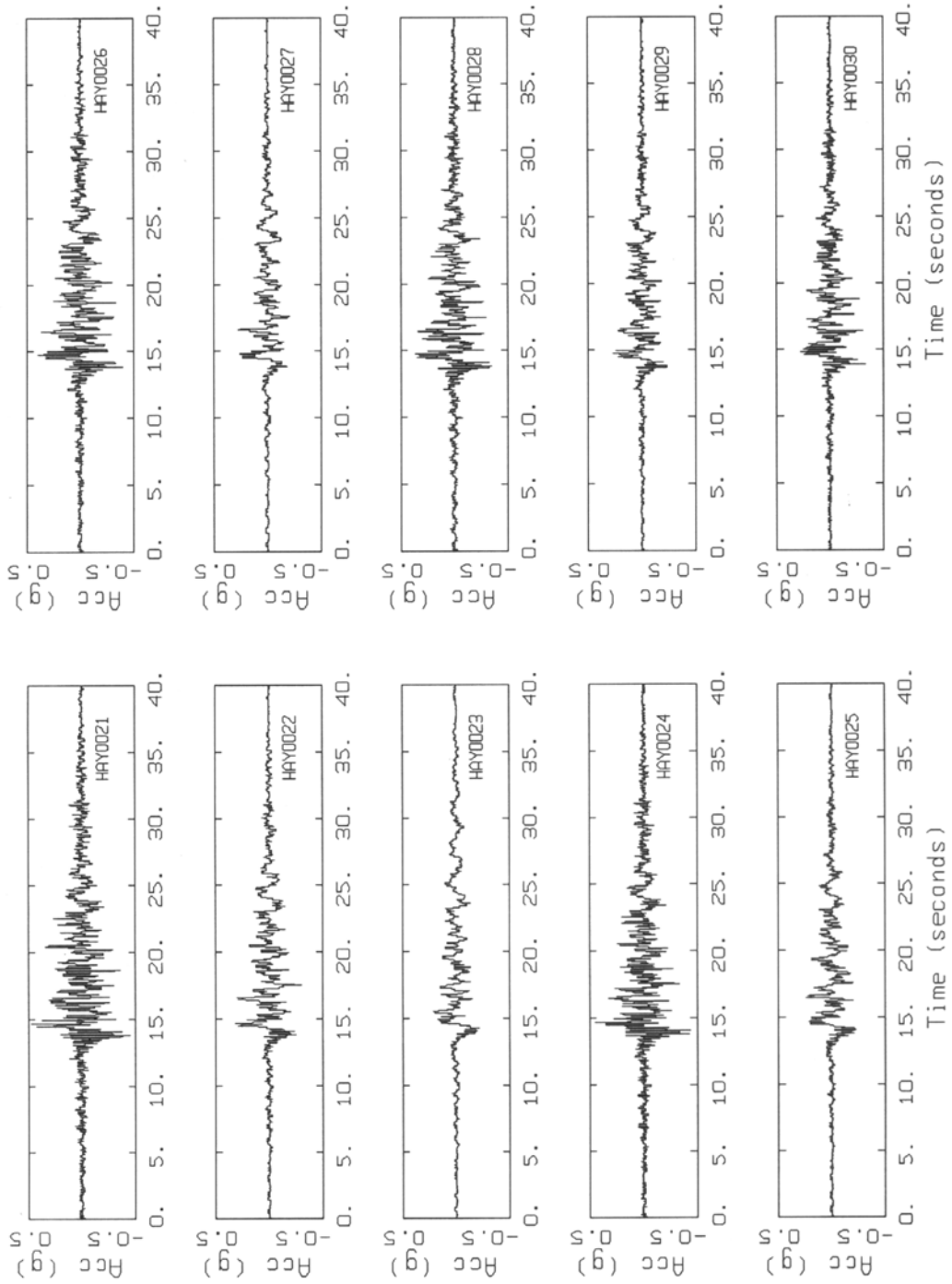
HAYWARD, M 7.1, SOFT SOIL, D = 5.0 KM, SITE

Appendix



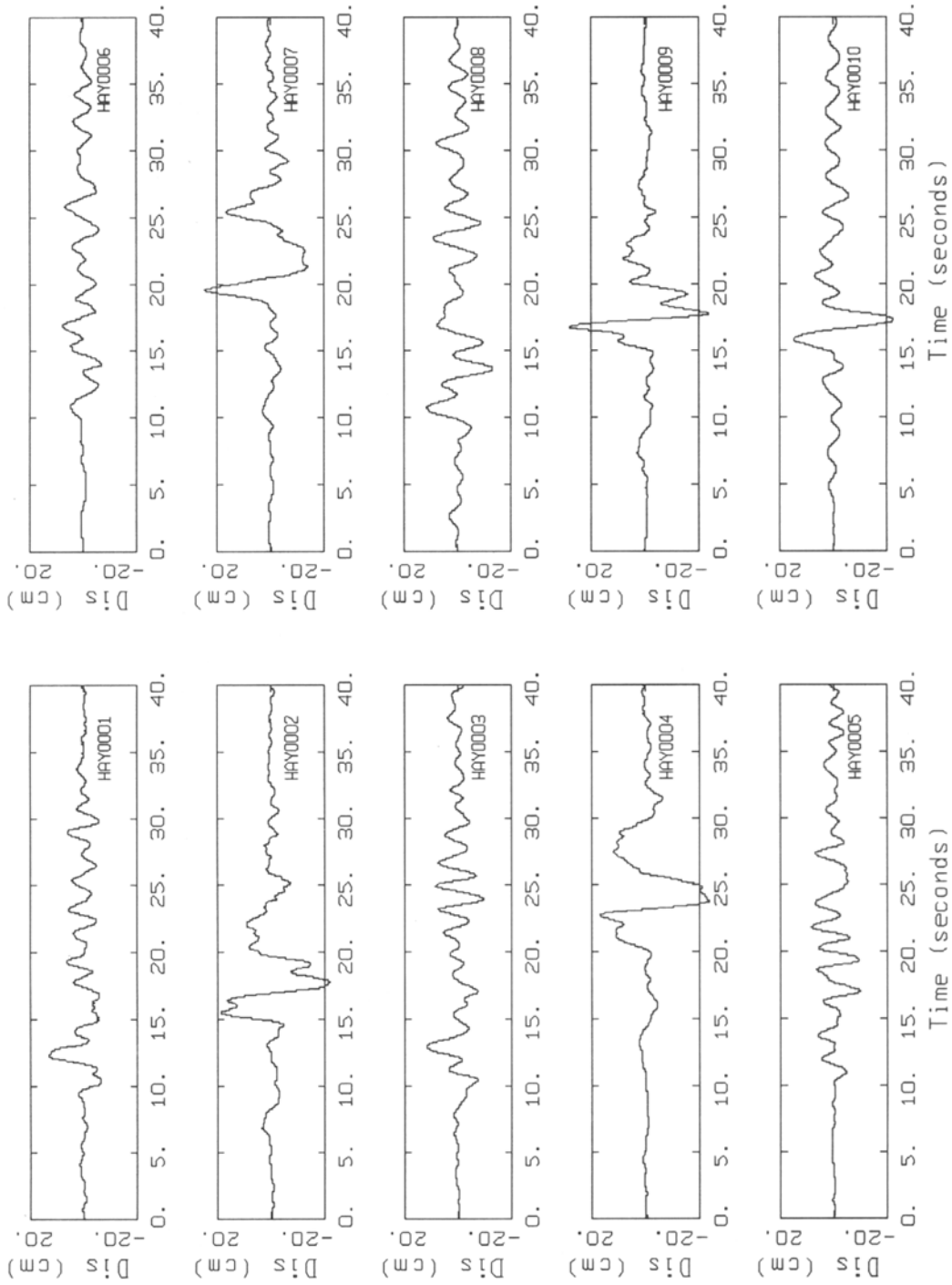
HAYWARD, M 7.1, SOFT SOIL, D = 7.5 KM, SITE

Appendix



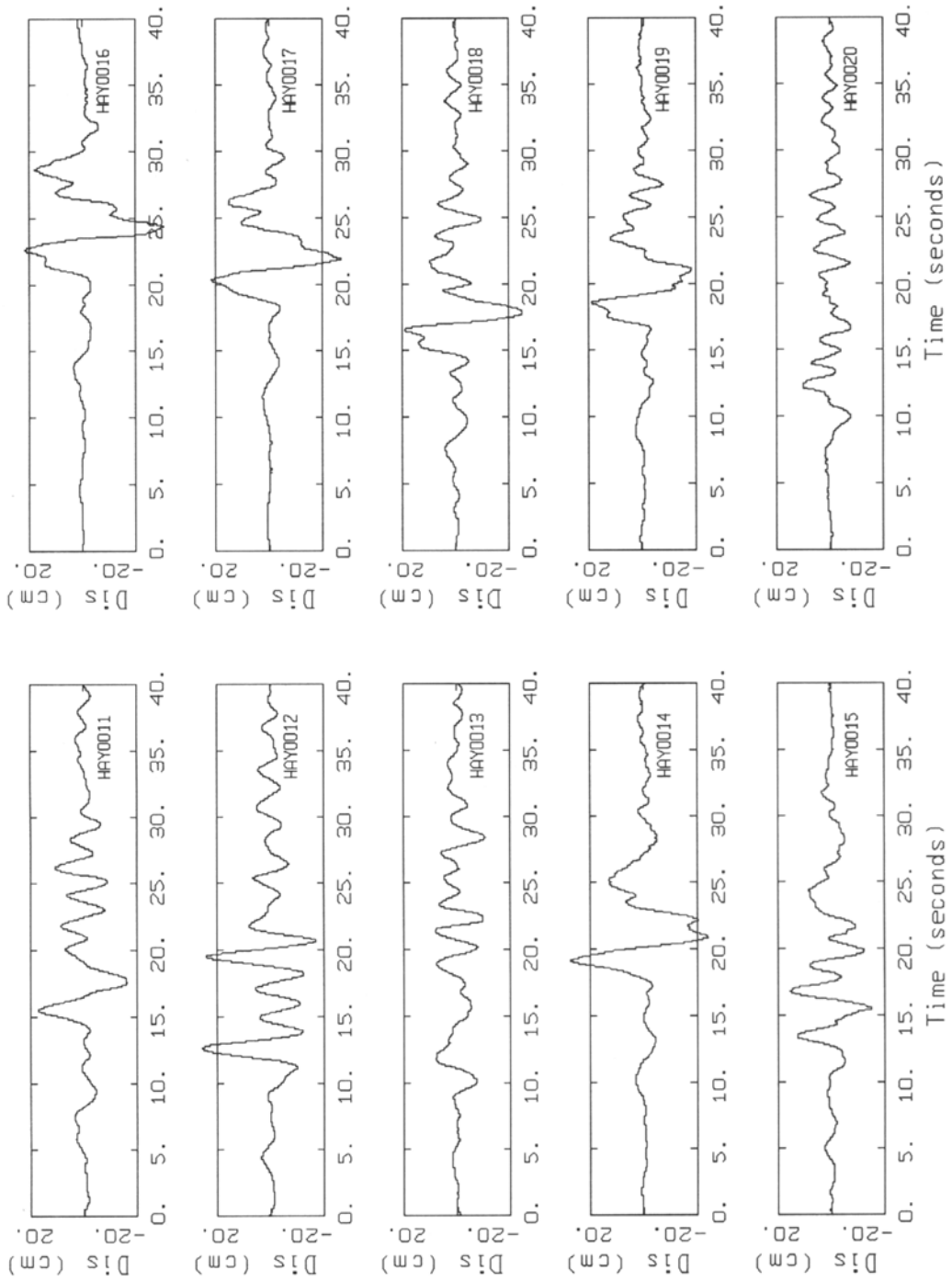
HAYWARD, M 7.1, SOFT SOIL, D = 7.5 KM, SITE

Appendix



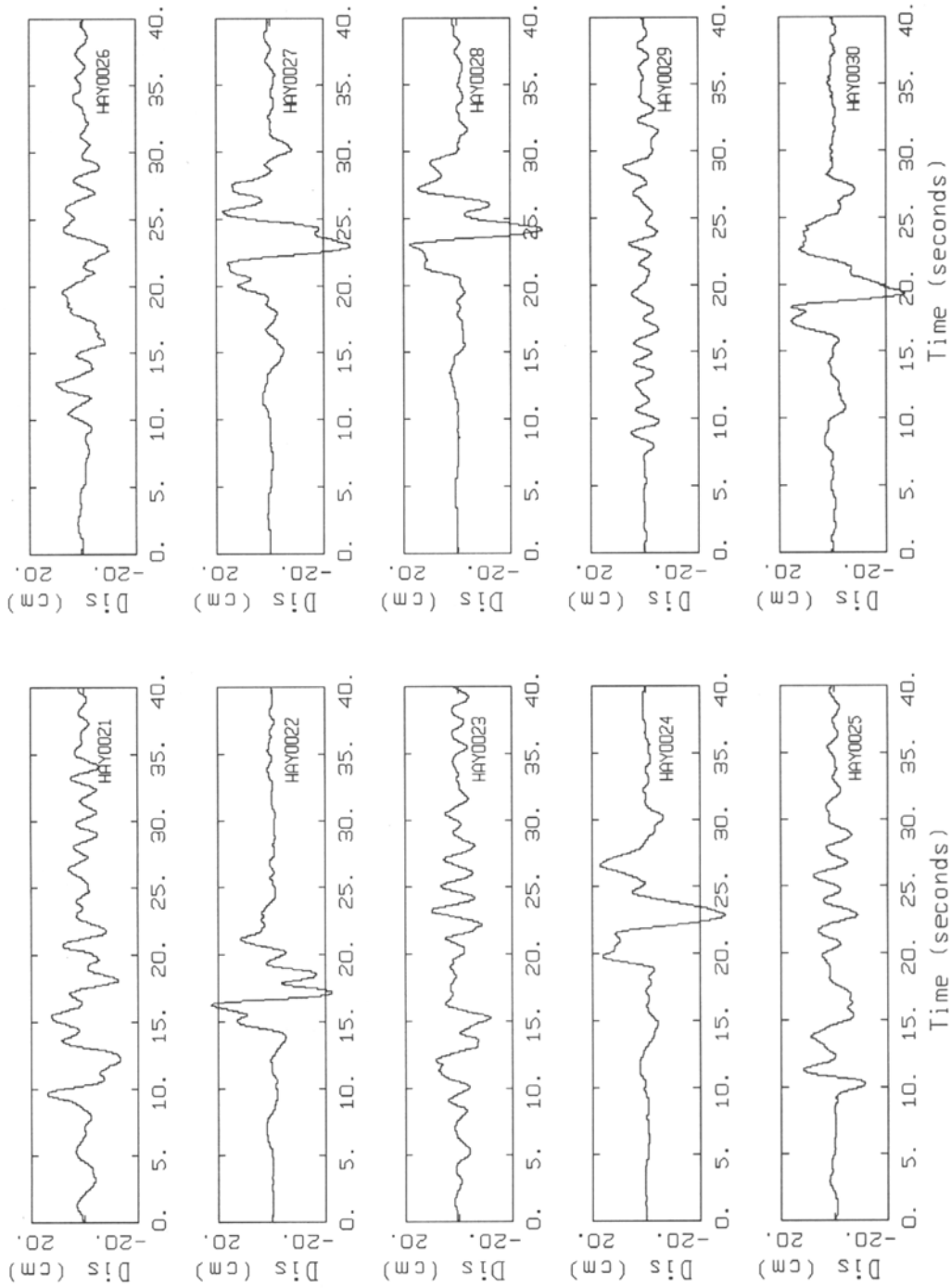
HAYWARD, M 7.1, SOFT SOIL, D = 5.0 KM, SITE

Appendix



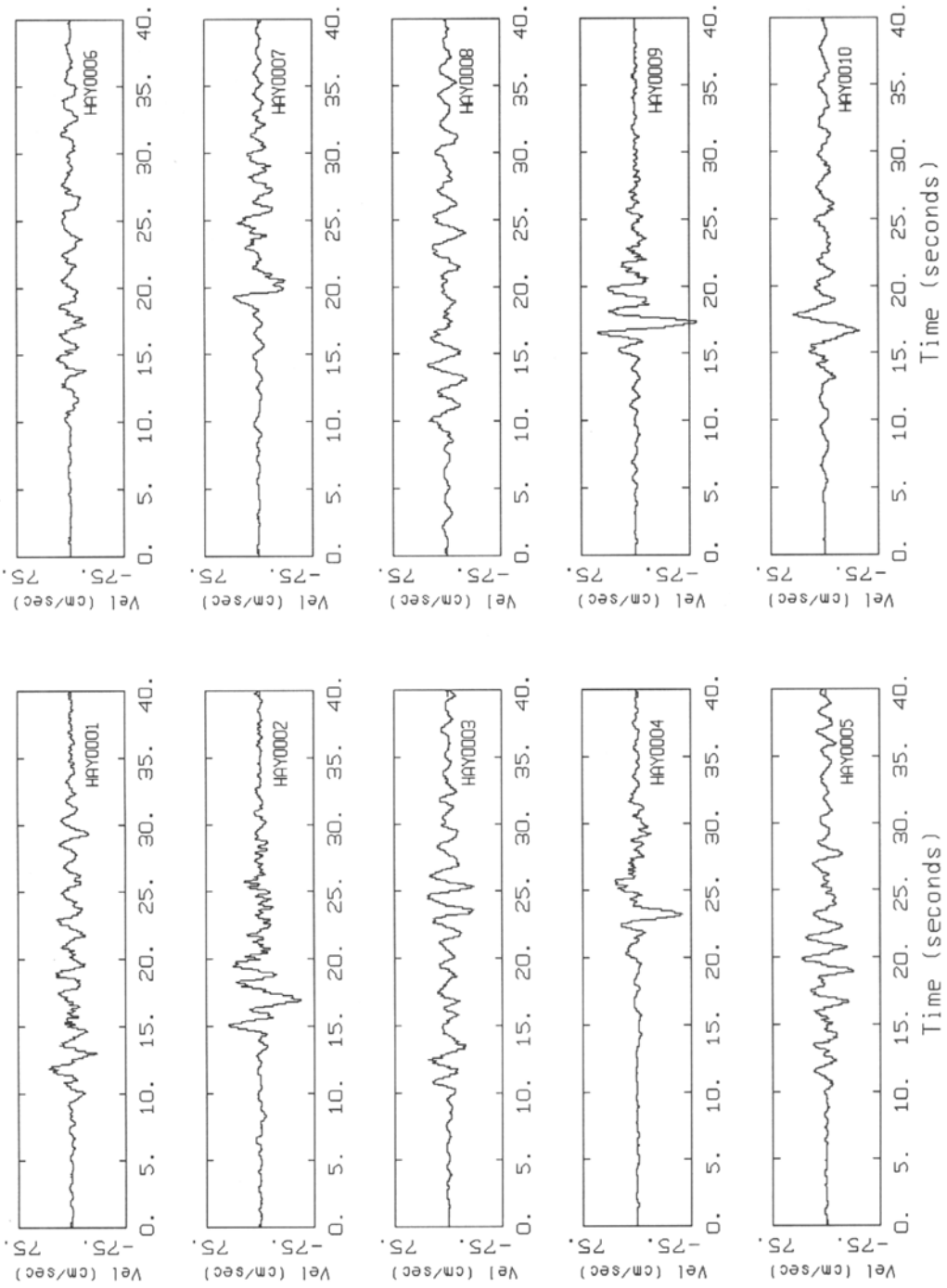
HAYWARD, M 7.1, SOFT SOIL, D = 5.0 KM, SITE

Appendix



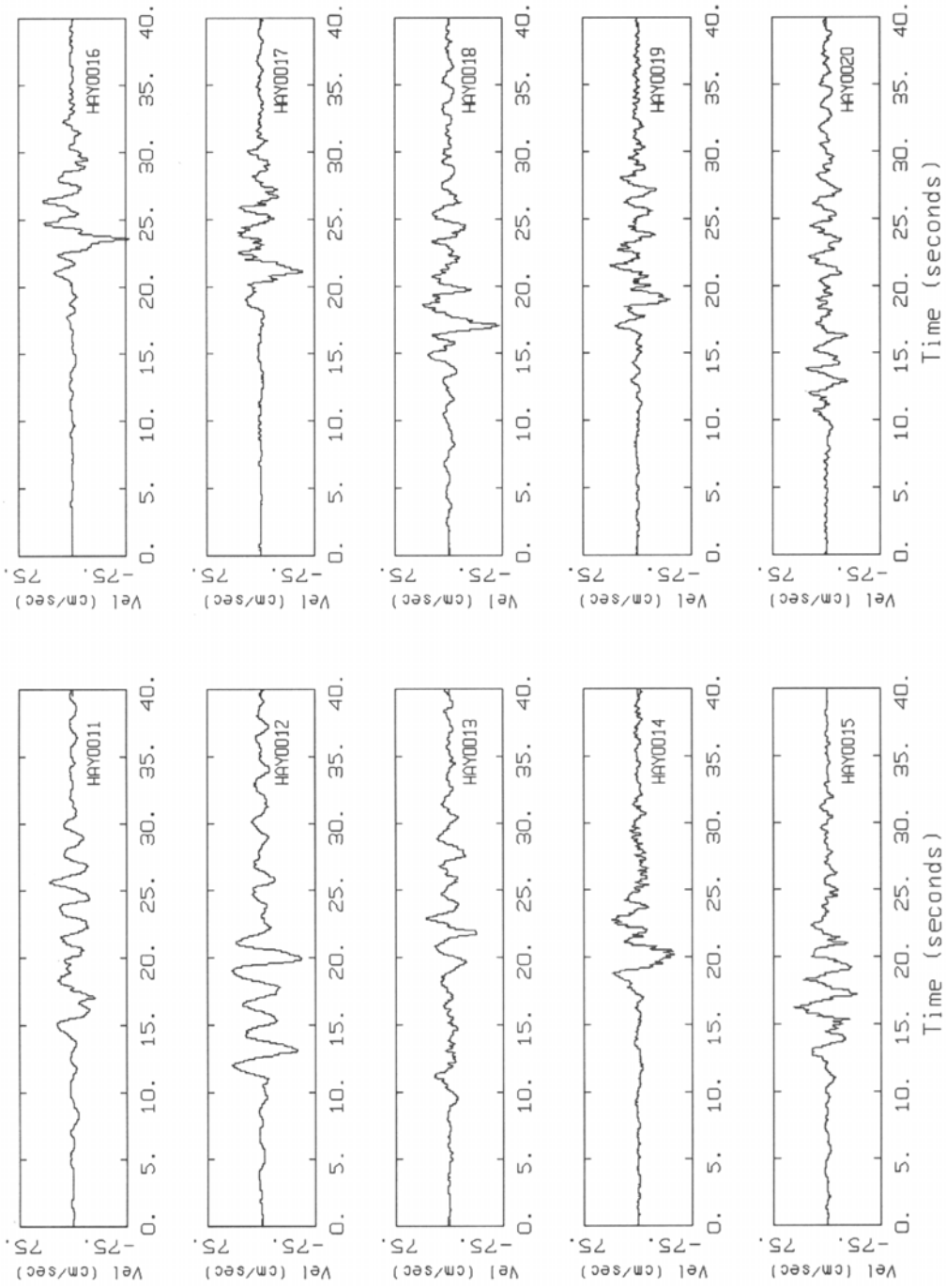
HAYWARD, M 7.1, SOFT SOIL, D = 5.0 KM, SITE

Appendix



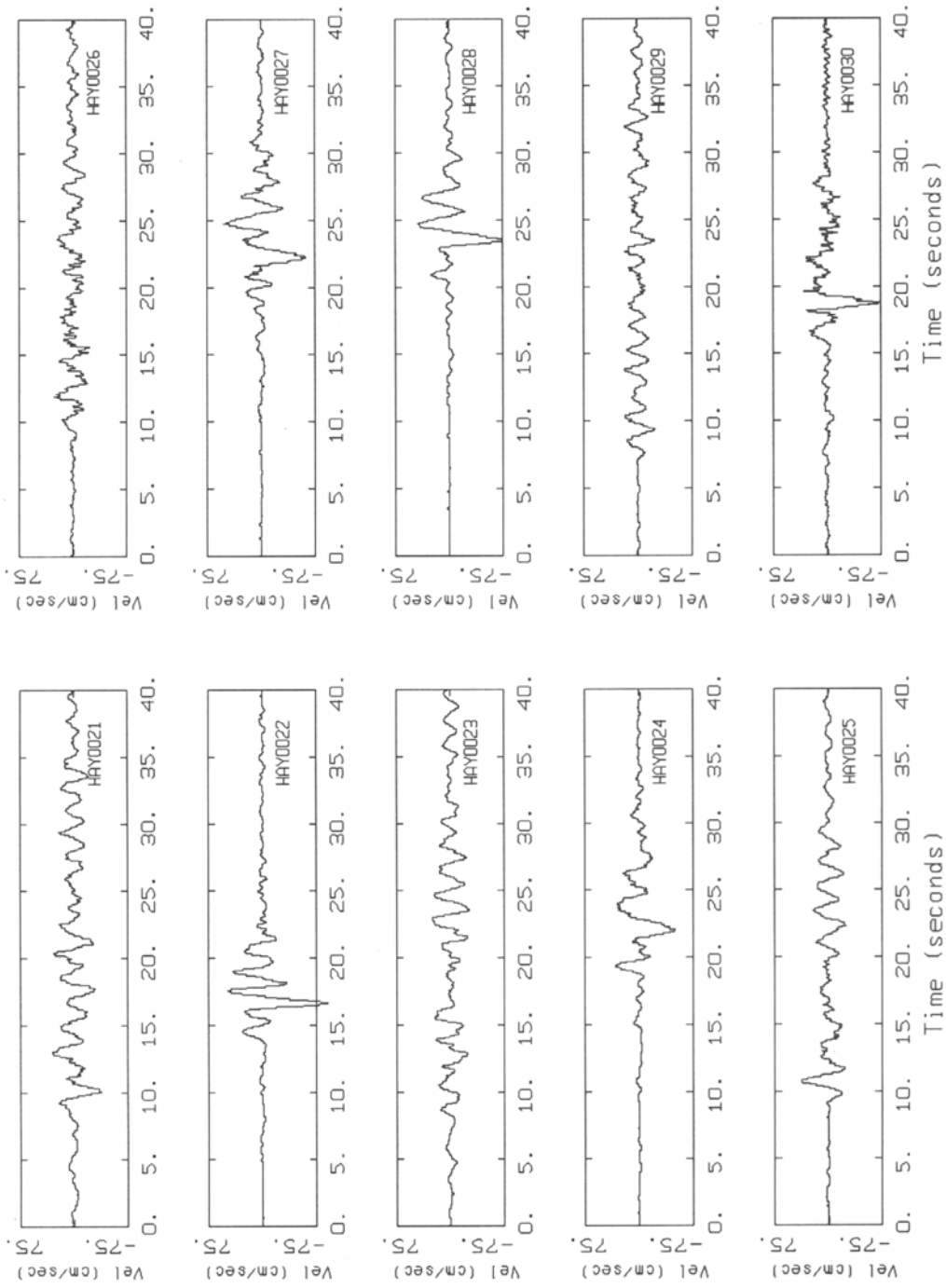
HAYWARD, M 7.1, SOFT SOIL, D = 5.0 KM, SITE

Appendix



HAYWARD, M 7.1, SOFT SOIL, D = 5.0 KM, SITE

Appendix

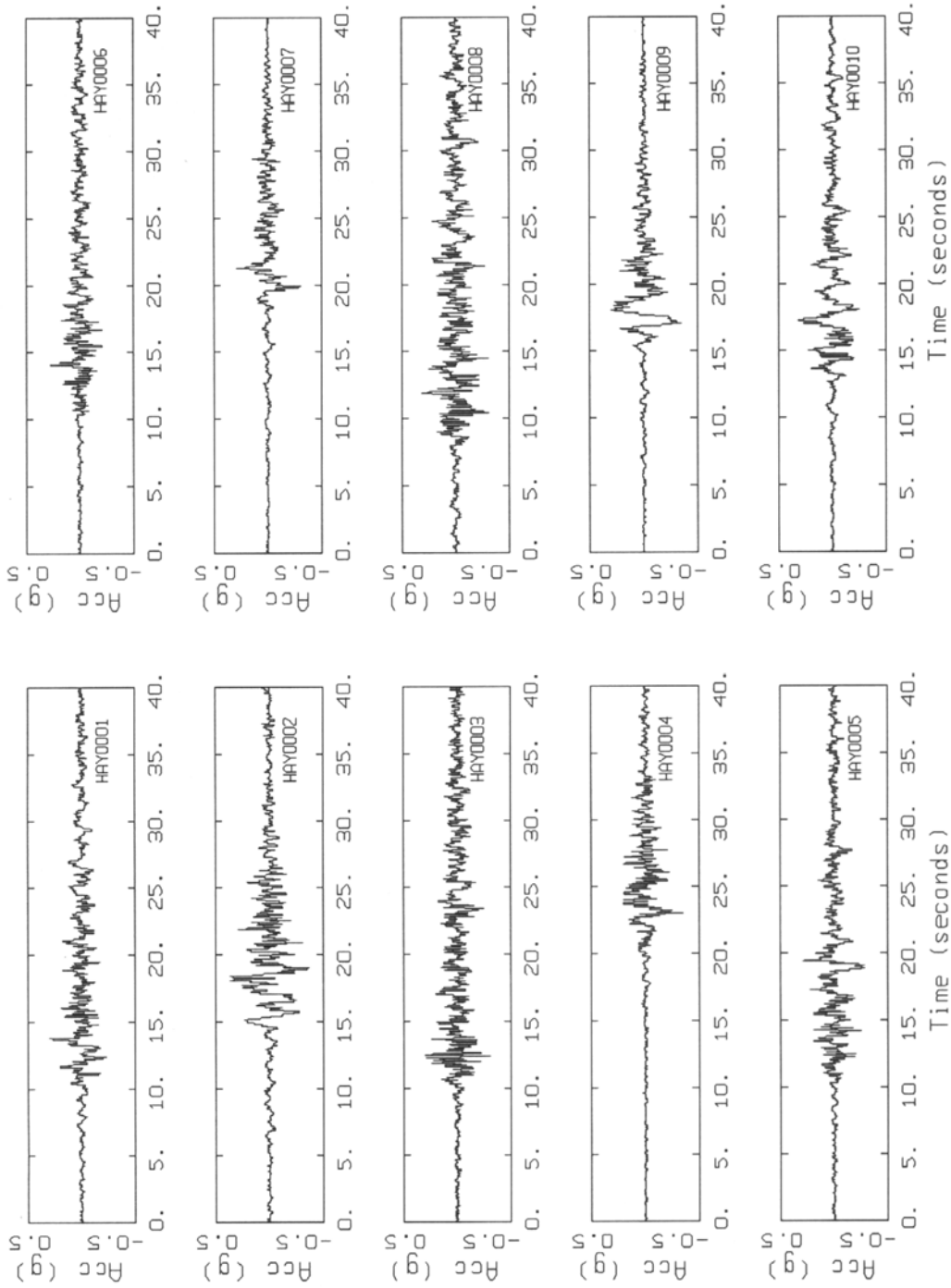


HAYWARD, M 7.1, SOFT SOIL, D = 5.0 KM, SITE

Appendix

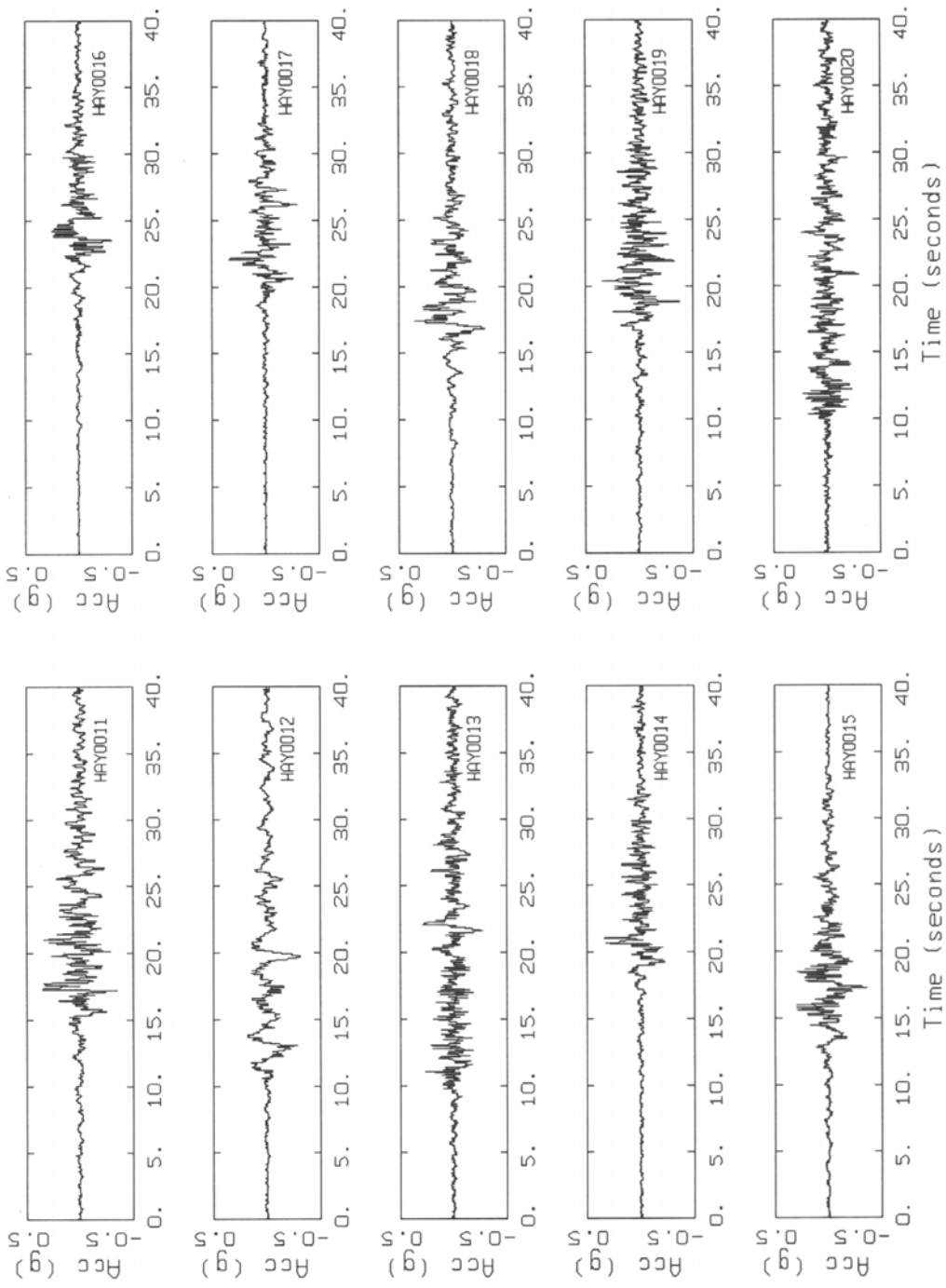
Figure Set A16. Plots of acceleration, velocity, and displacement time histories for an average horizontal component. Variation of source parameters.

Appendix



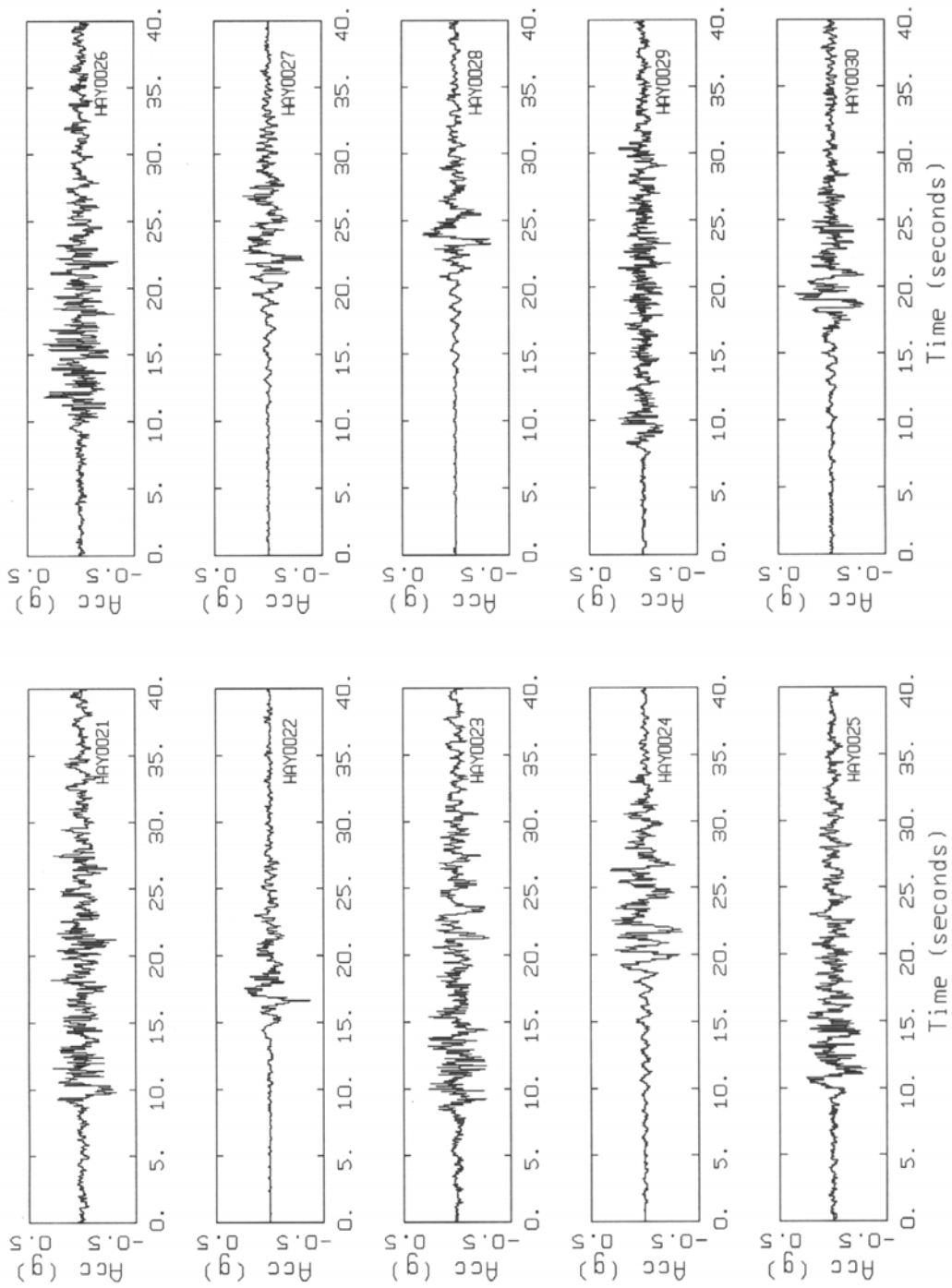
HAYWARD, M 7.1, SOFT SOIL, D = 5.0 KM, SOURCE

Appendix



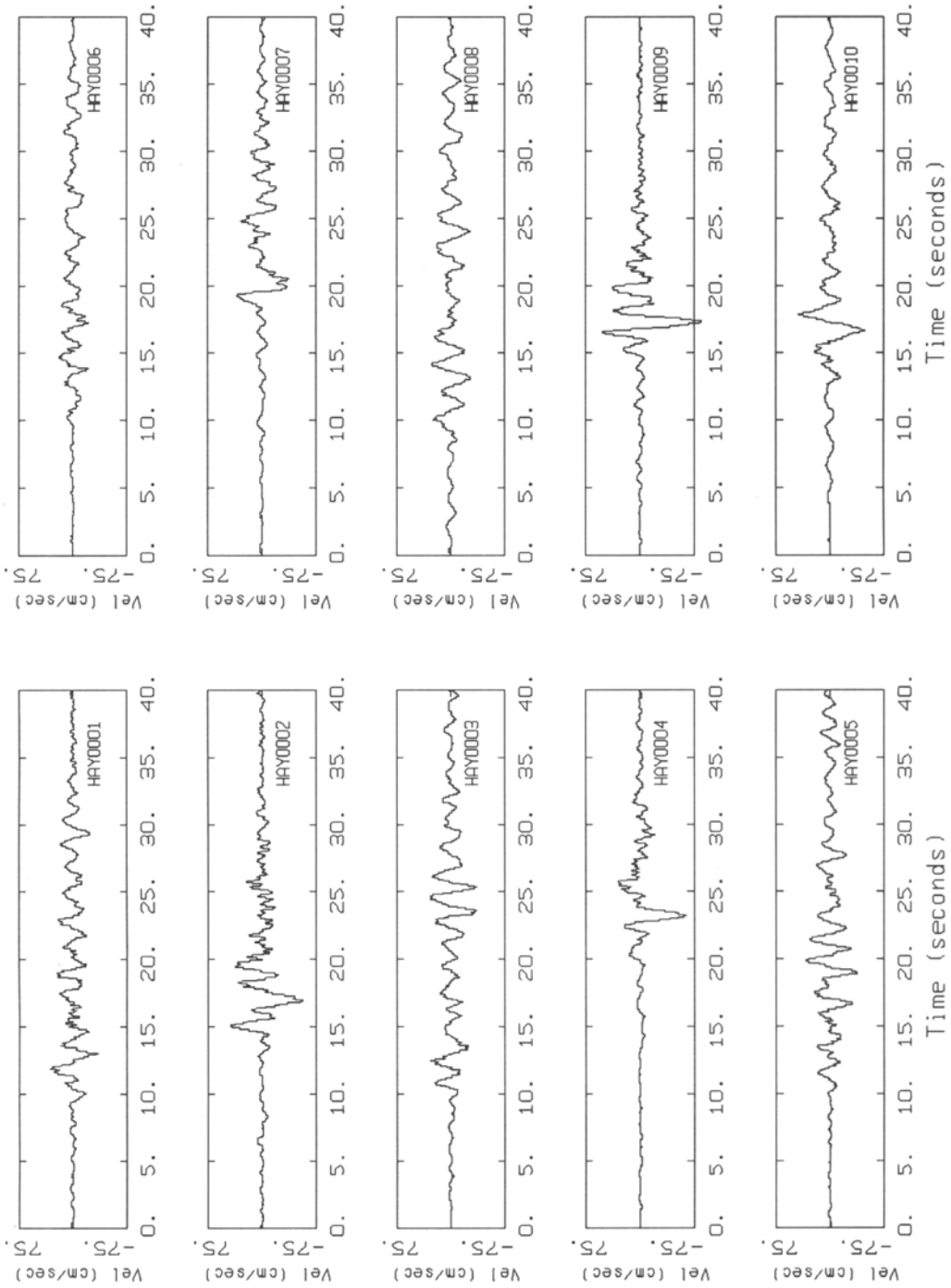
HAYWARD, M 7.1, SOFT SOIL, D = 7.5 KM, SOURCE

Appendix



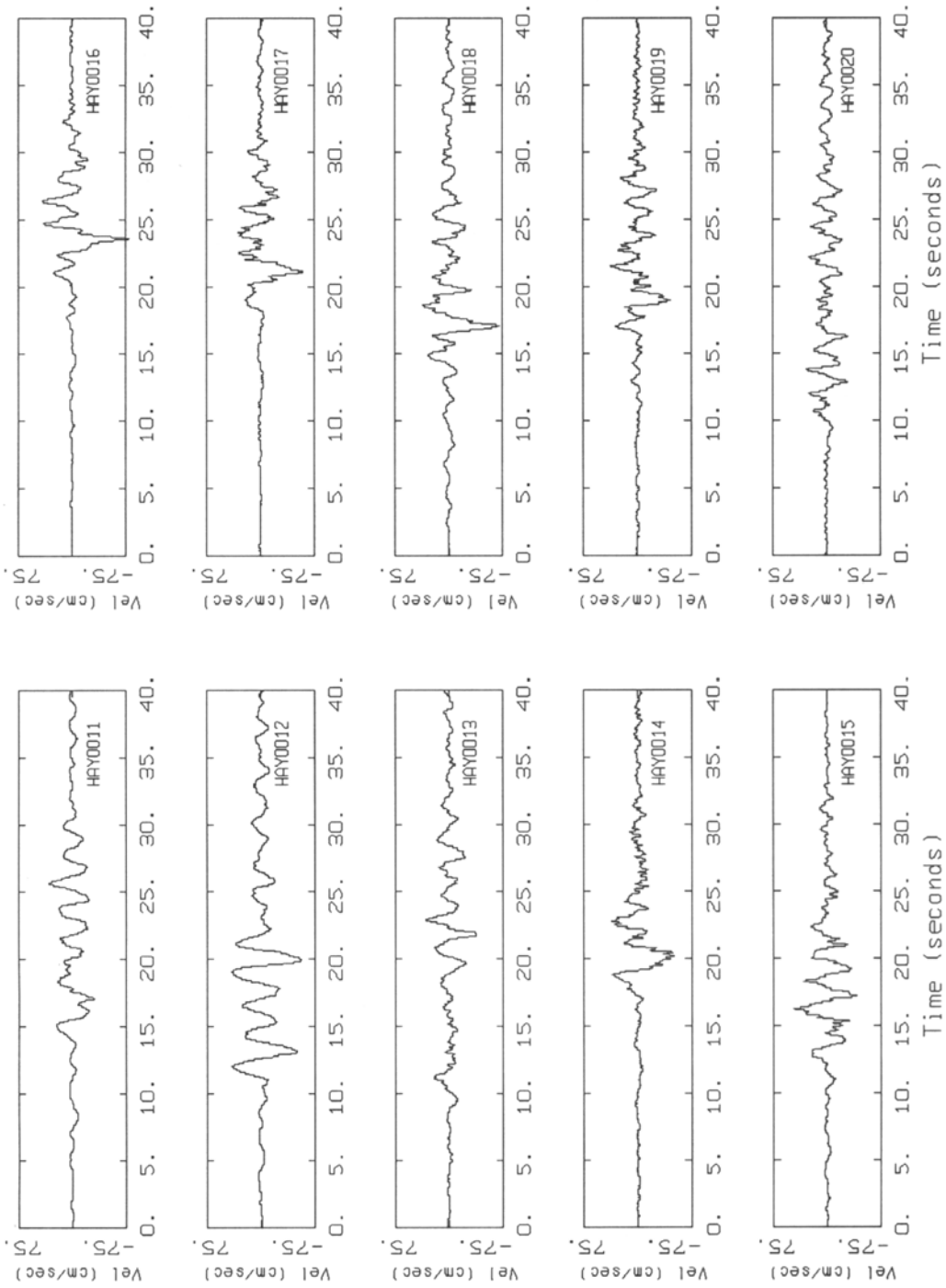
HAYWARD, M 7.1, SOFT SOIL, D = 7.5 KM, SOURCE

Appendix



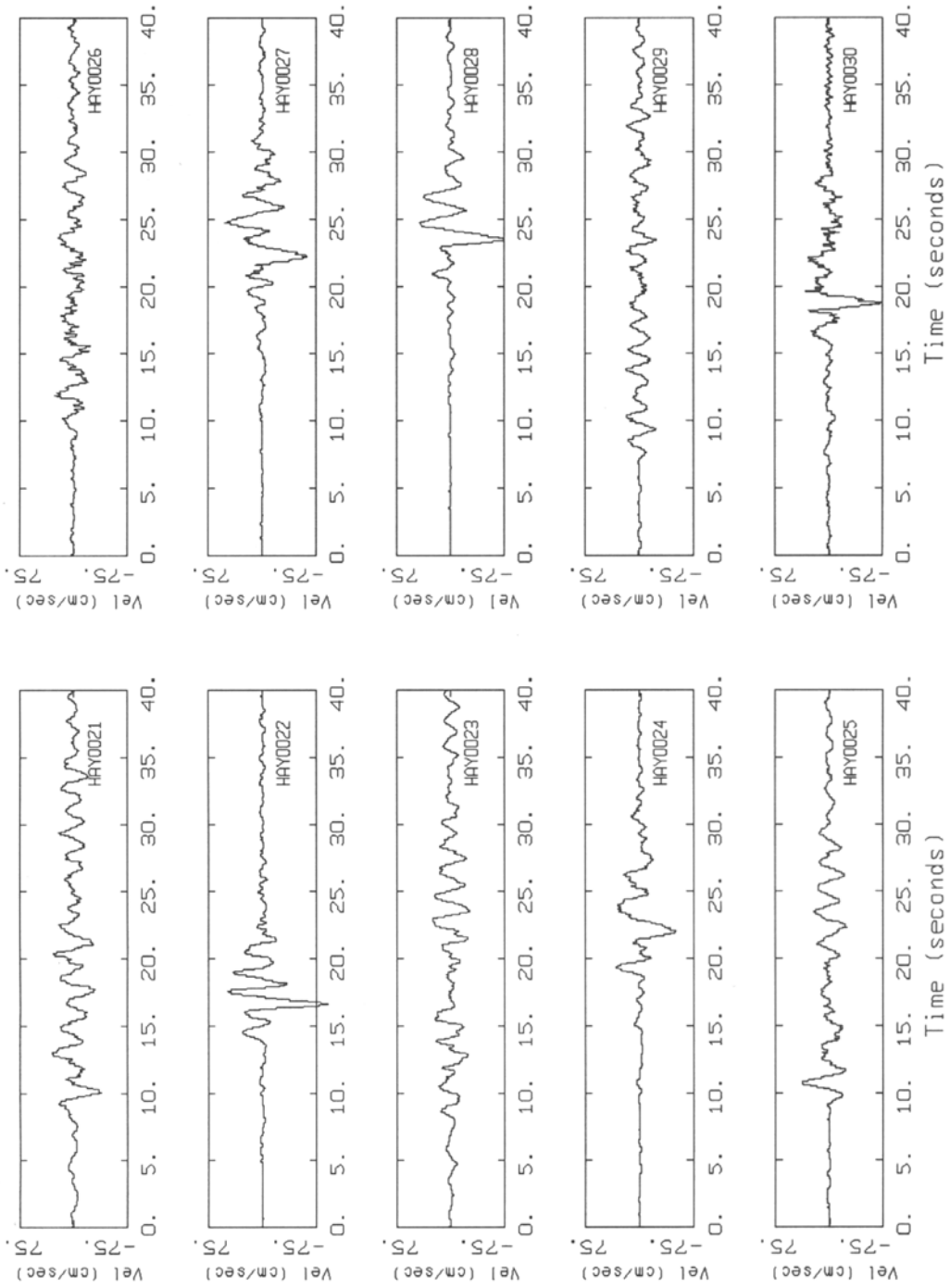
HAYWARD, M 7.1, SOFT SOIL, D = 5.0 KM, SOURCE

Appendix



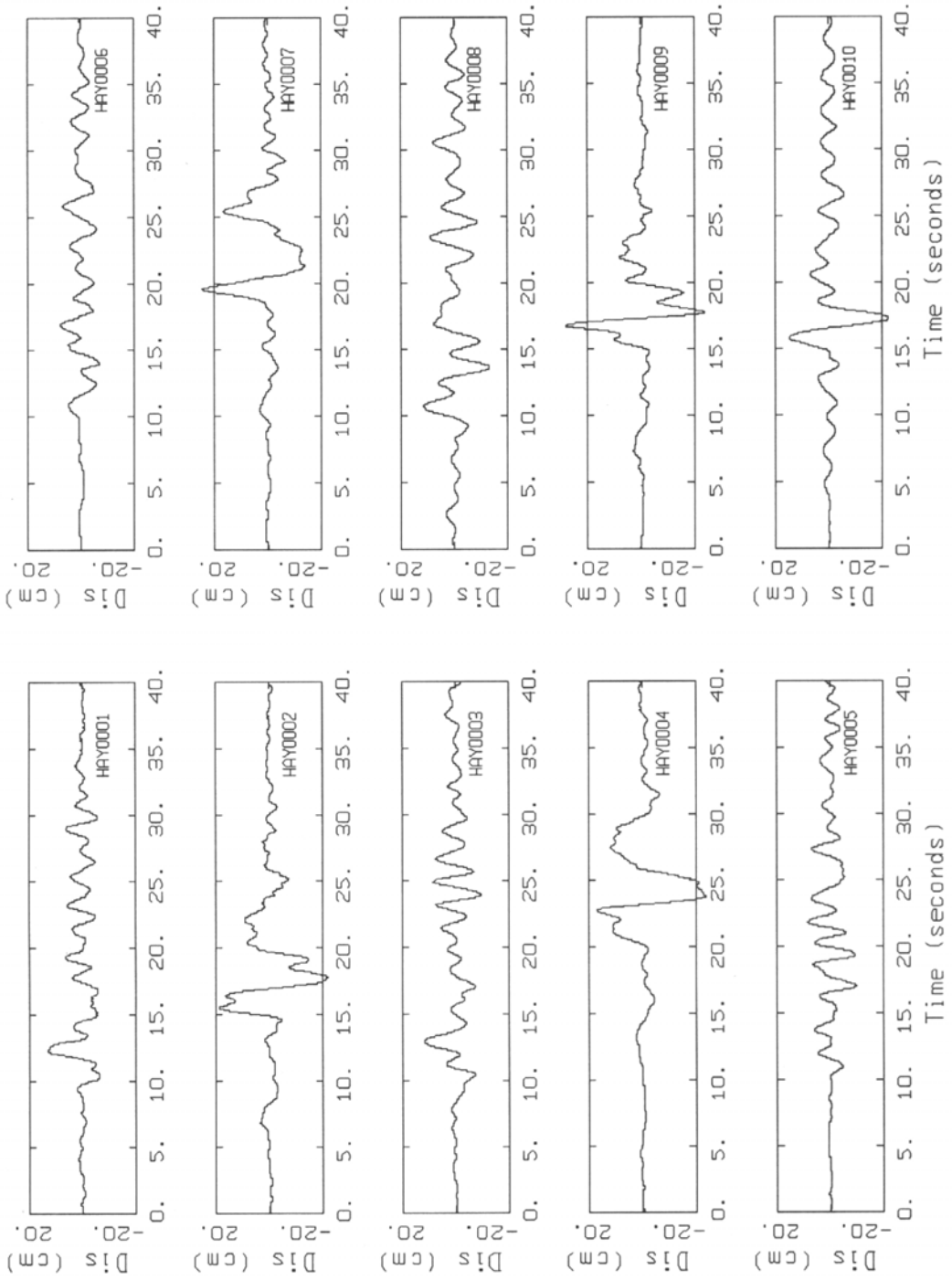
HAYWARD, M 7.1, SOFT SOIL, D = 5.0 KM, SOURCE

Appendix



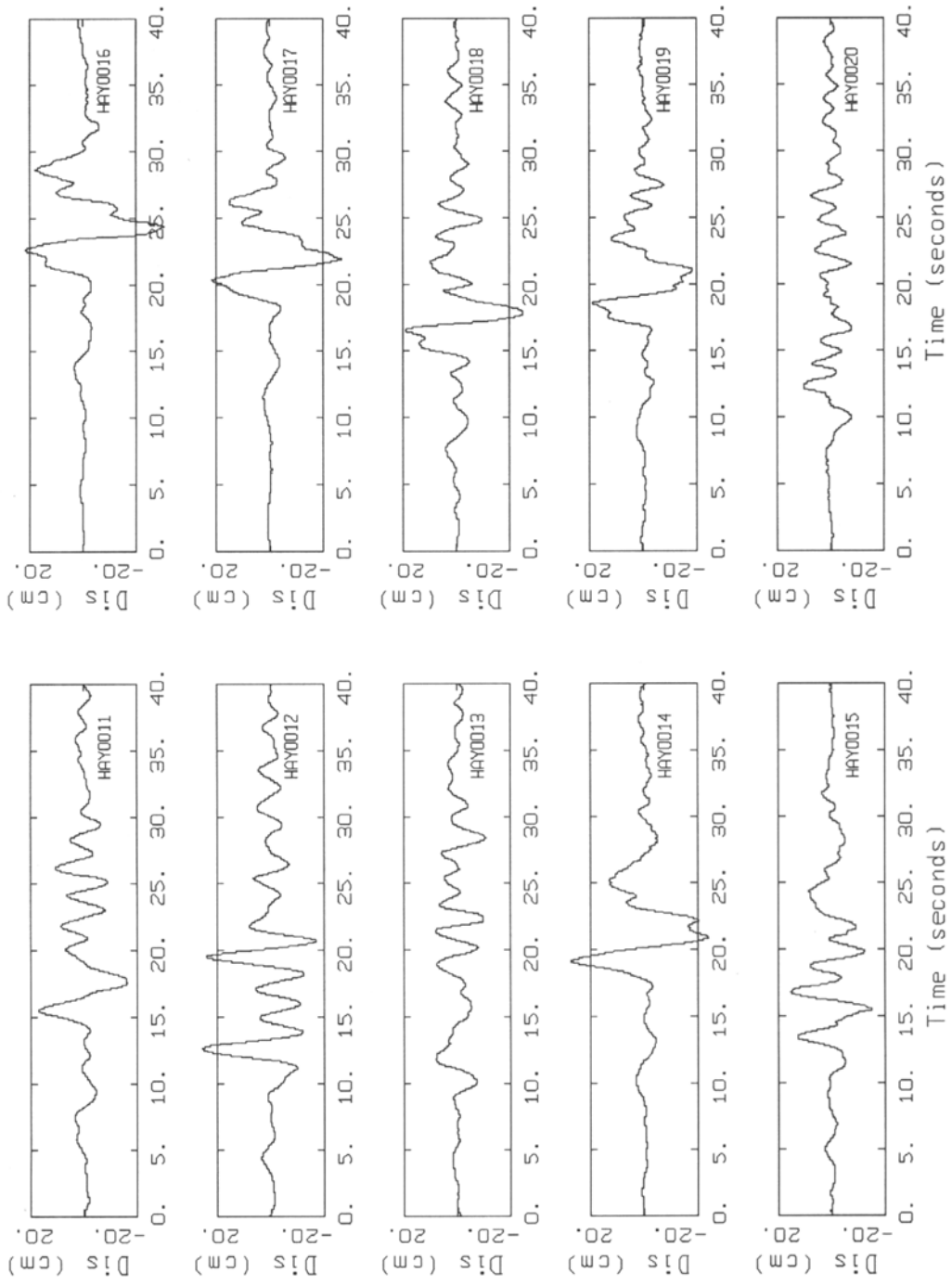
HAYWARD, M 7.1, SOFT SOIL, D = 5.0 KM, SOURCE

Appendix



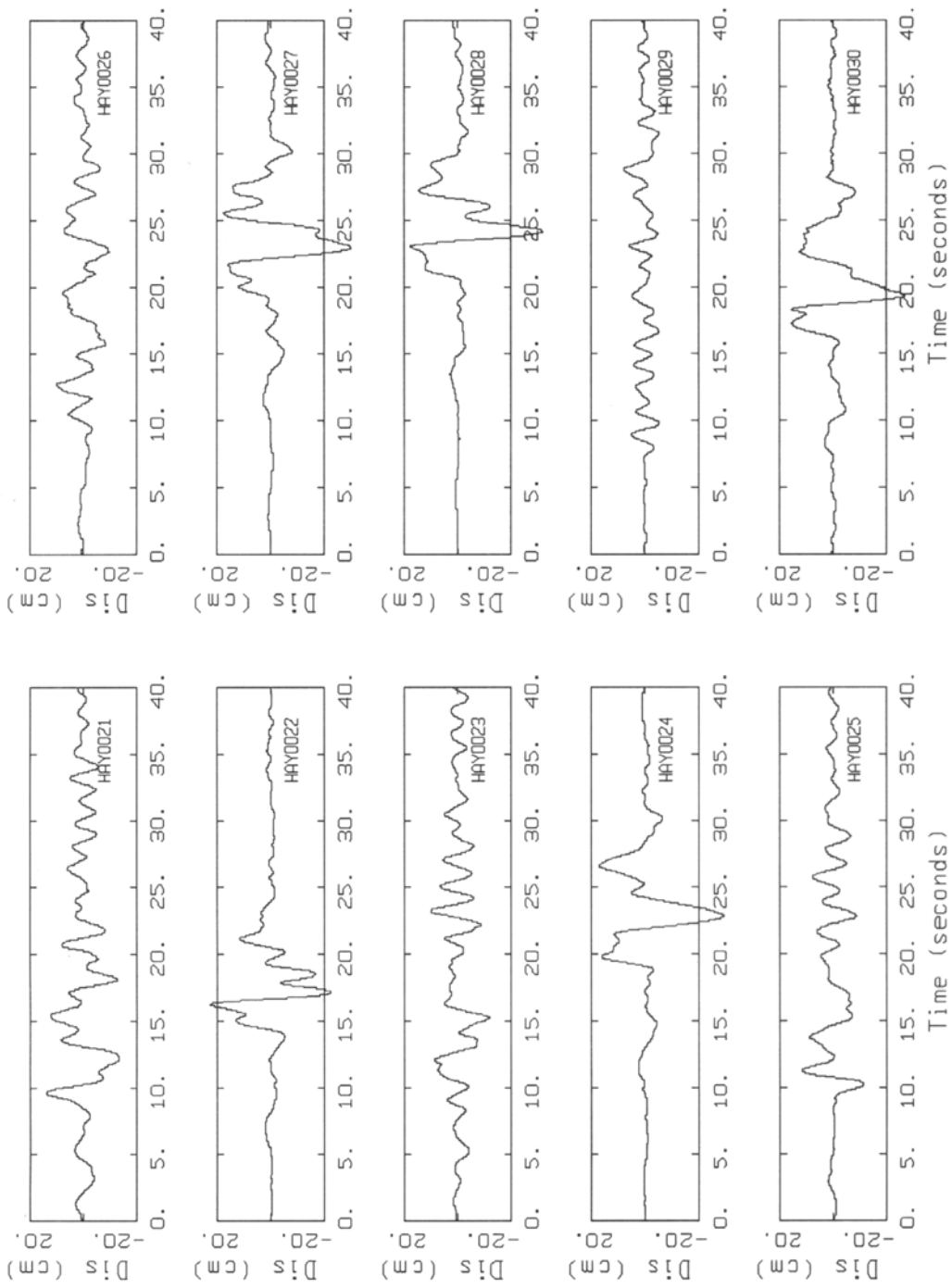
HAYWARD, M 7.1, SOFT SOIL, D = 5.0 KM, SOURCE

Appendix



HAYWARD, M 7.1, SOFT SOIL, D = 5.0 KM, SOURCE

Appendix



HAYWARD, M 7.1, SOFT SOIL, D = 5.0 KM, SOURCE